

Figure 38. Efficacy of AAV-HITI at various doses in newborn MPS VI mice. A) Alcian blue staining of histological sections from liver, kidney, spleen. Scale bar 50 μ m. Quantification of GAGs in liver (B), kidney and AFgRNA MD (N=4), affected MPS VI mice treated with AAV-HITI-gRNA at medium doses; AFgRNA LD (N=4), affected MPS VI mice treated with AAV-HITI-gRNA at low doses E) Alcian blue staining of histological sections from mitral heart valve and myocardium. Alcian Blue quantifications in the mitral heart valve and in myocardium are reported as Alcian blue positive area/total area. Scale bar 50 μ m. NR, unaffected untreated mice; AF (N=6), affected MPS VI mice, and AFgRNA MD (N=4), affected MPS VI mice treated with AAV-HITI-gRNA at medium doses; AFgRNA LD (N=4), affected MPS VI mice treated with AAV-HITI-gRNA at low doses. F-H) Measurement of skull length/width ratio (F), femur (G) and tibia (H) lengths; data are reported as the percentage of normal length (% of NR). NR, unaffected untreated mice; AF (N= 9), affected MPS VI mice, and AFgRNA MD (N=4,), affected MPS VI mice treated with AAV-HITI-gRNA at medium dose; and AFgRNA LD (N=4,), affected MPS VI mice treated with AAV-HITI-gRNA at low doses. Statistical differences were assessed by ordinary one-way ANOVA and Tukey's multiplecomparisons test.

Liver-directed AAV-HITI is effective in adult mice

To understand the applicability of AAV-HITI in an adult liver, MPS VI and Hema mice were randomly administered systemically at 6 weeks of age with the low dose of 1.2×10^{13} total GC/kg of AAV-HITI vectors. Similarly to the analysis performed in newborn mice, I measured serum ARSB activity in sera samples obtained from AFgRNA-treated MPS VI animals at different timepoints and found detectable ARSB levels at 90 days of age (1-month after a single AAV-HITI treatment). This activity became supraphysiological at the subsequent timepoints (Figure 39A). Moreover, AFgRNA-treated mice showed decreased levels of urinary (Figure 39B), and tissue GAGs compared to the AF control mice (Figure 40A-D). GAGs storage was also reduced in histological sections from the heart mitral valve and myocardium (Figure 40E) while I did not observe significant improvement in the analyzed bones (Figure 40F-H). In Hema mice

at 30 days post AAV-HITI delivery we observed: F8 protein levels around 36% of normal (**Figure 39C**); therapeutic levels of F8 activity (**Figure 39D**); and reduced clotting time (**Figure 39E**). These data indicate that AAV-HITI is effective in adult liver at moderate AAV doses in addition to newborn.

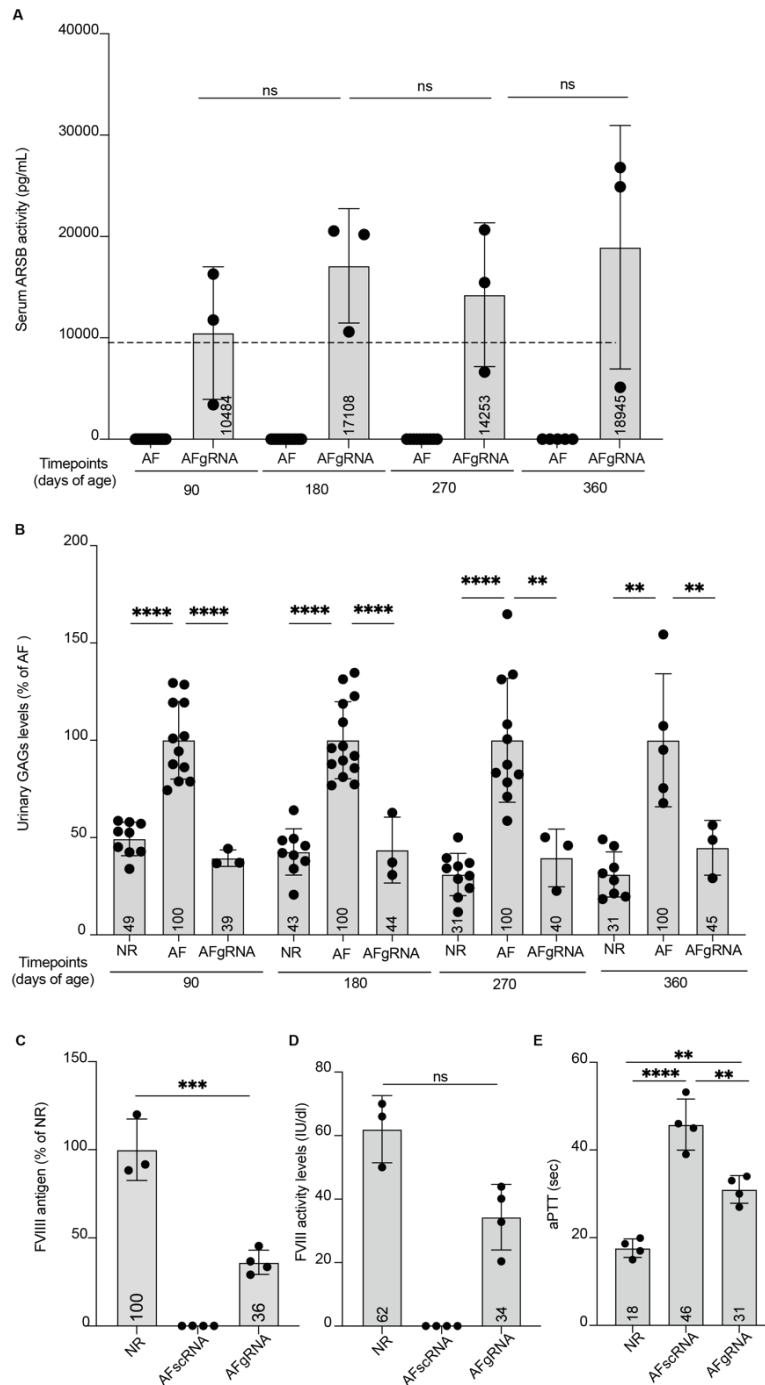


Figure 39. Liver-directed AAV-HITI in adult mice. A) Serum ARSB activity analyzed at different timepoints in MPS VI mice left untreated (AF, N=14) or treated with AAV-HITI-

gRNA (AFgRNA, N=3) at the total dose of 1.2×10^{13} total GC/kg. **B)** Urinary GAG levels at different timepoints in MPSVI mice left untreated (AF, N=14) or treated with AAV-HITI-gRNA (AFgRNA, N=3) reported as a percentage of GAG levels in untreated MPS VI mice. NR, sera samples from normal animals. Statistical differences were assessed by Kruskal-Wallis test. The differences in the number of analyzed samples within the same group of treatment was due to sample availability. Each dot corresponds to a single animal within each group at different timepoints. **A-B)** The differences in the number of analyzed samples within the same group of treatment at different timepoints was due to sample availability. **C)** F8 antigen levels detected in AAV-HITI (AFscRNA, N=4; AFgRNA, N=4) treated adult Hema mice and normal controls (NR, N=3) 1-month post AAV-HITI treatment. P-value*** = 0.0001 between NR and AFgRNA. **D)** F8 activity levels evaluated in Hema mice (AFgRNA, N=4; AFscRNA, N=4) and normal controls (NR, N=3) by chromogenic assay 1-month post AAV-HITI treatment. Statistical differences were assessed by ordinary one-way ANOVA test. P-value between NR and AFgRNA = 0.0783. **E)** Activated partial thromboplastin time (aPTT) measured 1-month post AAV-HITI treatment in Hema AAV-HITI (AFgRNA, N= 4 and AFscRNA, N= 4) mice and normal controls (NR; N= 4). P-values: **** <0.0001 between NR and AFscRNA; p-value ** = 0.0028 between NR and AFgRNA; p-value ** = 0.0014 between AFscRNA and AFgRNA. All data are represented as mean \pm standard deviation.

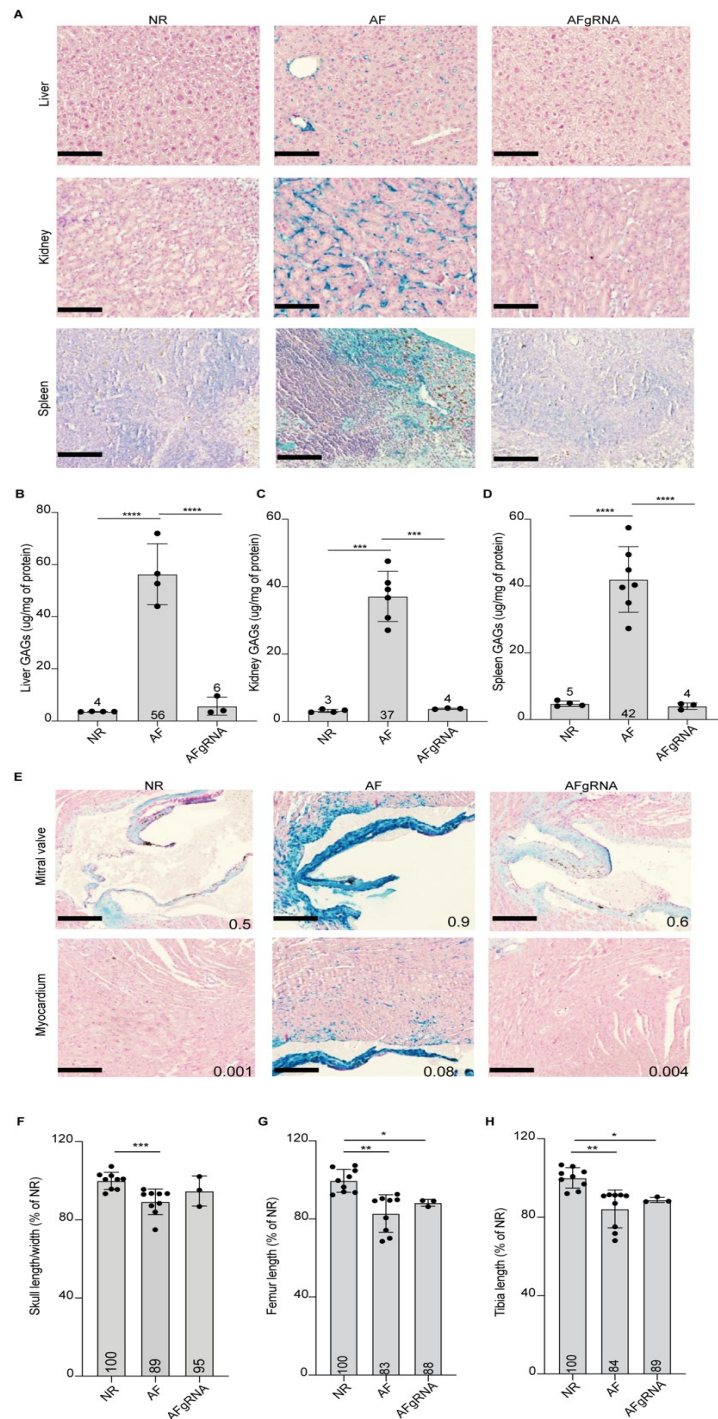


Figure 40. Efficiency of AAV-HITI in MPS VI mice. A) Alcian blue staining of histological sections from liver, kidney, spleen. Scale bar 50µm. Quantification of GAGs in liver (B), kidney (C), and spleen (D). E) Alcian Blue quantification in the mitral heart valve and in myocardium are reported as Alcian blue positive area/total area. Scale bar 50µm. F-H) Measurement of skull length/width ratio (F), femur (G) and tibia (H) lengths; data are reported as the percentage of normal length (% of NR). Statistical differences were assessed by ordinary one-way ANOVA and Tukey's multiple comparisons test.

DISCUSSION

AAV-mediated liver-directed gene therapy offers promise for treating liver diseases by enabling systemic production of therapeutic proteins like coagulation factors or lysosomal enzymes¹⁴⁹. AAVs are attractive tools for therapy due to their low immunogenicity, ability to infect non-dividing cells, and stable transgene expression, leading to approved therapies and various ongoing trials¹⁵⁰. However, their limited cargo capacity (~4.7 kb) poses challenges for large gene transfers, such as the *F8* gene for haemophilia A¹⁵¹. Additionally, AAV genomes can be diluted over time in newborns due to liver cell proliferation, reducing the therapeutic efficacy²⁹ and repeated AAV administrations can also increase immune responses, raising safety concerns¹⁵³. To address these challenges, my Ph.D. project explored advanced strategies like intein-mediated protein trans-splicing (PTS)⁸¹ and CRISPR-Cas9 gene editing to expand AAV cargo capacity and enable durable genome correction. In Specific Aim 1, I developed an AAV-intein-mediated PTS system for haemophilia A (HemA), a bleeding disorder caused by mutations in the large *F8* gene. Although therapies like Emicizumab¹⁵⁴ have advanced, a permanent cure remains elusive. While recent clinical trials have explored AAV-based gene therapies for HemA, challenges persist, including immune responses and concerns about long-term vector expression. The approved gene therapy using a smaller *F8* variant (SQF8) in 2023 (marked as Roctavian) represented progress, but limitations such as immune reactivity, long-term transgene expression and truncated genomes from oversize vectors remain problematic. To overcome the size limitation of *F8*, I employed an AAV protein trans-splicing (PTS) approach based on split inteins, using two vectors equipped with Npu DnaE inteins¹¹⁹ to reconstitute the full-length, highly secreted *F8*-N6 variant. Careful construct design is critical when using intein-mediated PTS to ensure precise splicing and preserve the functional integrity of the reconstituted protein. The selection of junction points must retain essential amino acids for

efficient trans-splicing, and the splitting point should avoid critical structural domains to prevent misfolding. In my approach, I split the F8N6 variant at Serine 962 within its B-domain, a non-essential region for F8 functionality. Additionally, each polypeptide included an expression cassette within its respective AAV-intein vector. These design features enabled the efficient delivery of split genes, overcoming AAV packaging limitations and avoiding the production of poorly defined truncated genomes, which could trigger immune responses or safety concerns. In the context of HemA, the development of anti-F8 antibodies following AAV treatment is a known complication, though the cause remains unclear. Interestingly, my approach did not induce anti-F8 antibodies or elevate pro/anti-inflammatory cytokines, which were observed in mice treated with a single AAV vector expressing the F8V3 variant. This, is one of the most promising B-domain deleted (BDD) versions of F8⁵⁹ currently under evaluation in the clinic (NCT03001830). Yet, the size of the AAV-F8-CodopV3 genome is over the canonical vector cargo capacity and results in truncated genomes. The reasons for immune differences between the two AAV systems (AAV-CodopV3 and AAV-N6-intein) are not clear or easy to investigate. Possible explanations could be that i. the difference in the B-domain structure between the CodopV3 and the N6 variants is responsible for the higher immunoreactivity of V3 than N6; ii. F8 antigen levels may differ between the various groups, as we engineered N6 to be expressed at similar therapeutic levels than V3 using lower vector doses, which improves the burden of both AAV manufacturing and anti-AAV immune responses; iii. the single oversized AAV-CodopV3 vector contains truncated genomes that may result in shorter immunogenic products. Despite these results, some challenges remain, such as the generation of excised inteins as by-products, which could theoretically cause toxicity. However, no toxicity has been observed in preclinical studies^{81,155,156} nor in this study. Future refinements, such as integrating degrons for selective intein degradation post-splicing¹⁵⁷, could enhance the safety of this approach

without affecting therapeutic protein levels. Nevertheless, the potential for protein misfolding or incomplete splicing, which could lead to the accumulation of non-functional or even toxic protein products should be carefully evaluated in each study ⁸⁴.

In Specific Aim 2, I addressed the loss of episomal AAV genomes in proliferative tissues by leveraging homology-independent targeted integration (HITI) for genome editing¹⁴⁷. HITI uses non-homologous end-joining to achieve targeted integration in both newborn and adult tissues without requiring large homology arms, making it suitable for large transgenes. I demonstrated that AAV-HITI enabled significant levels of full-length donor DNA integration after CRISPR/Cas9 cleavage, with a slight preference for the correct orientation, highlighting the importance of the inverted gRNA sites at both extremities of the donor DNA. Importantly, AAV-HITI integrates two technologies: AAV vectors and CRISPR/Cas9 both requiring thorough safety evaluation. It is well known that AAV integrates into the genome at low frequency ¹⁵⁸. Despite the rarity of these integrations, several mouse studies have been conducted to assess the potential genotoxicity, particularly after neonatal exposure ^{159,160}. Findings from these studies suggest that factors such as treatment age, vector dosage, and vector design may influence the likelihood of genotoxic events associated with AAV vectors ¹⁵⁹. Nonetheless, no definitive evidence of AAV-related genotoxicity has been observed to date. In my study I found that AAV fragments occasionally integrated at CRISPR-induced double-stranded breaks, though at a low frequency with most of these integrations falling within the AAV inverted terminal repeat (ITR) sequences, in line with previously reported data ^{161–163}. Moreover, full-length AAV-SpCas9 genome integrated at low levels and did not result in detectable long-term protein expression. A further critical consideration in genome editing is minimizing genotoxicity. CAST-Seq analysis¹²⁹ showed no evidence of chromosomal rearrangements or off-target mutations. Moreover, in

this study I used a weak hybrid liver specific promoter (HLP) to drive SpCas9 expression and no promoter in the donor DNA. This design should further decrease genotoxicity risks ¹⁶⁴. Lastly, the absence of hepatocellular carcinoma (HCC) up to 1-year after neonatal AAV-HITI treatment supports the platform's safety. Despite these results, to exclude potential AAV-HITI-induced genotoxicity associated with HCC development in mice, longer follow-up to 18-24 months of age will be necessary ¹⁶⁵. Additionally, AAV-HITI did not affect albumin levels, indicating safe gene insertion at the albumin locus. However, the potential for cryptic splice site creation warrants ongoing monitoring, especially when applying HITI to other genes. Lastly, I demonstrated that AAV-HITI directed to the 3' albumin locus provided sustained, stable expression of therapeutic transgenes in both newborns and adults, even at lower AAV doses, in two different mouse models of genetic diseases. These promising results suggest that AAV-HITI could be effective in human applications, though additional studies are needed. For instance, unwanted AAV genome integration at the on-target site could be mitigated using non-viral systems such as lipid nanoparticles (LNP) for nuclease delivery which provide transient expression ¹⁶⁶. Testing AAV-HITI in humanized liver models and optimizing gRNA sequences for human albumin will be key steps toward clinical translation.

CONCLUSION

Throughout my Ph.D., I focused on developing innovative AAV-based liver-directed gene therapies to address the major challenges associated with current AAV systems. My research employed cutting-edge techniques such as intein-mediated protein trans-splicing (PTS) and genome editing (AAV-HITI) to overcome these limitations. I successfully demonstrated the efficacy and safety of these approaches in animal models of genetic diseases, highlighting their therapeutic potential. By harnessing the unique capability of split inteins to splice proteins, I reconstituted the large, full-length F8N6 protein within the liver, validating the effectiveness of this approach in a mouse model of haemophilia A. Importantly, I observed no immune responses toward the *F8* transgene, underscoring the immunological safety of this method. Additionally, I implemented the mutation independent AAV-HITI platform to achieve stable integration of therapeutic transgenes at the mouse albumin locus, ensuring long-term transgene expression. I conducted an extensive long-term study that confirmed the sustained efficacy and safety of this platform in two different mouse models. Importantly, through detailed molecular analysis I evaluated the different AAV-HITI outcomes at the on-target site. Moreover, my work demonstrated that high doses of AAV-HITI did not result in hepatocellular carcinoma (HCC) development or genotoxicity, supporting its safety even at elevated AAV doses. Furthermore, I achieved significant and sustained therapeutic transgene expression, with results lasting up to one year following a single AAV administration in newborn mice models of mucopolysaccharidosis VI and haemophilia A. Notably, I also demonstrated the success of the AAV-HITI system in adult mice at lower AAV doses, broadening its application to adult liver-targeted therapies. All together these findings establish that these new AAV-mediated liver-directed strategies are promising approaches for treating genetic disorders from early to adult-onset diseases, thereby expanding the scope

of AAV-mediated gene therapy to a wider range of conditions requiring liver-directed interventions.

REFERENCES

1. Bowen, D.J. (2002). Haemophilia A and haemophilia B: molecular insights. [erratum appears in *Mol Pathol* 2002 Jun;55(3):208.] [republished from *Mol Pathol*. 2002 Feb;55(1):1-18 ; 11836440.]. [Review] [162 refs] . *Mol. Pathol.* .
2. Antonarakis, S.E., Kazazian, H.H., and Tuddenham, E.G.D. (1995). Molecular etiology of factor VIII deficiency in hemophilia A. *Hum. Mutat.* <https://doi.org/10.1002/humu.1380050102>.
3. Bolton-Maggs, P.H.B., and Pasi, K.J. (2003). Haemophilias A and B. In *Lancet* [https://doi.org/10.1016/S0140-6736\(03\)13405-8](https://doi.org/10.1016/S0140-6736(03)13405-8).
4. Oldenburg, J., Mahlangu, J.N., Kim, B., Schmitt, C., Callaghan, M.U., Young, G., Santagostino, E., Kruse-Jarres, R., Negrier, C., Kessler, C., et al. (2017). Emicizumab Prophylaxis in Hemophilia A with Inhibitors. *N. Engl. J. Med.* 377, 809–818. <https://doi.org/10.1056/nejmoa1703068>.
5. Mahlangu, J., Oldenburg, J., Paz-Priel, I., Negrier, C., Niggli, M., Mancuso, M.E., Schmitt, C., Jiménez-Yuste, V., Kempton, C., Dhalluin, C., et al. (2018). Emicizumab prophylaxis in patients who have hemophilia a without inhibitors. *N. Engl. J. Med.* <https://doi.org/10.1056/NEJMoa1803550>.
6. Samelson-Jones, B.J., Small, J.C., and George, L.A. (2024). Roctavian Gene Therapy for Hemophilia A. *Blood Adv.* 8, 5179–5189. <https://doi.org/10.1182/bloodadvances.2023011847>.
7. Manco-Johnson, M.J., Abshire, T.C., Shapiro, A.D., Riske, B., Hacker, M.R., Kilcoyne, R., Ingram, J.D., Manco-Johnson, M.L., Funk, S., Jacobson, L., et al. (2007). Prophylaxis versus episodic treatment to prevent joint disease in boys with severe hemophilia. *N. Engl. J. Med.* <https://doi.org/10.1056/NEJMoa067659>.
8. Nathwani, A.C., Davidoff, A.M., and Tuddenham, E.G.D. (2004). Prospects for gene therapy of haemophilia, <https://doi.org/10.1111/j.1365-2516.2004.00926.x> <https://doi.org/10.1111/j.1365-2516.2004.00926.x>.
9. Nathwani, A.C., Davidoff, A.M., and Tuddenham, E.G.D. (2017). Advances in Gene Therapy for Hemophilia, <https://doi.org/10.1089/hum.2017.167> <https://doi.org/10.1089/hum.2017.167>.

10. Toole, J.J., Pittman, D.D., and Orr, E.C. (1986). A large region (≈ 95 kDa) of human factor VIII is dispensable for in vitro procoagulant activity. *Proc. Natl. Acad. Sci. U. S. A.* <https://doi.org/10.1073/pnas.83.16.5939>.
11. Pittman, D., Alderman, E., Tomkinson, K., Wang, J., Giles, A., and Kaufman, R. (1993). Biochemical, immunological, and in vivo functional characterization of B-domain-deleted factor VIII. *Blood* *81*, 2925–2935. <https://doi.org/10.1182/blood.v81.11.2925.2925>.
12. Bunting, S., Zhang, L., Xie, L., Bullens, S., Mahimkar, R., Fong, S., Sandza, K., Harmon, D., Yates, B., Handyside, B., et al. (2018). Gene Therapy with BMN 270 Results in Therapeutic Levels of FVIII in Mice and Primates and Normalization of Bleeding in Hemophilic Mice. *Mol. Ther.* *26*, 496–509. <https://doi.org/10.1016/j.ymthe.2017.12.009>.
13. Rangarajan, S., Walsh, L., Lester, W., Perry, D., Madan, B., Laffan, M., Yu, H., Vettermann, C., Pierce, G.F., Wong, W.Y., et al. (2017). AAV5–Factor VIII Gene Transfer in Severe Hemophilia A. *N. Engl. J. Med.* *377*, 2519–2530. <https://doi.org/10.1056/nejmoa1708483>.
14. Belaramani, K.M., Chan, T.C.H., Hau, E.W.L., Yeung, M.C.W., Kwok, A.M.K., Lo, I.F.M., Law, T.H.F., Wu, H., Wong, S.S.N., Lam, S.W., et al. (2024). Expanded Newborn Screening for Inborn Errors of Metabolism in Hong Kong: Results and Outcome of a 7 Year Journey. *Int. J. Neonatal Screen.* *10*, 1–14. <https://doi.org/10.3390/ijns10010023>.
15. Carter, M.T., Srour, M., Au, P.Y.B., Buhas, D., Dyack, S., Eaton, A., Inbar-Feigenberg, M., Howley, H., Kawamura, A., Lewis, S.M.E., et al. (2023). Genetic and metabolic investigations for neurodevelopmental disorders: Position statement of the Canadian College of Medical Geneticists (CCMG). *J. Med. Genet.* *60*, 523–532. <https://doi.org/10.1136/jmg-2022-108962>.
16. Muenzer, J. (2011). Overview of the mucopolysaccharidoses. *Rheumatology* *50*, 4–12. <https://doi.org/10.1093/rheumatology/ker394>.
17. Parenti, G., Medina, D.L., and Ballabio, A. (2021). The rapidly evolving view of lysosomal storage diseases. *EMBO Mol. Med.* *13*, 1–21. <https://doi.org/10.15252/emmm.202012836>.

18. Platt, F.M., Boland, B., and van der Spoel, A.C. (2012). Lysosomal storage disorders: The cellular impact of lysosomal dysfunction. *J. Cell Biol.* *199*, 723–734. <https://doi.org/10.1083/jcb.201208152>.
19. Eskelinen, E.L. (2005). Maturation of autophagic vacuoles in Mammalian cells. *Autophagy* *1*, 1–10. <https://doi.org/10.4161/auto.1.1.1270>.
20. Luzio, J.P., Pryor, P.R., and Bright, N.A. (2007). Lysosomes: Fusion and function. *Nat. Rev. Mol. Cell Biol.* *8*, 622–632. <https://doi.org/10.1038/nrm2217>.
21. Ferla, R., Claudiani, P., Cotugno, G., Saccone, P., De Leonibus, E., and Auricchio, A. (2014). Similar therapeutic efficacy between a single administration of gene therapy and multiple administrations of recombinant enzyme in a mouse model of lysosomal storage disease. *Hum. Gene Ther.* *25*, 609–618. <https://doi.org/10.1089/hum.2013.213>.
22. Brunetti-Pierri, N., Ferla, R., Ginocchio, V.M., Rossi, A., Fecarotta, S., Romano, R., Parenti, G., Yildiz, Y., Zancan, S., Pecorella, V., et al. (2022). Liver-Directed Adeno-Associated Virus–Mediated Gene Therapy for Mucopolysaccharidosis Type VI. *NEJM Evid. J.* 1–12. <https://doi.org/10.1056/evidoa2200052>.
23. Bailey, J., Oliveri, A., and Levin, E. (2013). 基因的改变 NIH Public Access. *Bone* *23*, 1–7. <https://doi.org/10.1016/j.ymgme.2010.09.010.Clinical>.
24. Cotugno, G., Tessitore, A., Capalbo, A., Annunziata, P., Strisciuglio, C., Faella, A., Aurilio, M., Di Tommaso, M., Russo, F., Mancini, A., et al. (2010). Different serum enzyme levels are required to rescue the various systemic features of the mucopolysaccharidoses. *Hum. Gene Ther.* *21*, 555–569. <https://doi.org/10.1089/hum.2009.189>.
25. Cotugno, G., Annunziata, P., Tessitore, A., O'Malley, T., Capalbo, A., Faella, A., Bartolomeo, R., O'Donnell, P., Wang, P., Russo, F., et al. (2011). Long-term amelioration of feline mucopolysaccharidosis VI after AAV-mediated liver gene transfer. *Mol. Ther.* *19*, 461–469. <https://doi.org/10.1038/mt.2010.257>.
26. Ferla, R., O'Malley, T., Calcedo, R., O'Donnell, P., Wang, P., Cotugno, G., Claudiani, P., Wilson, J.M., Haskins, M., and Auricchio, A. (2013). Gene therapy for mucopolysaccharidosis type VI is effective in cats without pre-existing immunity to AAV8. *Hum. Gene Ther.* *24*, 163–169. <https://doi.org/10.1089/hum.2012.179>.

27. Alliegro, M., Ferla, R., Nusco, E., De Leonibus, C., Settembre, C., and Auricchio, A. (2016). Low-dose gene therapy reduces the frequency of enzyme replacement therapy in a mouse model of lysosomal storage disease. *Mol. Ther.* 24, 2054–2063. <https://doi.org/10.1038/mt.2016.181>.
28. Ferla, R., Alliegro, M., Marteau, J.B., Dell’Anno, M., Nusco, E., Pouillot, S., Galimberti, S., Valsecchi, M.G., Zuliani, V., and Auricchio, A. (2017). Non-clinical Safety and Efficacy of an AAV2/8 Vector Administered Intravenously for Treatment of Mucopolysaccharidosis Type VI. *Mol. Ther. Methods Clin. Dev.* 6, 143–158. <https://doi.org/10.1016/j.omtm.2017.07.004>.
29. Ehrhardt, A., Xu, H., and Kay, M.A. (2003). Episomal Persistence of Recombinant Adenoviral Vector Genomes during the Cell Cycle In Vivo. *J. Virol.* 77, 7689–7695. <https://doi.org/10.1128/jvi.77.13.7689-7695.2003>.
30. Cotugno, G., Annunziata, P., Barone, M.V., Karali, M., Banfi, S., and Auricchio, A. (2012). Impact of age at administration, lysosomal storage, and transgene regulatory elements on AAV2/8-mediated rat liver transduction. *PLoS One* 7. <https://doi.org/10.1371/journal.pone.0033286>.
31. Wang, L., Wang, H., Bell, P., McMenemy, D., and Wilson, J.M. (2012). Hepatic gene transfer in Neonatal mice by Adeno-associated virus serotype 8 vector. *Hum. Gene Ther.* 23, 533–539. <https://doi.org/10.1089/hum.2011.183>.
32. Cunningham, S.C., Spinoulas, A., Carpenter, K.H., Wilcken, B., Kuchel, P.W., and Alexander, I.E. (2009). AAV2/8-mediated correction of OTC deficiency is robust in adult but not neonatal Spfash mice. *Mol. Ther.* 17, 1340–1346. <https://doi.org/10.1038/mt.2009.88>.
33. Naldini, L. (2015). Gene therapy returns to centre stage. *Nature* 526, 351–360. <https://doi.org/10.1038/nature15818>.
34. Doudna, J.A., and Charpentier, E. (2014). The new frontier of genome engineering with CRISPR-Cas9. *Science* (80-.). 346. <https://doi.org/10.1126/science.1258096>.
35. Goswami, R., Subramanian, G., Silayeva, L., Newkirk, I., Doctor, D., Chawla, K., Chattopadhyay, S., Chandra, D., Chilukuri, N., and Betapudi, V. (2019). Gene therapy leaves a vicious cycle. *Front. Oncol.* 9, 1–25. <https://doi.org/10.3389/fonc.2019.00297>.

36. Rosenberg, S.A., Restifo, N.P., Yang, J.C., Morgan, R.A., and Dudley, M.E. (2008). Adoptive cell transfer: A clinical path to effective cancer immunotherapy. *Nat. Rev. Cancer* 8, 299–308. <https://doi.org/10.1038/nrc2355>.
37. Ramamoorth, M., and Narvekar, A. (2015). Non viral vectors in gene therapy - An overview. *J. Clin. Diagnostic Res.* 9, GE01–GE06. <https://doi.org/10.7860/JCDR/2015/10443.5394>.
38. Milone, M.C., and O’Doherty, U. (2018). Clinical use of lentiviral vectors. *Leukemia* 32, 1529–1541. <https://doi.org/10.1038/s41375-018-0106-0>.
39. Ginn, S.L., Amaya, A.K., Alexander, I.E., Edelstein, M., and Abedi, M.R. (2018). Gene therapy clinical trials worldwide to 2017: An update. *J. Gene Med.* 20, 1–16. <https://doi.org/10.1002/jgm.3015>.
40. Wang, J.H., Gessler, D.J., Zhan, W., Gallagher, T.L., and Gao, G. (2024). Adeno-associated virus as a delivery vector for gene therapy of human diseases. *Signal Transduct. Target. Ther.* 9. <https://doi.org/10.1038/s41392-024-01780-w>.
41. Wang, C., Pan, C., Yong, H., Wang, F., Bo, T., Zhao, Y., Ma, B., He, W., and Li, M. (2023). Emerging non-viral vectors for gene delivery. 1–18.
42. Hock, F.J., and Gralinski, M.R. (2020). *Drug Discovery and Evaluation: Methods in Clinical Pharmacology: Second Edition* <https://doi.org/10.1007/978-3-319-68864-0>.
43. Daya, S., and Berns, K.I. (2008). Gene therapy using adeno-associated virus vectors. *Clin. Microbiol. Rev.* 21, 583–593. <https://doi.org/10.1128/CMR.00008-08>.
44. Sonntag, F., Köther, K., Schmidt, K., Weghofer, M., Raupp, C., Nieto, K., Kuck, A., Gerlach, B., Böttcher, B., Müller, O.J., et al. (2011). The Assembly-Activating Protein Promotes Capsid Assembly of Different Adeno-Associated Virus Serotypes. *J. Virol.* 85, 12686–12697. <https://doi.org/10.1128/jvi.05359-11>.
45. Elmore, Z.C., Patrick Havlik, L., Oh, D.K., Anderson, L., Daaboul, G., Devlin, G.W., Vincent, H.A., and Asokan, A. (2021). The membrane associated accessory protein is an adeno-associated viral egress factor. *Nat. Commun.* 12, 1–13. <https://doi.org/10.1038/s41467-021-26485-4>.
46. Summerford, C., and Samulski, R.J. (1998). Membrane-Associated Heparan Sulfate Proteoglycan Is a Receptor for Adeno-Associated Virus Type 2 Virions. *J. Virol.* 72,

- 1438–1445. <https://doi.org/10.1128/jvi.72.2.1438-1445.1998>.
47. Nonnenmacher, M., and Weber, T. (2012). Intracellular transport of recombinant adeno-associated virus vectors. *Gene Ther.* *19*, 649–658. <https://doi.org/10.1038/gt.2012.6>.
 48. Dhungel, B.P., Bailey, C.G., and Rasko, J.E.J. (2021). Journey to the Center of the Cell: Tracing the Path of AAV Transduction. *Trends Mol. Med.* *27*, 172–184. <https://doi.org/10.1016/j.molmed.2020.09.010>.
 49. Ferrari, F.K., Samulski, T., Shenk, T., and Samulski, R.J. (1996). Second-strand synthesis is a rate-limiting step for efficient transduction by recombinant adeno-associated virus vectors. *J. Virol.* *70*, 3227–3234. <https://doi.org/10.1128/jvi.70.5.3227-3234.1996>.
 50. Balakrishnan, B., and Jayandharan, G. (2014). Basic Biology of Adeno-Associated Virus (AAV) Vectors Used in Gene Therapy. *Curr. Gene Ther.* *14*, 86–100. <https://doi.org/10.2174/1566523214666140302193709>.
 51. Kotin, R.M., Linden, R.M., and Berns, K.I. (1992). Characterization of a preferred site on human chromosome 19q for integration of adeno-associated virus DNA by non-homologous recombination. *EMBO J.* *11*, 5071–5078. <https://doi.org/10.1002/j.1460-2075.1992.tb05614.x>.
 52. Wright, J.F. (2008). Manufacturing and characterizing AAV-based vectors for use in clinical studies. *Gene Ther.* *15*, 840–848. <https://doi.org/10.1038/gt.2008.65>.
 53. Soon, G.S.T., and Torbenson, M. (2023). The Liver and Glycogen: In Sickness and in Health. *Int. J. Mol. Sci.* *24*. <https://doi.org/10.3390/ijms24076133>.
 54. Nathwani, A.C., Reiss, U.M., Tuddenham, E.G.D., Rosales, C., Chowdary, P., McIntosh, J., Peruta, M. Della, Lheriteau, E., Patel, N., Raj, D., et al. (2015). Long term gene therapy for FiX. *N Engl J Med* *371*, 1994–2004. <https://doi.org/10.1056/NEJMoa1407309.Long-Term>.
 55. Pasi, K.J., Rangarajan, S., Mitchell, N., Lester, W., Symington, E., Madan, B., Laffan, M., Russell, C.B., Li, M., Pierce, G.F., et al. (2020). Multiyear follow-up of aav5-hfviii-sq gene therapy for hemophilia a. *N. Engl. J. Med.* <https://doi.org/10.1056/NEJMoa1908490>.

56. Miesbach, W., Meijer, K., Coppens, M., Kampmann, P., Klamroth, R., Schutgens, R., Tangelder, M., Castaman, G., Schwäble, J., Bonig, H., et al. (2018). Gene therapy with adeno-associated virus vector 5–human factor IX in adults with hemophilia B. *Blood* *131*, 1022–1031. <https://doi.org/10.1182/blood-2017-09-804419>.
57. Anguela, X.M., and High, K.A. (2024). Hemophilia B and gene therapy: a new chapter with etranacogene dezaparvovec. *Blood Adv.* *8*, 1796–1803. <https://doi.org/10.1182/bloodadvances.2023010511>.
58. Mücke, M.M., Fong, S., Foster, G.R., Lillicrap, D., Miesbach, W., and Zeuzem, S. (2024). Adeno-associated viruses for gene therapy – clinical implications and liver-related complications, a guide for hepatologists. *J. Hepatol.* *80*, 352–361. <https://doi.org/10.1016/j.jhep.2023.10.029>.
59. Nathwani, A.C., Tuddenham, E., Chowdhary, P., McIntosh, J., Lee, D., Rosales, C., Phillips, M., Pie, J., Junfang, Z., Meagher, M.M., et al. (2018). GO-8: Preliminary Results of a Phase I/II Dose Escalation Trial of Gene Therapy for Haemophilia a Using a Novel Human Factor VIII Variant. *Blood*. <https://doi.org/10.1182/blood-2018-99-118256>.
60. Symington, E., Rangarajan, S., Lester, W., Madan, B., Pierce, G.F., Raheja, P., Millar, C., Osmond, D., Li, M., and Robinson, T.M. (2024). Valoctocogene roxaparvovec gene therapy provides durable haemostatic control for up to 7 years for haemophilia A. *Haemophilia*, 1138–1147. <https://doi.org/10.1111/hae.15071>.
61. Mingozzi, F., and High, K.A. (2013). Immune responses to AAV vectors: Overcoming barriers to successful gene therapy. *Blood* *122*, 23–36. <https://doi.org/10.1182/blood-2013-01-306647>.
62. Manini, A., Abati, E., Nuredini, A., Corti, S., and Comi, G. Pietro (2022). Adeno-Associated Virus (AAV)-Mediated Gene Therapy for Duchenne Muscular Dystrophy: The Issue of Transgene Persistence. *Front. Neurol.* *12*. <https://doi.org/10.3389/fneur.2021.814174>.
63. Chamberlain, J.R., and Chamberlain, J.S. (2017). Progress toward Gene Therapy for Duchenne Muscular Dystrophy. *Mol. Ther.* *25*, 1125–1131. <https://doi.org/10.1016/j.ymthe.2017.02.019>.

64. Cunningham, S.C., Dane, A.P., Spinoulas, A., and Alexander, I.E. (2008). Gene delivery to the juvenile mouse liver using AAV2/8 vectors. *Mol. Ther.* *16*, 1081–1088. <https://doi.org/10.1038/mt.2008.72>.
65. Zabaleta, N., Unzu, C., Weber, N.D., and Gonzalez-Aseguinolaza, G. (2023). Gene therapy for liver diseases — progress and challenges. *Nat. Rev. Gastroenterol. Hepatol.* *20*, 288–305. <https://doi.org/10.1038/s41575-022-00729-0>.
66. Paulk, N.K., Pekrun, K., Zhu, E., Nygaard, S., Li, B., Xu, J., Chu, K., Leborgne, C., Dane, A.P., Haft, A., et al. (2018). Bioengineered AAV Capsids with Combined High Human Liver Transduction In Vivo and Unique Humoral Seroreactivity. *Mol. Ther.* *26*, 289–303. <https://doi.org/10.1016/j.ymthe.2017.09.021>.
67. Cabanes-Creus, M., Navarro, R.G., Zhu, E., Baltazar, G., Liao, S.H.Y., Drouyer, M., Amaya, A.K., Scott, S., Nguyen, L.H., Westhaus, A., et al. (2022). Novel human liver-tropic AAV variants define transferable domains that markedly enhance the human tropism of AAV7 and AAV8. *Mol. Ther. Methods Clin. Dev.* *24*, 88–101. <https://doi.org/10.1016/j.omtm.2021.11.011>.
68. Kremer, L.P.M., Cerrizuela, S., Dehler, S., Stiehl, T., Weinmann, J., Abendroth, H., Kleber, S., Laure, A., El Andari, J., Anders, S., et al. (2021). High throughput screening of novel AAV capsids identifies variants for transduction of adult NSCs within the subventricular zone. *Mol. Ther. Methods Clin. Dev.* *23*, 33–50. <https://doi.org/10.1016/j.omtm.2021.07.001>.
69. Rode, L., Bär, C., Groß, S., Rossi, A., Meumann, N., Viereck, J., Abbas, N., Xiao, K., Riedel, I., Gietz, A., et al. (2022). AAV capsid engineering identified two novel variants with improved in vivo tropism for cardiomyocytes. *Mol. Ther.* *30*, 3601–3618. <https://doi.org/10.1016/j.ymthe.2022.07.003>.
70. Wagner, H.J., Weber, W., and Fussenegger, M. (2021). Synthetic Biology: Emerging Concepts to Design and Advance Adeno-Associated Viral Vectors for Gene Therapy. *Adv. Sci.* *8*, 1–22. <https://doi.org/10.1002/advs.202004018>.
71. Prasad, S., Dimmock, D.P., Greenberg, B., Walia, J.S., Sadhu, C., Tavakkoli, F., and Lipshutz, G.S. (2022). Immune Responses and Immunosuppressive Strategies for Adeno-Associated Virus-Based Gene Therapy for Treatment of Central Nervous System Disorders: Current Knowledge and Approaches. *Hum. Gene Ther.* *33*, 1228–

1245. <https://doi.org/10.1089/hum.2022.138>.
72. Hamilton, B.A., and Wright, J.F. (2021). Challenges Posed by Immune Responses to AAV Vectors: Addressing Root Causes. *Front. Immunol.* *12*, 1–8. <https://doi.org/10.3389/fimmu.2021.675897>.
73. Song, L.P., and Huang, H.L. (2003). Protein splicing and its application. *Sheng Wu Gong Cheng Xue Bao* *19*, 249–254. https://doi.org/10.1007/0-306-47572-3_10.
74. Perler, F.B., and Allewell, N.M. (2014). Evolution, mechanisms, and applications of Intein-mediated protein splicing. *J. Biol. Chem.* *289*, 14488–14489. <https://doi.org/10.1074/jbc.R114.570531>.
75. Wood, D.W., Belfort, M., and Lennon, C.W. (2023). Inteins—mechanism of protein splicing, emerging regulatory roles, and applications in protein engineering. *Front. Microbiol.* *14*, 1–7. <https://doi.org/10.3389/fmicb.2023.1305848>.
76. Sarmiento, C., and Camarero, J.A. (2019). Biotechnological Applications of Protein Splicing. *Curr. Protein Pept. Sci.* *20*, 408–424. <https://doi.org/10.2174/1389203720666190208110416>.
77. Wang, H., Wang, L., Zhong, B., and Dai, Z. (2022). Protein Splicing of Inteins: A Powerful Tool in Synthetic Biology. *Front. Bioeng. Biotechnol.* *10*, 1–9. <https://doi.org/10.3389/fbioe.2022.810180>.
78. Wu, H., Hu, Z., and Liu, X.Q. (1998). Protein trans-splicing by a split intein encoded in a split DnaE gene of *Synechocystis* sp. PCC6803. *Proc. Natl. Acad. Sci. U. S. A.* *95*, 9226–9231. <https://doi.org/10.1073/pnas.95.16.9226>.
79. Li, Y. (2015). Split-inteins and their bioapplications, <https://doi.org/10.1007/s10529-015-1905-2> <https://doi.org/10.1007/s10529-015-1905-2>.
80. Tasfaout, H., Halbert, C.L., McMillen, T.S., Allen, J.M., Reyes, T.R., Flint, G. V., Grimm, D., Hauschka, S.D., Regnier, M., and Chamberlain, J.S. (2024). Split intein-mediated protein trans-splicing to express large dystrophins. *Nature* *632*, 192–200. <https://doi.org/10.1038/s41586-024-07710-8>.
81. Tornabene, P., Trapani, I., Minopoli, R., Centrulo, M., Lupo, M., De Simone, S., Tiberi, P., Dell’Aquila, F., Marrocco, E., Iodice, C., et al. (2019). Intein-mediated protein trans-splicing expands adeno-associated virus transfer capacity in the retina.

- Sci. Transl. Med. <https://doi.org/10.1126/scitranslmed.aav4523>.
82. Esposito, F., Lyubenova, H., Tornabene, P., Auricchio, S., Iuliano, A., Nusco, E., Merlin, S., Olgasi, C., Manni, G., Gargaro, M., et al. (2022). Liver gene therapy with intein-mediated F8 trans-splicing corrects mouse haemophilia A. *EMBO Mol. Med.* *14*, 1–15. <https://doi.org/10.15252/emmm.202115199>.
 83. Padula, A., Petruzzelli, R., Philbert, S.A., Church, S.J., Esposito, F., Campione, S., Monti, M., Capolongo, F., Perna, C., Nusco, E., et al. (2022). Full-length ATP7B reconstituted through protein trans-splicing corrects Wilson disease in mice. *Mol. Ther. Methods Clin. Dev.* *26*, 495–504. <https://doi.org/10.1016/j.omtm.2022.08.004>.
 84. Zhou, Y., Zhang, C., Xiao, W., Herzog, R.W., and Han, R. (2024). Systemic delivery of full-length dystrophin in Duchenne muscular dystrophy mice. *Nat. Commun.* *15*. <https://doi.org/10.1038/s41467-024-50569-6>.
 85. Yao, Z., Aboualizadeh, F., Kroll, J., Akula, I., Snider, J., Lyakisheva, A., Tang, P., Kotlyar, M., Jurisica, I., Boxem, M., et al. (2020). Split Intein-Mediated Protein Ligation for detecting protein-protein interactions and their inhibition. *Nat. Commun.* *11*. <https://doi.org/10.1038/s41467-020-16299-1>.
 86. Truong, D.J.J., Kühner, K., Kühn, R., Werfel, S., Engelhardt, S., Wurst, W., and Ortiz, O. (2015). Development of an intein-mediated split-Cas9 system for gene therapy. *Nucleic Acids Res.* *43*, 6450–6458. <https://doi.org/10.1093/nar/gkv601>.
 87. Horvath, P., and Barrangou, R. (2010). CRISPR/Cas, the immune system of Bacteria and Archaea. *Science (80-.)*. *327*, 167–170. <https://doi.org/10.1126/science.1179555>.
 88. Gasiunas, G., Barrangou, R., Horvath, P., and Siksnys, V. (2012). Cas9-crRNA ribonucleoprotein complex mediates specific DNA cleavage for adaptive immunity in bacteria. *Proc. Natl. Acad. Sci. U. S. A.* *109*, 2579–2586. <https://doi.org/10.1073/pnas.1208507109>.
 89. Qiao, H., Wu, J., Zhang, X., Luo, J., Wang, H., and Ming, D. (2021). The Advance of CRISPR-Cas9-Based and NIR/CRISPR-Cas9-Based Imaging System. *Front. Chem.* *9*, 1–17. <https://doi.org/10.3389/fchem.2021.786354>.
 90. Jinek, M., Chylinski, K., Fonfara, I., Hauer, M., Doudna, J.A., and Charpentier, E. (2012). A programmable dual-RNA-guided DNA endonuclease in adaptive bacterial

- immunity. *Science* (80-.). 337, 816–821. <https://doi.org/10.1126/science.1225829>.
91. Kleinstiver, B.P., Pattanayak, V., Prew, M.S., Tsai, S.Q., Nguyen, N.T., Zheng, Z., and Joung, J.K. (2016). High-fidelity CRISPR-Cas9 nucleases with no detectable genome-wide off-target effects. *Nature* 529, 490–495. <https://doi.org/10.1038/nature16526>.
 92. Hsu, P.D., Scott, D.A., Weinstein, J.A., Ran, F.A., Konermann, S., Agarwala, V., Li, Y., Fine, E.J., Wu, X., Shalem, O., et al. (2013). DNA targeting specificity of RNA-guided Cas9 nucleases. *Nat. Biotechnol.* 31, 827–832. <https://doi.org/10.1038/nbt.2647>.
 93. Komor, A.C., Kim, Y.B., Packer, M.S., Zuris, J.A., and Liu, D.R. (2016). Programmable editing of a target base in genomic DNA without double-stranded DNA cleavage. *Nature* 533, 420–424. <https://doi.org/10.1038/nature17946>.
 94. Chavez, M., Chen, X., Finn, P.B., and Qi, L.S. (2023). Advances in CRISPR therapeutics. *Nat. Rev. Nephrol.* 19, 9–22. <https://doi.org/10.1038/s41581-022-00636-2>.
 95. Tornabene, P., Ferla, R., Llado-Santaularia, M., Centrulo, M., Dell’Anno, M., Esposito, F., Marrocco, E., Pone, E., Minopoli, R., Iodice, C., et al. (2022). Therapeutic homology-independent targeted integration in retina and liver. *Nat. Commun.* 13, 1–14. <https://doi.org/10.1038/s41467-022-29550-8>.
 96. Wang, Q., Zhong, X., Li, Q., Su, J., Liu, Y., Mo, L., Deng, H., and Yang, Y. (2020). CRISPR-Cas9-Mediated In Vivo Gene Integration at the Albumin Locus Recovers Hemostasis in Neonatal and Adult Hemophilia B Mice. *Mol. Ther. - Methods Clin. Dev.* 18, 520–531. <https://doi.org/10.1016/j.omtm.2020.06.025>.
 97. Syed, A., and Tainer, J.A. (2018). The MRE11-RAD50-NBS1 Complex Conducts the Orchestration of Damage Signaling and Outcomes to Stress in DNA Replication and Repair. *Annu. Rev. Biochem.* 87, 263–294. <https://doi.org/10.1146/annurev-biochem-062917-012415>.
 98. Zhao, F., Kim, W., Kloeber, J.A., and Lou, Z. (2020). DNA end resection and its role in DNA replication and DSB repair choice in mammalian cells. *Exp. Mol. Med.* 52, 1705–1714. <https://doi.org/10.1038/s12276-020-00519-1>.
 99. Longhese, M.P., Bonetti, D., Manfrini, N., and Clerici, M. (2010). Mechanisms and

- regulation of DNA end resection. *EMBO J.* *29*, 2864–2874.
<https://doi.org/10.1038/emboj.2010.165>.
100. Jasin, M., and Rothstein, R. (2013). Repair of strand breaks by homologous recombination. *Cold Spring Harb. Perspect. Biol.* *5*, 1–18.
<https://doi.org/10.1101/cshperspect.a012740>.
 101. Lu, D., Danilowicz, C., Tashjian, T.F., Prévost, C., Godoy, V.G., and Prentiss, M. (2019). Slow extension of the invading DNA strand in a D-loop formed by RecA-mediated homologous recombination may enhance recognition of DNA homology. *J. Biol. Chem.* *294*, 8606–8616. <https://doi.org/10.1074/jbc.RA119.007554>.
 102. Krejci, L., Altmannova, V., Spirek, M., and Zhao, X. (2012). Homologous recombination and its regulation. *Nucleic Acids Res.* *40*, 5795–5818.
<https://doi.org/10.1093/nar/gks270>.
 103. Li, X., and Heyer, W.D. (2008). Homologous recombination in DNA repair and DNA damage tolerance. *Cell Res.* *18*, 99–113. <https://doi.org/10.1038/cr.2008.1>.
 104. Ran, F.A., Hsu, P.D., Wright, J., Agarwala, V., Scott, D.A., and Zhang, F. (2013). Genome engineering using the CRISPR-Cas9 system. *Nat. Protoc.* *8*, 2281–2308.
<https://doi.org/10.1038/nprot.2013.143>.
 105. Porro, F., Bortolussi, G., Barzel, A., De Caneva, A., Iaconcig, A., Vodret, S., Zentilin, L., Kay, M.A., and Muro, A.F. (2017). Promoterless gene targeting without nucleases rescues lethality of a Crigler-Najjar syndrome mouse model. *EMBO Mol. Med.* *9*, 1346–1355. <https://doi.org/10.15252/emmm.201707601>.
 106. Azhagiri, M.K.K., Babu, P., Venkatesan, V., and Thangavel, S. (2021). Homology-directed gene-editing approaches for hematopoietic stem and progenitor cell gene therapy. *Stem Cell Res. Ther.* *12*, 1–12. <https://doi.org/10.1186/s13287-021-02565-6>.
 107. Fu, J., Fu, Y.W., Zhao, J.J., Yang, Z.X., Li, S.A., Li, G.H., Quan, Z.J., Zhang, F., Zhang, J.P., Zhang, X.B., et al. (2022). Improved and Flexible HDR Editing by Targeting Introns in iPSCs. *Stem Cell Rev. Reports* *18*, 1822–1833.
<https://doi.org/10.1007/s12015-022-10331-1>.
 108. Li, X., Sun, B., Qian, H., Ma, J., Paolino, M., and Zhang, Z. (2022). A high-efficiency and versatile CRISPR/Cas9-mediated HDR-based biallelic editing system. *J. Zhejiang*

- Univ. Sci. B 23, 141–152. <https://doi.org/10.1631/jzus.B2100196>.
109. Lieber, M.R. (2011). The mechanism of DSB repair by the NHEJ. *Annu. Rev. Biochem.* 79, 181–211. <https://doi.org/10.1146/annurev.biochem.052308.093131>.The.
 110. Chang, H.H.Y., Pannunzio, N.R., Adachi, N., and Lieber, M.R. (2017). Non-homologous DNA end joining and alternative pathways to double-strand break repair. *Nat. Rev. Mol. Cell Biol.* 18, 495–506. <https://doi.org/10.1038/nrm.2017.48>.
 111. Pannunzio, N.R., Watanabe, G., and Lieber, M.R. (2018). Nonhomologous DNA end-joining for repair of DNA double-strand breaks. *J. Biol. Chem.* 293, 10512–10523. <https://doi.org/10.1074/jbc.TM117.000374>.
 112. Maresca, M., Lin, V.G., Guo, N., and Yang, Y. (2013). Obligate ligation-gated recombination (ObLiGaRe): Custom-designed nuclease-mediated targeted integration through nonhomologous end joining. *Genome Res.* 23, 539–546. <https://doi.org/10.1101/gr.145441.112>.
 113. Zhang, J.P., Cheng, X.X., Zhao, M., Li, G.H., Xu, J., Zhang, F., Yin, M. Di, Meng, F.Y., Dai, X.Y., Fu, Y.W., et al. (2019). Curing hemophilia A by NHEJ-mediated ectopic F8 insertion in the mouse. *Genome Biol.* 20, 1–17. <https://doi.org/10.1186/s13059-019-1907-9>.
 114. Suzuki, K., Tsunekawa, Y., Hernandez-Benitez, R., Wu, J., Zhu, J., Kim, E.J., Hatanaka, F., Yamamoto, M., Araoka, T., Li, Z., et al. (2016). In vivo genome editing via CRISPR/Cas9 mediated homology-independent targeted integration. *Nature* 540, 144–149. <https://doi.org/10.1038/nature20565>.
 115. Esposito, F., Dell’Aquila, F., Rhiel, M., Auricchio, S., Chmielewski, K.O., Andrieux, G., Ferla, R., Horrach, P.S., Padmanabhan, A., Di Cunto, R., et al. (2024). Safe and effective liver-directed AAV-mediated homology-independent targeted integration in mouse models of inherited diseases. *Cell Reports Med.* 5, 101619. <https://doi.org/10.1016/j.xcrm.2024.101619>.
 116. Auricchio, A., Hildinger, M., O’Connor, E., Gao, G.P., and Wilson, J.M. (2001). Isolation of highly infectious and pure adeno-associated virus type 2 vectors with a single-step gravity-flow column. *Hum. Gene Ther.* 12, 71–76. <https://doi.org/10.1089/104303401450988>.

117. Shah, N.H., Eryilmaz, E., Cowburn, D., and Muir, T.W. (2013). Extein residues play an intimate role in the rate-limiting step of protein trans-splicing. *J. Am. Chem. Soc.* <https://doi.org/10.1021/ja401015p>.
118. Cheriyan, M., Chan, S.H., and Perler, F. (2014). Traceless splicing enabled by substrate-induced activation of the *Nostoc punctiforme* Npu DnaE intein after mutation of a catalytic cysteine to serine. *J. Mol. Biol.* *426*, 4018–4029. <https://doi.org/10.1016/j.jmb.2014.10.025>.
119. Iwai, H., Züger, S., Jin, J., and Tam, P.H. (2006). Highly efficient protein trans-splicing by a naturally split DnaE intein from *Nostoc punctiforme*. *FEBS Lett.* <https://doi.org/10.1016/j.febslet.2006.02.045>.
120. McIntosh, J., Lenting, P.J., Rosales, C., Lee, D., Rabbanian, S., Raj, D., Patel, N., Tuddenham, E.G.D., Christophe, O.D., McVey, J.H., et al. (2013). Therapeutic levels of FVIII following a single peripheral vein administration of rAAV vector encoding a novel human factor VIII variant. *Blood*. <https://doi.org/10.1182/blood-2012-10-462200>.
121. Yan, Z., Yan, H., and Ou, H. (2012). Human thyroxine binding globulin (TBG) promoter directs efficient and sustaining transgene expression in liver-specific pattern. *Gene* *506*, 289–294. <https://doi.org/10.1016/j.gene.2012.07.009>.
122. Levitt, N., Briggs, D., Gil, A., and Proudfoot, N.J. (1989). Definition of an efficient synthetic poly(A) site. *Genes Dev.* <https://doi.org/10.1101/gad.3.7.1019>.
123. Doria, M., Ferrara, A., and Auricchio, A. (2013). AAV2/8 vectors purified from culture medium with a simple and rapid protocol transduce murine liver, muscle, and retina efficiently. *Hum. Gene Ther. Methods* *24*, 392–398. <https://doi.org/10.1089/hgtb.2013.155>.
124. Maddalena, A., Tornabene, P., Tiberi, P., Minopoli, R., Manfredi, A., Mutarelli, M., Rossi, S., Simonelli, F., Naggert, J.K., Cacchiarelli, D., et al. (2018). Triple Vectors Expand AAV Transfer Capacity in the Retina. *Mol. Ther.* *26*, 524–541. <https://doi.org/10.1016/j.ymthe.2017.11.019>.
125. Sambrook, J., and Russell, D.W. 2001. *Molecular cloning: a laboratory manual*. Cold Spring Harbor Laboratory Press. Cold Spring Harbor, New York, USA. 999 pp.

126. Lampe, S.E.G., Kaspar, B.K., and Foust, K.D. (2014). Intravenous injections in neonatal mice. *J. Vis. Exp.*, 2–7. <https://doi.org/10.3791/52037>.
127. Nakai, H., Fuess, S., Storm, T.A., Muramatsu, S., Nara, Y., and Kay, M.A. (2005). Unrestricted Hepatocyte Transduction with Adeno-Associated Virus Serotype 8 Vectors in Mice. *J. Virol.* 79, 214–224. <https://doi.org/10.1128/jvi.79.1.214-224.2005>.
128. Tornabene, P., Ferla, R., Llado-Santaularia, M., Centrulo, M., Dell’Anno, M., Esposito, F., Marrocco, E., Pone, E., Minopoli, R., Iodice, C., et al. (2022). Therapeutic homology-independent targeted integration in retina and liver. *Nat. Commun.* 13, 1963. <https://doi.org/10.1038/s41467-022-29550-8>.
129. Turchiano, G., Andrieux, G., Klermund, J., Blattner, G., Pennucci, V., el Gaz, M., Monaco, G., Poddar, S., Mussolino, C., Cornu, T.I., et al. (2021). Quantitative evaluation of chromosomal rearrangements in gene-edited human stem cells by CAST-Seq. *Cell Stem Cell* 28, 1136-1147.e5. <https://doi.org/10.1016/j.stem.2021.02.002>.
130. Currin, A., Swainston, N., Dunstan, M.S., Jervis, A.J., Mulherin, P., Robinson, C.J., Taylor, S., Carbonell, P., Hollywood, K.A., Yan, C., et al. (2019). Highly multiplexed, fast and accurate nanopore sequencing for verification of synthetic DNA constructs and sequence libraries. *Synth. Biol.* 4, 1–8. <https://doi.org/10.1093/synbio/ysz025>.
131. Tange, O. (2018). GNU Parallel 2018. Ole Tange.
132. Srivathsan, A., Lee, L., Katoh, K., Hartop, E., Narayanan Kutty, S., Wong, J., Yeo, D., and Meier, R. (2021). MinION barcodes: biodiversity discovery and identification by everyone, for everyone. *bioRxiv*, 2021.03.09.434692.
133. Li, H. (2018). Minimap2: Pairwise alignment for nucleotide sequences. *Bioinformatics* 34, 3094–3100. <https://doi.org/10.1093/bioinformatics/bty191>.
134. Danecek, P., Bonfield, J.K., Liddle, J., Marshall, J., Ohan, V., Pollard, M.O., Whitwham, A., Keane, T., McCarthy, S.A., and Davies, R.M. (2021). Twelve years of SAMtools and BCFtools. *Gigascience* 10, 1–4. <https://doi.org/10.1093/gigascience/giab008>.
135. Clement, K., Rees, H., Canver, M.C., Gehrke, J.M., Farouni, R., Hsu, J.Y., Cole, M.A., Liu, D.R., Joung, J.K., Bauer, D.E., et al. (2019). CRISPResso2 provides accurate and rapid genome editing sequence analysis. *Nat. Biotechnol.* 37, 224–226.

<https://doi.org/10.1038/s41587-019-0032-3>.

136. Li, H. (2013). Aligning sequence reads, clone sequences and assembly contigs with BWA-MEM. *00*, 1–3.
137. Miao, H.Z., Sirachainan, N., Palmer, L., Kucab, P., Cunningham, M.A., Kaufman, R.J., and Pipe, S.W. (2004). Bioengineering of coagulation factor VIII for improved secretion. *Blood*. <https://doi.org/10.1182/blood-2003-10-3591>.
138. Sandberg, H., Almstedt, A., Brandt, J., Gray, E., Holmquist, L., Oswaldsson, U., Sebring, S., and Mikaelsson, M. (2001). Structural and functional characteristics of the B-domain-deleted recombinant factor VIII protein, r-VIII SQ. *Thromb. Haemost.* <https://doi.org/10.1055/s-0037-1612910>.
139. Ward, N.J., Buckley, S.M.K., Waddington, S.N., VandenDriessche, T., Chuah, M.K.L., Nathwani, A.C., McIntosh, J., Tuddenham, E.G.D., Kinnon, C., Thrasher, A.J., et al. (2011). Codon optimization of human factor VIII cDNAs leads to high-level expression. *Blood*. <https://doi.org/10.1182/blood-2010-05-282707>.
140. Nathwani, A.C. Gene therapy for hemophilia | Gene therapy for hemophilia. 569–578.
141. Zhu, F.X., Liu, Z.L., Wang, X.L., Miao, J., Qu, H.G., and Chi, X.Y. (2013). Inter-chain disulfide bond improved protein trans-splicing increases plasma coagulation activity in C57BL/6 mice following portal vein FVIII gene delivery by dual vectors. *Sci. China Life Sci.* <https://doi.org/10.1007/s11427-013-4455-7>.
142. Castaman, G., Di Minno, G., De Cristofaro, R., and Peyvandi, F. (2022). The Arrival of Gene Therapy for Patients with Hemophilia A. *Int. J. Mol. Sci.* *23*, 1–18. <https://doi.org/10.3390/ijms231810228>.
143. Rosenkilde, M.M., and Schwartz, T.W. (2004). The chemokine system - A major regulator of angiogenesis in health and disease. *Apmis* *112*, 481–495. <https://doi.org/10.1111/j.1600-0463.2004.apm11207-0808.x>.
144. Boström, E.A., Kindstedt, E., Sulniute, R., Palmqvist, P., Majster, M., Holm, C.K., Zwickler, S., Clark, R., Önell, S., Johansson, I., et al. (2015). Increased eotaxin and MCP-1 levels in serum from individuals with periodontitis and in human gingival fibroblasts exposed to pro-inflammatory cytokines. *PLoS One* *10*, 1–19.












- <https://doi.org/10.1371/journal.pone.0134608>.
145. Sharma, R., Anguela, X.M., Doyon, Y., Wechsler, T., DeKolver, R.C., Sproul, S., Paschon, D.E., Miller, J.C., Davidson, R.J., Shivak, D., et al. (2015). In vivo genome editing of the albumin locus as a platform for protein replacement therapy. *Blood* 126, 1777–1784. <https://doi.org/10.1182/blood-2014-12-615492>.
 146. Suzuki, K., Tsunekawa, Y., Hernandez-Benitez, R., Wu, J., Zhu, J., Kim, E.J., Hatanaka, F., Yamamoto, M., Araoka, T., Li, Z., et al. (2016). Homology-independent targeted integration. *Nature* 540, 144–149. <https://doi.org/10.1038/nature20565>.In.
 147. Suzuki, K., and Izpisua Belmonte, J.C. (2018). In vivo genome editing via the HITI method as a tool for gene therapy. *J. Hum. Genet.* 63, 157–164. <https://doi.org/10.1038/s10038-017-0352-4>.
 148. Nozawa, T., Furukawa, N., Aikawa, C., Watanabe, T., Haobam, B., Kurokawa, K., Maruyama, F., and Nakagawa, I. (2011). CRISPR inhibition of prophage acquisition in streptococcus pyogenes. *PLoS One* 6. <https://doi.org/10.1371/journal.pone.0019543>.
 149. Chuecos, M.A., and Lagor, W.R. (2024). Liver directed adeno-associated viral vectors to treat metabolic disease. *J. Inherit. Metab. Dis.* 47, 22–40. <https://doi.org/10.1002/jimd.12637>.
 150. Au, H.K.E., Isalan, M., and Mielcarek, M. (2022). Gene Therapy Advances: A Meta-Analysis of AAV Usage in Clinical Settings. *Front. Med.* 8, 1–14. <https://doi.org/10.3389/fmed.2021.809118>.
 151. Chao, H., Sun, L., Bruce, A., Xiao, X., and Walsh, C.E. (2002). Expression of human factor VIII by splicing between dimerized AAV vectors. *Mol. Ther.* 5, 716–722. <https://doi.org/10.1006/mthe.2002.0607>.
 152. Strauch, O.F., Stypmann, J., Reinheckel, T., Martinez, E., Haverkamp, W., and Peters, C. (2003). Cardiac and Ocular Pathologies in a Mouse Model of Mucopolysaccharidosis Type VI. *Pediatr. Res.* 54, 701–708. <https://doi.org/10.1203/01.PDR.0000084085.65972.3F>.
 153. Mingozzi, F., Maus, M. V., Hui, D.J., Sabatino, D.E., Murphy, S.L., Rasko, J.E.J., Ragni, M. V., Manno, C.S., Sommer, J., Jiang, H., et al. (2007). CD18+ T-cell responses to adeno-associated virus capsid in humans. *Nat. Med.* 13, 419–422.

- <https://doi.org/10.1038/nm1549>.
154. Young, G., Pipe, S.W., Kenet, G., Oldenburg, J., Safavi, M., Czirok, T., Nissen, F., and Mahlangu, J. (2024). Emicizumab is well tolerated and effective in people with congenital hemophilia A regardless of age, severity of disease, or inhibitor status: a scoping review. *Res. Pract. Thromb. Haemost.* *8*, 102415.
<https://doi.org/10.1016/j.rpth.2024.102415>.
 155. Chen, L., Zhu, F., Li, J., Lu, H., Jiang, H., Sarkar, R., Arruda, V.R., Wang, J., Zhao, J., Pierce, G.F., et al. (2007). The enhancing effects of the light chain on heavy chain secretion in split delivery of factor VIII gene. *Mol. Ther.*
<https://doi.org/10.1038/sj.mt.6300268>.
 156. Zhu, F.X., Liu, Z.L., Chi, X.Y., and Qu, H.G. (2010). Protein trans-splicing based dual-vector delivery of the coagulation factor VIII gene. *Sci. China Life Sci.*
<https://doi.org/10.1007/s11427-010-4011-7>.
 157. Tornabene, P., Trapani, I., Centrulo, M., Marrocco, E., Minopoli, R., Lupo, M., Iodice, C., Gesualdo, C., Simonelli, F., Surace, E.M., et al. (2021). Inclusion of a degron reduces levelsof undesired inteins after AAV-mediated proteintans-splicing in the retina. *Mol. Ther. - Methods Clin. Dev.* *23*, 448–459.
<https://doi.org/10.1016/j.omtm.2021.10.004>.
 158. Deyle, D.R., and Russell, D.W. (2009). Adeno-associated virus vector integration. *Curr. Opin. Mol. Ther.* *11*, 442–447.
 159. Sabatino, D.E., Bushman, F.D., Chandler, R.J., Crystal, R.G., Davidson, B.L., Dolmetsch, R., Eggan, K.C., Gao, G., Gil-Farina, I., Kay, M.A., et al. (2022). Evaluating the state of the science for adeno-associated virus integration: An integrated perspective. *Mol. Ther.* *30*, 2646–2663.
<https://doi.org/10.1016/j.ymthe.2022.06.004>.
 160. Chandler, R.J., LaFave, M.C., Varshney, G.K., Burgess, S.M., and Venditti, C.P. (2016). Genotoxicity in mice following AAV gene delivery: A safety concern for human gene therapy? *Mol. Ther.* *24*, 198–201. <https://doi.org/10.1038/mt.2016.17>.
 161. Hanlon, K.S., Kleinstiver, B.P., Garcia, S.P., Zaborowski, M.P., Volak, A., Spirig, S.E., Muller, A., Sousa, A.A., Tsai, S.Q., Bengtsson, N.E., et al. (2019). High levels of

- AAV vector integration into CRISPR-induced DNA breaks. *Nat. Commun.* *10*, 1–11. <https://doi.org/10.1038/s41467-019-12449-2>.
162. Nelson, C.E., Wu, Y., Gemberling, M.P., Oliver, M.L., Waller, M.A., Bohning, J.D., Robinson-Hamm, J.N., Bulaklak, K., Castellanos Rivera, R.M., Collier, J.H., et al. (2019). Long-term evaluation of AAV-CRISPR genome editing for Duchenne muscular dystrophy. *Nat. Med.* *25*, 427–432. <https://doi.org/10.1038/s41591-019-0344-3>.
163. Simpson, B.P., Yrigollen, C.M., Izda, A., and Davidson, B.L. (2023). Targeted long-read sequencing captures CRISPR editing and AAV integration outcomes in brain (The Author(s)) <https://doi.org/10.1016/j.ymthe.2023.01.004>.
164. Chandler, R.J., La Fave, M.C., Varshney, G.K., Trivedi, N.S., Carrillo-Carrasco, N., Senac, J.S., Wu, W., Hoffmann, V., Elkahloun, A.G., Burgess, S.M., et al. (2015). Vector design influences hepatic genotoxicity after adeno-associated virus gene therapy. *J. Clin. Invest.* *125*, 870–880. <https://doi.org/10.1172/JCI79213>.
165. Ferla, R., Alliegro, M., Dell’Anno, M., Nusco, E., Cullen, J.M., Smith, S.N., Wolfsberg, T.G., O’Donnell, P., Wang, P., Nguyen, A.D., et al. (2021). Low incidence of hepatocellular carcinoma in mice and cats treated with systemic adeno-associated viral vectors. *Mol. Ther. - Methods Clin. Dev.* *20*, 247–257. <https://doi.org/10.1016/j.omtm.2020.11.015>.
166. Han, J.P., Kim, M.J., Choi, B.S., Lee, J.H., Lee, G.S., Jeong, M., Lee, Y., Kim, E.A., Oh, H.K., Go, N., et al. (2022). In vivo delivery of CRISPR-Cas9 using lipid nanoparticles enables antithrombin gene editing for sustainable hemophilia A and B therapy. *Sci. Adv.* *8*, 1–10. <https://doi.org/10.1126/sciadv.abj6901>.

APPENDIX

Liver gene therapy with intein-mediated F8 *trans*-splicing corrects mouse haemophilia A

Federica Esposito¹ , Hristiana Lyubenova¹ , Patrizia Tornabene¹ , Stefano Auricchio¹, Antonella Iuliano¹ , Edoardo Nusco¹, Simone Merlin² , Cristina Olgasi² , Giorgia Manni³ , Marco Gargaro³ , Francesca Fallarino³ , Antonia Follenzi²  & Alberto Auricchio^{1,4,*} 

Abstract

Liver gene therapy with adeno-associated viral (AAV) vectors is under clinical investigation for haemophilia A (HemA), the most common inherited X-linked bleeding disorder. Major limitations are the large size of the F8 transgene, which makes packaging in a single AAV vector a challenge, as well as the development of circulating anti-F8 antibodies which neutralise F8 activity. Taking advantage of split-intein-mediated protein *trans*-splicing, we divided the coding sequence of the large and highly secreted F8-N6 variant in two separate AAV-intein vectors whose co-administration to HemA mice results in the expression of therapeutic levels of F8 over time. This occurred without eliciting circulating anti-F8 antibodies unlike animals treated with the single oversized AAV-F8 vector under clinical development. Therefore, liver gene therapy with AAV-F8-N6 intein should be considered as a potential therapeutic strategy for HemA.

Keywords AAV vectors; haemophilia A; liver gene therapy; protein *trans*-splicing

Subject Categories Genetics, Gene Therapy & Genetic Disease; Haematology; Methods & Resources

DOI 10.15252/emmm.202115199 | Received 13 October 2021 | Revised 1 April 2022 | Accepted 11 April 2022 | Published online 2 May 2022

EMBO Mol Med (2022) 14: e15199

Introduction

Haemophilia A (HemA) is the most common inherited X-linked recessive coagulation disorder caused by the partial or complete deficiency of coagulation F8. F8 activity levels are inversely proportional to bleeding risk; severely affected patients (about 50% of all cases) have circulating protein levels of < 1% (Antonarakis *et al*, 1995; White *et al*, 2001; Bowen, 2002). Levels of F8 activity between 1 and 5% result in a moderate phenotype, levels between 5 and 50% give a mild phenotype, and levels above 50% are associated with normal haemostasis (White *et al*, 2001).

The current management of HemA involves prophylactic administration of recombinant or plasma-derived F8. Lifelong intravenous infusions are required as often as 2–3 times weekly in severely affected patients. The chances of developing neutralising anti-F8 antibodies (inhibitors) remain high with about 30% of patients having to discontinue treatment (Cafuir & Kempton, 2017). This is potentially overcome by the recently approved bispecific antibody Emicizumab, which has significantly broadened the treatment options for HemA, allowing treatment of even younger patients which was previously unfeasible with standard care (Mahlangu *et al*, 2018; Oldenburg *et al*, 2018). Emicizumab is injected subcutaneously every 1–4 weeks with almost no bleeding occurring in the majority of patients. However, the management of spontaneous bleeds on Emicizumab still requires standard infusions (Butterfield *et al*, 2019).

Regardless of the various existing treatment options, the possibility of curing HemA rather than managing the disease remains the hope of many patients. In the last two decades, gene therapy for HemA has been under extensive investigation after it was observed that even modest improvements in the F8 levels (by 1–2%) can significantly reduce the risk of spontaneous bleeding events and the need for F8 replacement infusions (Manco-Johnson *et al*, 2007).

Adeno-associated viral (AAV) vectors have emerged as the most promising *in vivo* gene therapy approach for HemA, because of their excellent safety profile and their ability to direct long-term transgene expression from post-mitotic tissues such as the liver (Nathwani *et al*, 2004, 2017). However, HemA poses a great challenge to AAV gene therapy because of the size (7 kb) of the F8 coding sequence (CDS) to be transferred which exceeds the canonical AAV cargo capacity of ~4.7 kb. For this reason, all of the AAV-based products under clinical investigation consist of B-domain-deleted (BDD) versions of the F8 transgene, which are ~4.4 kb in size (Makris, 2020). However, using a transgene of this size leaves limited space in the vector for the necessary regulatory elements, thus restricting the choice of promoters and polyA signals. Moreover, all these vector genomes are on the verge of AAV's normal cargo capacity and are thus at risk of being improperly packaged as a library of heterogeneous truncated genomes. Despite the ability of such oversize

1 Telethon Institute of Genetics and Medicine (TIGEM), Pozzuoli, Italy

2 Department of Health Sciences, University of Piemonte Orientale "Amedeo Avogadro", Novara, Italy

3 Department of Medicine and Surgery, University of Perugia, Perugia, Italy

4 Medical Genetics, Department of Advanced Biomedical Sciences, Federico II University, Naples, Italy

*Corresponding author. Tel: +39 081 19230605; E-mail: auricchio@tigem.it

vectors to successfully express large proteins, their long-term efficiency and safety are yet to be confirmed (Grieger & Samulski, 2005; Dong et al, 2010; Hirsch et al, 2010; Wu et al, 2010).

As an alternative, different groups have explored strategies based on co-delivery of dual AAV vectors to reconstitute F8. Each vector encodes for one of the two chains, which should then re-associate and produce the biologically active heterodimer F8. However, the main drawback of this approach is the apparent chain imbalance, which derives from less efficient secretion of the heavy chain than the light one. This results in the production of higher amounts of inactive protein compared with full-length F8 (Burton et al, 1999; Scallan et al, 2003; Chen et al, 2009; Zhu et al, 2012).

More recently, protein *trans*-splicing (PTS) has been evaluated to reconstitute large proteins via AAV vectors. PTS is used by unicellular organisms across all three domains of life to reconstitute large proteins from shorter precursors that include split-inteins (intervening proteins) at their extremities. Following translation, split-inteins mediate their association and self-excision from the host protein in an independent process that does not require any energy supply (Mills et al, 2014; Li, 2015). PTS has been used with limited success to reconstitute F8 (Chen et al, 2007), while we have recently shown that AAV-intein-mediated PTS in the retina results in therapeutic levels of protein reconstitution which in some instances match those achieved by single AAV vectors (Tornabene et al, 2019).

Encouraged by these results, we explored the efficiency of liver gene therapy with AAV-intein vectors to reconstitute the large and highly active F8-N6 variant (N6) (5 kb) (Miao et al, 2004; Ward et al, 2011).

Results

AAV-intein-mediated protein *trans*-splicing in mouse liver

We assessed the potential of split-intein-mediated protein *trans*-splicing in liver by comparing the efficiency of adeno-associated viral (AAV) vector intein to that of a single AAV vector. To do so, we used the reporter enhanced green fluorescent protein (eGFP) whose coding sequence (CDS) fits well within a single AAV. The full-length eGFP CDS was divided into two separate halves at Cysteine 71 and fused to either the N- and C-terminal halves of the DnaE split-inteins from *Nostoc punctiforme* (Npu; Iwai et al, 2006) (Fig 1A). These were cloned under the human thyroxine binding globulin (TBG) liver promoter (Yan et al, 2012) and separately packaged into AAV8 vectors that efficiently target liver. A single AAV8 vector carrying the full-length eGFP CDS under the same TBG promoter was produced for the *in vivo* comparison. Five-week-old C57/BL6 mice were injected retro-orbitally with either the single or the two AAV-intein vectors at the dose of 5×10^{11} GC of each vector per animal. Livers were harvested 4-week post-injection (4 wpi) and Western blot (WB) analysis of liver lysates followed by quantification of the eGFP bands showed that AAV-intein reconstitute about 76% of the full-length eGFP protein produced by the single vector (Fig 1B and C).

In vitro characterisation of human F8 variants

After assessing that AAV-intein transduce efficiently liver, we set up to select the best F8 transgenic variant to be expressed via

AAV-intein vectors. To this end, we compared the wild-type F8 coding sequence (CDS) to 3 commonly used B-domain-deleted (BDD), which lack F8 amino acids from 740 to 1649 (Miao et al, 2004) versions (Figs 2A and EV1 for exact amino acid differences). Specifically, the 3 BDD constructs carry different codon-optimised linkers in the place of the B domain, which are designed to promote efficient F8 secretion by mimicking some of the natural F8 post-translational modifications (Miao et al, 2004): F8-N6 (N6) contains 11 amino acids from the modified SQ activation peptide (SQ^m) from Ward et al (2011), followed by the N6 human B domain spacer involving 6 (N)-linked glycosylation sites (Miao et al, 2004); F8-SQ (SQ) contains the original SQ linker described by Sandberg et al (2001). This variant is available for clinical use as a replacement recombinant F8 product (ReFacto, Wyeth Pharma; Toole et al, 1986) and is also under investigation in more than one AAV gene therapy clinical trial (Butterfield et al, 2019). The F8-V3 variant (V3) consists of a small 17-aa peptide, which contains the original 6 (N)-linked glycosylation triplets from the N6 inserted into and flanked by the SQ linker (McIntosh et al, 2013). This variant has been previously described as another small version of BDD F8, able to achieve high levels of F8 activity in mice and non-human primates (McIntosh et al, 2013) as well as in human subjects (Nathwani et al, 2018).

All four variants were independently cloned into an AAV backbone plasmid under the control of the CMV promoter, including both a short synthetic polyadenylation signal (Levitt et al, 1989) and a triple flag tag (3xFlag) to allow for easy detection of the proteins. The constructs were tested by transient transfection in the human embryonic kidney cell line 293 (HEK293). WB analysis of the cell lysates 72-h post-transfection (hpt) revealed bands of the expected size (Fig 2B). To detect the biological activity of each variant, cells were cultured for 12 h following transfection, after which they were kept in serum-free medium until the time point of 72 hpt when F8 activity was measured by chromogenic assay on media of transfected cells. All variants produced detectable F8 activity levels (Fig 2C). Wild-type F8 had fairly low mean levels of activity of 8.4 International Unit/decilitre (IU/dl), followed by SQ with 27.4 IU/dl, V3 with 57.6 IU/dl and N6 with the highest mean levels of 71.6 IU/dl. There was a significant difference in potency of the wild-type F8 and both the N6 and V3 constructs, which was determined by the Kruskal–Wallis rank-sum test; this difference was more significant for the N6 (** $P \leq 0.001$) than for the V3 variant (* $P \leq 0.05$). In addition, enzyme-linked immunosorbent assay (ELISA) analysis of media from transfected cells showed that N6 is the most secreted F8 variant (Fig EV2). Based on this, we selected N6 as the variant to be tested by AAV-intein in comparison with one of the traditional single AAV replacement gene therapy, which is under clinical investigation (NCT03001830).

AAV-intein-mediated protein *trans*-splicing efficiently reconstitutes N6 *in vitro*

To test the efficiency of intein-mediated N6 protein *trans*-splicing (PTS), we split the large coding sequence (CDS) into two fragments, that is, the 5' and 3' half, fused, respectively, to the N- and C-terminal halves of the DnaE split-inteins from *Nostoc punctiforme* (Npu; Iwai et al, 2006). The split CDS was cloned into two separate AAV plasmids which included the same regulatory elements as

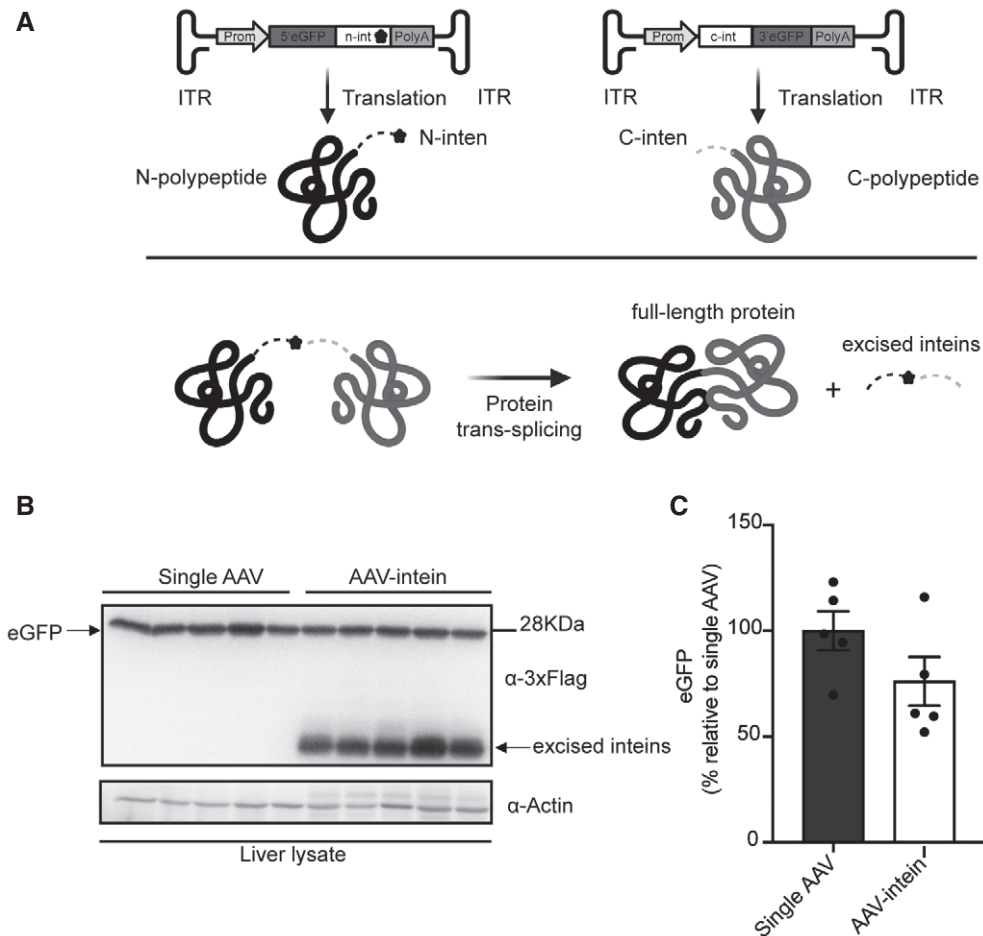


Figure 1. Intein-mediated protein *trans*-splicing in liver.

A Schematic representation of the enhanced green fluorescent protein (eGFP) intein constructs and of the intein-mediated protein *trans*-splicing. ITR—inverted terminal repeats; Prom—promoter; 5'eGFP—5'eGFP coding sequence (CDS); n-intein—N-terminal of DnaE intein; star symbol—3xFlag tag; PolyA—short synthetic polyadenylation signal; c-intein—C-terminal of DnaE intein; 3'eGFP—3' eGFP CDS.

B Western blot analysis of liver lysates (100 μg) shows that intein-mediated protein *trans*-splicing efficiently reconstitutes full-length eGFP. Single AAV: $n = 5$; AAV-intein: $n = 5$. Arrows indicate both full-length eGFP and excised inteins.

C Quantification of eGFP protein bands. Values are reported as mean \pm SEM. Each dot represents the eGFP protein band quantification from animals injected with either single AAV $n = 5$ or AAV-intein $n = 5$.

Source data are available online for this figure.

above, together with a 3xFlag to detect both N6 halves as well as the full-length protein and excised inteins. The splitting point was selected within the B domain, which is known to be dispensable for F8 expression and procoagulant activity (Pipe, 2009), thus aiming to preserve the integrity of the other more critical protein domains. To optimise the chosen splitting position, the intrinsic amino acid residue requirements for efficient protein *trans*-splicing with the *Npu* inteins were also considered. Specifically, the main prerequisite is the presence of an amino acid containing either a thiol or hydroxyl group (Cysteine, Serine or Threonine) as the first residue in the 3' half of the CDS (Shah et al, 2013; Cheriyan et al, 2014). The intein set was designed within the N6 linker (Ser962, considering the signal peptide) of the N6 variant. Moreover, to assess whether F8 activity in the medium of transfected cells was specifically due to the reconstitution of the full-length N6 after PTS, a set of N6 flanked by heterologous split-inteins was also designed. In this set, the N-

terminal of the 5' half of N6 CDS was fused to the split N-inteins DnaB from *Rhodothermus marinus* (*Rma*; Zhu et al, 2013; Tornabene et al, 2019) while the C-terminal of the 3' half was fused to the split C-intein DnaE. Both intein sets were tested by transient transfection into HEK293 cells. Seventy-two-hour post-transfection, cell lysates and medium were harvested, and N6 expression was evaluated by WB (Fig 3A and B). Both full-length N6 protein of the expected size (~190 kDa in cell lysate and ~170 kDa in the medium) and the excised DnaE inteins (~18 kDa) were detected only when the *Npu* inteins set was used. Quantification of the single halves after PTS shows that the 5' (~123 kDa) and 3' (~95 kDa) half are five-fold and fourfold more abundant than the full-length N6, respectively.

The activity levels of the secreted F8 in the medium were found to be ~60 IU/dl on average, while single halves as well as the heterologous intein set exhibited little to no activity (Fig 3C).

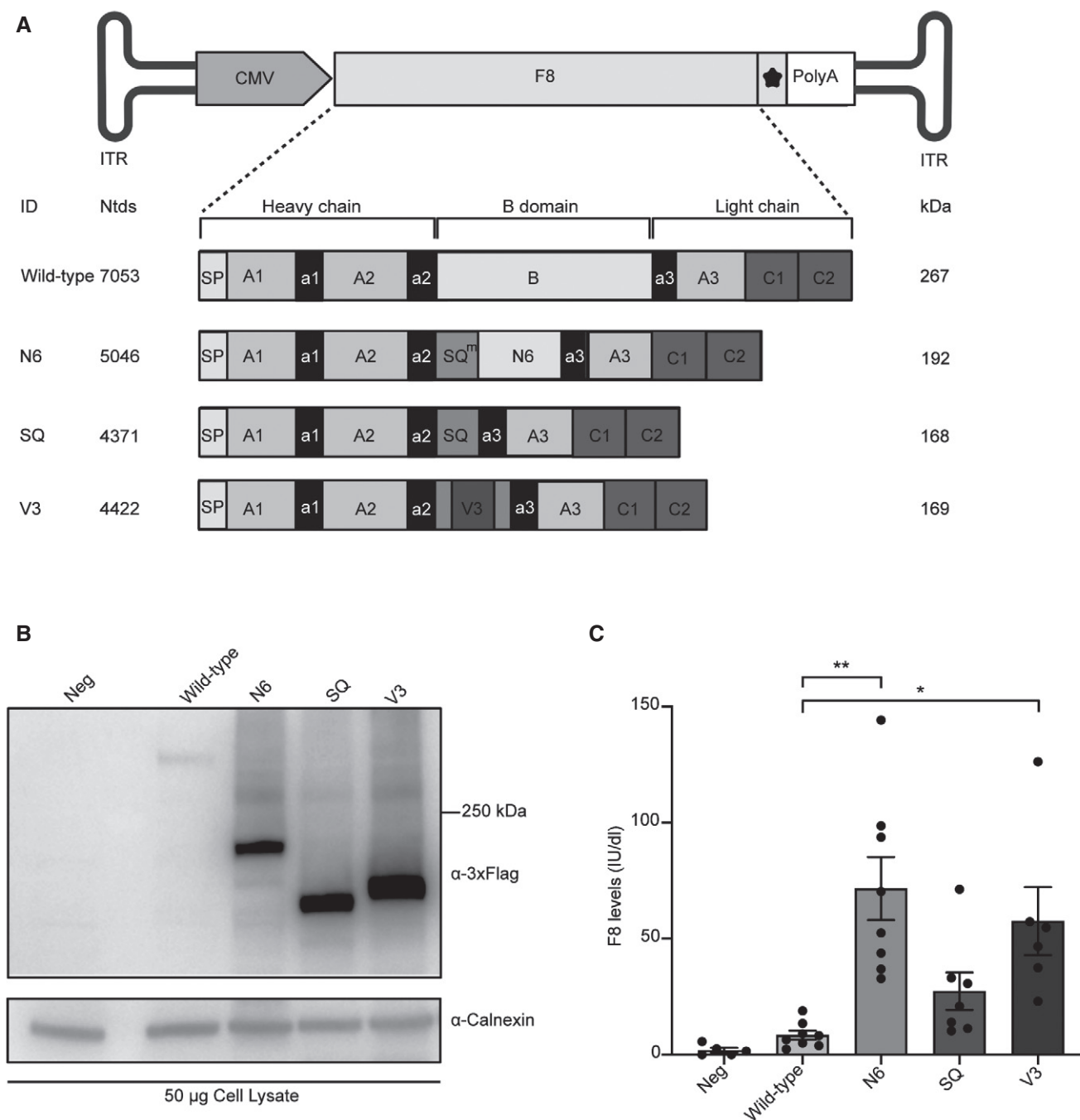


Figure 2. Comparison of human F8 variants *in vitro*.

A Schematic representation of the four different F8 variants that were cloned into an AAV plasmid: wild-type F8; N6 containing 11 amino acids of the modified SQ amino acid linker (SQ^N) followed by the human N6 B domain; SQ containing the SQ amino acid linker; V3 containing the V3 peptide in the middle of the SQ linker. ITR—inverted terminal repeats; CMV—cytomegalovirus promoter; star symbol—3xFlag tag; PolyA—short synthetic polyadenylation signal; Ntds—nucleotides; SP—signal peptide. Details on the exact amino acid differences in the B domain can be found in Fig EV1.

B Western blot analysis of lysates of HEK293 cells 72-h post-transfection with the various F8 variants. Neg—non-transfected cells.

C Chromogenic assay of F8 activity in the medium of transfected cells is reported as International Units/decilitre (IU/dl). Data are presented as mean \pm SEM. Each dot within the same group corresponds to a biological replicate: Neg $n = 5$; Wild-type $n = 8$; N6 $n = 8$; SQ $n = 7$; V3 $n = 6$. Significant differences between groups were assessed using the Kruskal–Wallis test followed by the *post hoc* analysis: Nemenyi's All-Pairs Rank Comparison Test. The Kruskal–Wallis test $P = 2.88e-05$. **indicates the significant difference between the N6 and the Wild-type groups: $P \leq 0.01$. *indicates the significant difference between the V3 and the Wild-type groups: $P \leq 0.05$. All P -values are reported in Appendix Table S1.

Source data are available online for this figure.

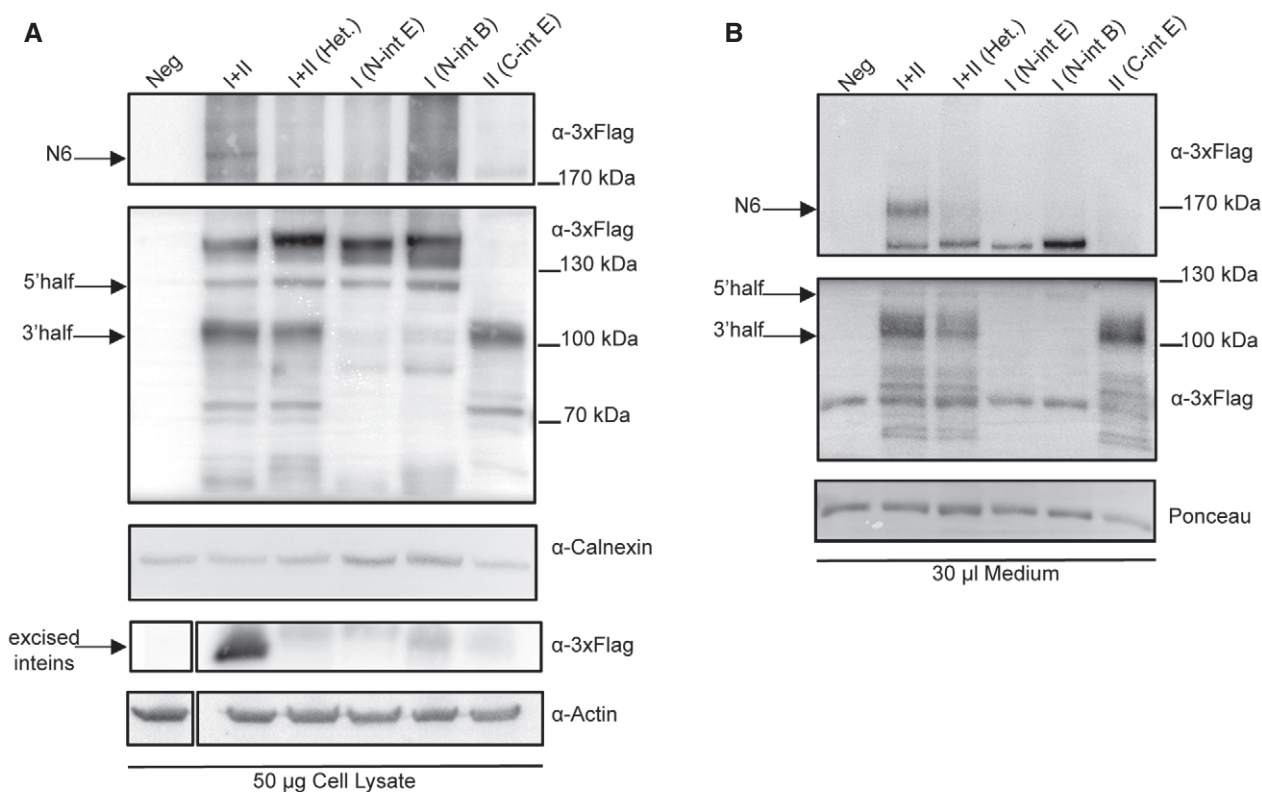


Figure 3. In vitro F8-N6 (N6) intein expression and activity.

A Western blot (WB) of protein lysates of HEK293 cells 72-h post-transfection ($n = 3$; biological replicates) with either *Npu* inteins or Heterologous (N-intein DnaB + C-intein DnaE) split-inteins. I + II, N6 split-intein proteins; I+II (Het.), heterologous split-intein proteins; I, 5'N6 coding sequence (CDS)-N-DnaE protein; I (N-int B), 5'N6 CDS-N-DnaB. II, C-DnaE-3'N6 CDS protein. Excised inteins (~12 kDa) are present only in the down part of the blot when I + II (*Npu* inteins) are provided. Arrows indicate the full-length N6 protein, single halves and excised inteins.

B WB of medium of the transfected cells showing the secreted proteins ($n = 3$; biological replicates). Arrows indicate the full-length N6 protein as well as single halves and excised inteins.

C Chromogenic assay performed on the medium of transfected cells to detect F8 activity levels reported as International Units/decilitre (IU/dl). Data are presented as mean \pm SEM. Each dot within each group represents a different biological replicate (n): I + II $n = 3$; I + II (Het.) $n = 3$; I (N-int E) $n = 3$; I (N-int B) $n = 3$; II (C-int E) $n = 3$; Neg $n = 4$. Significant differences between groups were assessed using Kruskal–Wallis rank-sum test Kruskal–Wallis, $P = 0.013$. *indicates the significant difference between the I + II and the I (N-int E) groups: $P \leq 0.05$. ***indicates the significant difference between the I + II and the Neg groups: $P \leq 0.001$. All P -values are reported in Appendix Table S1.

Source data are available online for this figure.

N6 codon optimisation increases F8 expression and activity *in vitro*

To further improve the efficiency of the N6 split-inteins, we codon-optimised the N6 CDS (CodopN6), as this has been previously reported to improve F8 levels (Ward *et al*, 2011; McIntosh *et al*, 2013). A fourfold increase in CodopN6 protein expression and secretion was observed by WB compared with the non-codon-optimised

N6 split-inteins (Fig 4A and B). Moreover, cells expressing CodopN6 had higher F8 activity levels (~200 IU/dl) than the corresponding non-codopN6 (~70 IU/dl) as assessed by chromogenic assay (Fig 4C). In addition, to demonstrate that PTS results in precise CodopN6 reconstitution, we transfected HEK293 cells with the CodopN6 intein plasmids and immunopurified the resultant full-length N6 protein. Liquid chromatography-mass spectrometry

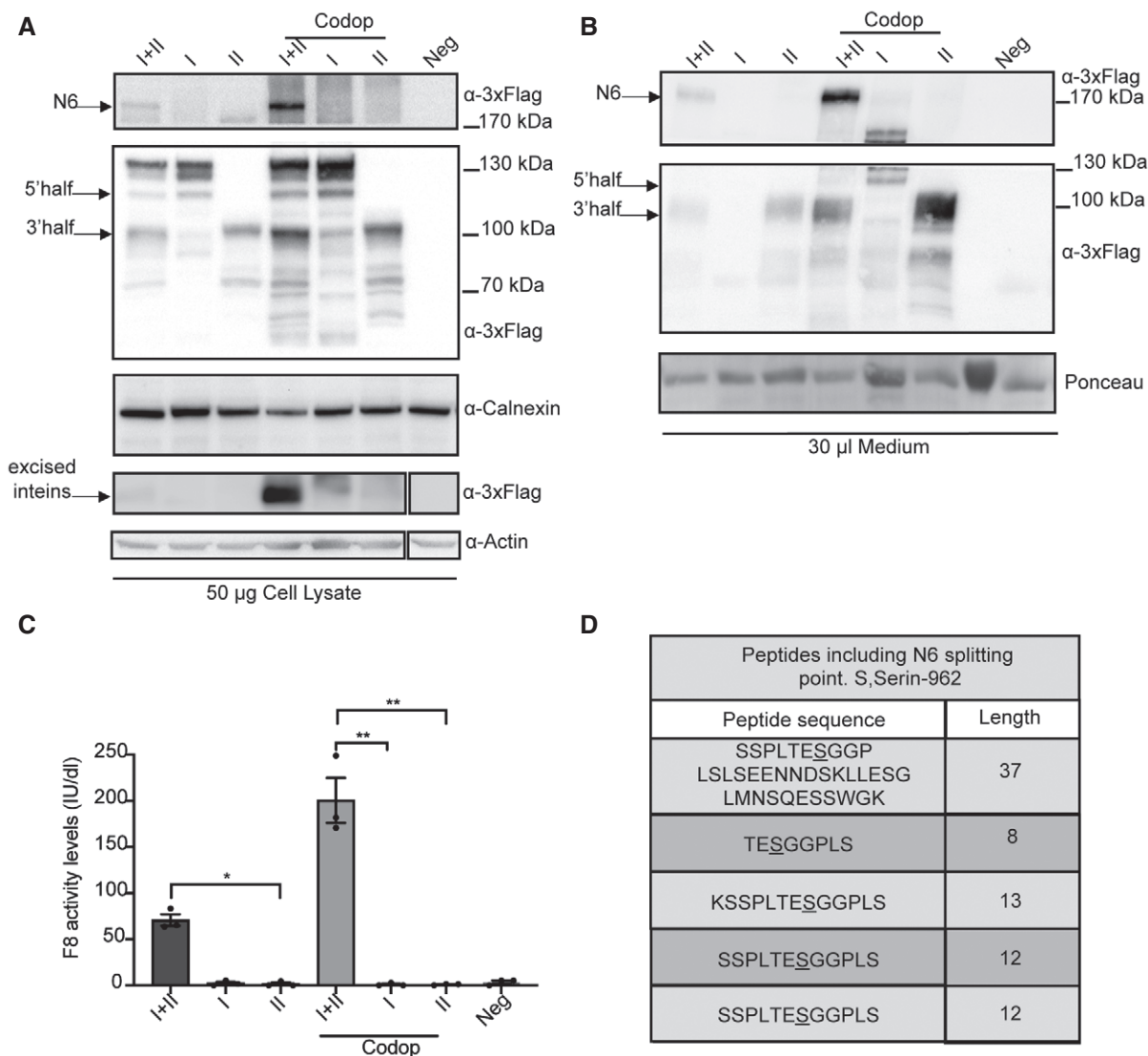


Figure 4. Codon optimisation of the N6 split-intein improves F8 activity levels.

- A Western blot (WB) of protein lysates of HEK293 cells 72 hpt with the AAV-N6 split-intein plasmids and with the codon-optimised set. I + II, N6 split-intein proteins; I, 5' N6 CDS-N-DnaE protein; II, C-DnaE-3'N6 CDS protein. ($n = 3$; biological replicates). Arrows indicate the full-length N6 protein, excised inteins and both single halves. Codop: codon-optimised.
- B WB of medium from the transfected cells showing increased secretion of the CodopN6 full-length protein compared with the non-codon-optimised. ($n = 3$; biological replicates). Arrows indicate the full-length N6 protein, excised inteins and both single halves.
- C Chromogenic assay performed on the medium from transfected cells to measure F8 activity levels reported as International Units/decilitre (IU/dl) ($n = 3$; biological replicates). Data are presented as mean \pm SEM. Significant differences between groups were assessed using Kruskal–Wallis test $P = 0.027$. *indicates the significant difference between the I + II (N6 split-intein) and the II (C-DnaE-3'N6 CDS) groups: $P \leq 0.05$. **indicates the significant difference between the Codop I + II and the I (5' N6 CDS-N-DnaE) codop groups: $P \leq 0.01$. **indicates the significant difference between the Codop I + II and the II (C-DnaE-3'N6 CDS) codop groups: $P \leq 0.01$. All P -values are reported in Appendix Table S1.
- D Peptides sequences obtained by LC-MS analysis which include the N6 splitting point which is correctly reconstituted; S: Ser 962 ($n = 5$; biological replicates).

Source data are available online for this figure.

(LC-MS) analysis showed reconstituted CodopN6 peptides with sequences at the splitting point, which were identical to full-length CodopN6 encoded by a single plasmid.

This was confirmed across 5 independent experiments and a total number of 211 individual peptides (Fig 4D).

Systemic administration of AAV-N6 intein results in therapeutic levels of F8 in HemaA mice

To determine the efficiency of liver gene therapy following systemic administration of either AAV-N6 intein (N6 intein), AAV-CodopN6 intein (CodopN6 intein) or the single AAV-codon-optimised F8-V3 (CodopV3; Nathwani *et al*, 2018) used as gold standard, we generated AAV8 in combination with the small hybrid liver promoter (HLP; McIntosh *et al*, 2013).

The resulting size of both the N6 intein and CodopN6 intein AAVs genomes (3.7 kb for the 5'half and 3 kb for the 3'half) fell well within the AAV packaging capacity, unlike the genome of the single AAV-CodopV3 (5.2 kb) which exceeds the capacity (Nathwani *et al*, 2018). The packaged genomic integrity of the 3' and 5' AAV-N6 intein was confirmed by alkaline Southern blot hybridisation of purified vector DNA with a probe specific for the HLP promoter. The lanes corresponding to AAV-intein vectors showed discrete bands of the expected molecular weight while the lane corresponding to the AAV8-Codop-V3 vector consisted of a heterogeneous population of truncated genomes of different sizes (Fig 5A).

The AAV-N6 intein vectors and the single AAV-CodopV3 were injected retro-orbitally in 7-11-week-old adults Hema^{B6;129S-F8tm1Kaz} mice, at a dose of 5×10^{11} genome copies (GC) of each vector per animal. Since the N6 intein codon optimisation allows higher levels of both F8 activity and expression *in vitro*, we hypothesised that this would allow the AAV vector dose to be lowered to obtain similar therapeutic efficacy to the non-codon-optimised N6. For this reason, the AAV-CodopN6 intein set was administered at the dose of 1.5×10^{11} genome copies of each vector. Blood plasma samples were collected for 16 weeks following vector administration at 4-week intervals. F8 activity was monitored using both the functional chromogenic assay and the activated partial thromboplastin time (aPTT).

After AAV-N6 intein administration, plasma F8 activity reached wild-type levels (~150 IU/dl) and remained stable up to 16-week post-injection (wpi). These mean levels were similar to those from animals which received the single AAV-CodopV3 (Fig 5B), which however showed a significant decrease or total loss of F8 activity over time in the majority of the treated animals (5 out of 8, Fig 5B).

Mice injected with the AAV-CodopN6 intein showed wild-type mean levels of F8 activity comparable to those obtained with the AAV-N6 intein vectors up to 12 wpi. A slight decrease in F8 activity levels was observed at 16 wpi in some of the animals (2 out of 5, Fig 5B), although the average levels were still in the wild-type range (Fig 5B). To confirm that the levels of F8 activity obtained resulted in improved blood clotting, we measured the activated partial thromboplastin time (aPTT) in mouse plasma at the time point of 16-week post-injection after AAV vector administration. We found that this was significantly decreased to normal levels in animals which received either the AAV-N6 intein or the AAV-CodopN6 intein treatment (Fig 5C). Moreover, to assess the possible correction of the haemophilic phenotype in the AAV-treated mice

compared with knockout untreated controls, we performed the tail-clip assay. For this purpose, a new round of injections was performed; three groups of animals were injected as previously described, and the assay was carried out at 4–16-week post-injection. All the groups of AAV-treated mice showed a trend in reduction of bleeding time (Fig 5D) and of blood loss (Fig 5E) compared with haemophilic untreated controls.

To demonstrate that transduced hepatocytes express the N6 full-length protein, we performed Western blot analysis on liver lysate samples from the AAV-CodopN6 intein injected group (Fig 5F), which revealed a band of the expected molecular weight.

Mice injected with AAV-CodopV3 develop anti-F8 antibodies

We evaluated anti-F8 antibodies development in AAV-treated animals: serum from animals administered with the single AAV-CodopV3 ($n = 8$), the AAV-N6 intein ($n = 5$) and the AAV-CodopN6 intein ($n = 5$) were analysed by an indirect enzyme-linked immunosorbent assay (ELISA). We found that anti-F8 antibody levels were precisely inversely correlated with the F8 activity. Specifically, of the $n = 8$ animals injected with the single AAV-CodopV3, $n = 5$ had high levels of anti-F8 antibodies and no detectable F8 activity ($*P < 0.05$) while the mice exhibiting high F8 activity levels ($n = 3$) had no anti-F8 antibodies ($***P < 0.0008$) (Fig 6A). All mice injected with AAV-N6 intein ($n = 5$) or with AAV-CodopN6 intein ($n = 5$) had high F8 activity levels and no detectable anti-F8 antibodies $*P < 0.05$ and $**P < 0.005$, respectively. We further investigated the possible inhibitory activity of the anti-F8 antibodies. The Bethesda assay performed on plasma samples of mice injected with the single AAV-CodopV3 with high levels of anti-F8 antibodies measured by indirect ELISA, confirmed the inhibitory activity of the anti-F8 antibodies in this group (Fig 6B).

To characterise immune responses to F8 variants in AAV-injected mice, we analysed their serum cytokines levels both at baseline and at 4-, 8- and 16-weeks post-injection. Mice injected with the single AAV-CodopV3 had significantly higher levels of the two pro-inflammatory cytokines eotaxin and interferon-gamma-induced protein 10 (IP-10) (Rosenkilde & Schwartz, 2004; Boström *et al*, 2015; Li *et al*, 2021) than animals injected with AAV-intein vectors (Fig 6C). Since neither pro- nor anti-inflammatory cytokines, such as IL-10 and TGF- β among those tested, were increased in the AAV-N6 intein-treated animals, N6 appears rather immunologically inert at the vector doses tested when compared to V3.

Discussion

After decades of extensive research on therapies for haemophilia A (HemA), numerous new technologies have emerged offering a broader range of disease management options for HemA patients. Yet, the problem of curing the disease remains unsolved. Liver gene therapy with single AAV vectors has the potential to fill this gap and is currently under evaluation in multiple clinical trials (Butterfield *et al*, 2019; Makris, 2020). However, the high F8 protein levels initially observed in some of the trials require high doses of viral vectors to be achieved (Makris, 2020). In addition, the durability of vector expression has recently been questioned because of the F8 declining levels observed in the gene therapy trial NCT02576795

(Pasi et al, 2020). Thus, we are still in the early stages of developing viable gene therapy for HemA and further improvements will be required to obtain safe and sustained F8 expression from human liver.

Here, we show that dual AAV vectors armed with *Npu* DnaE split-inteins efficiently and precisely reconstitute the large and

highly secreted F8-N6 (N6) variant in the mouse liver resulting in stable therapeutic levels of F8.

The N6 variant has been previously delivered in mice in the context of a single AAV, but its size (5 Kb) greatly exceeds the normal AAV cargo capacity. This construct was shown to achieve high

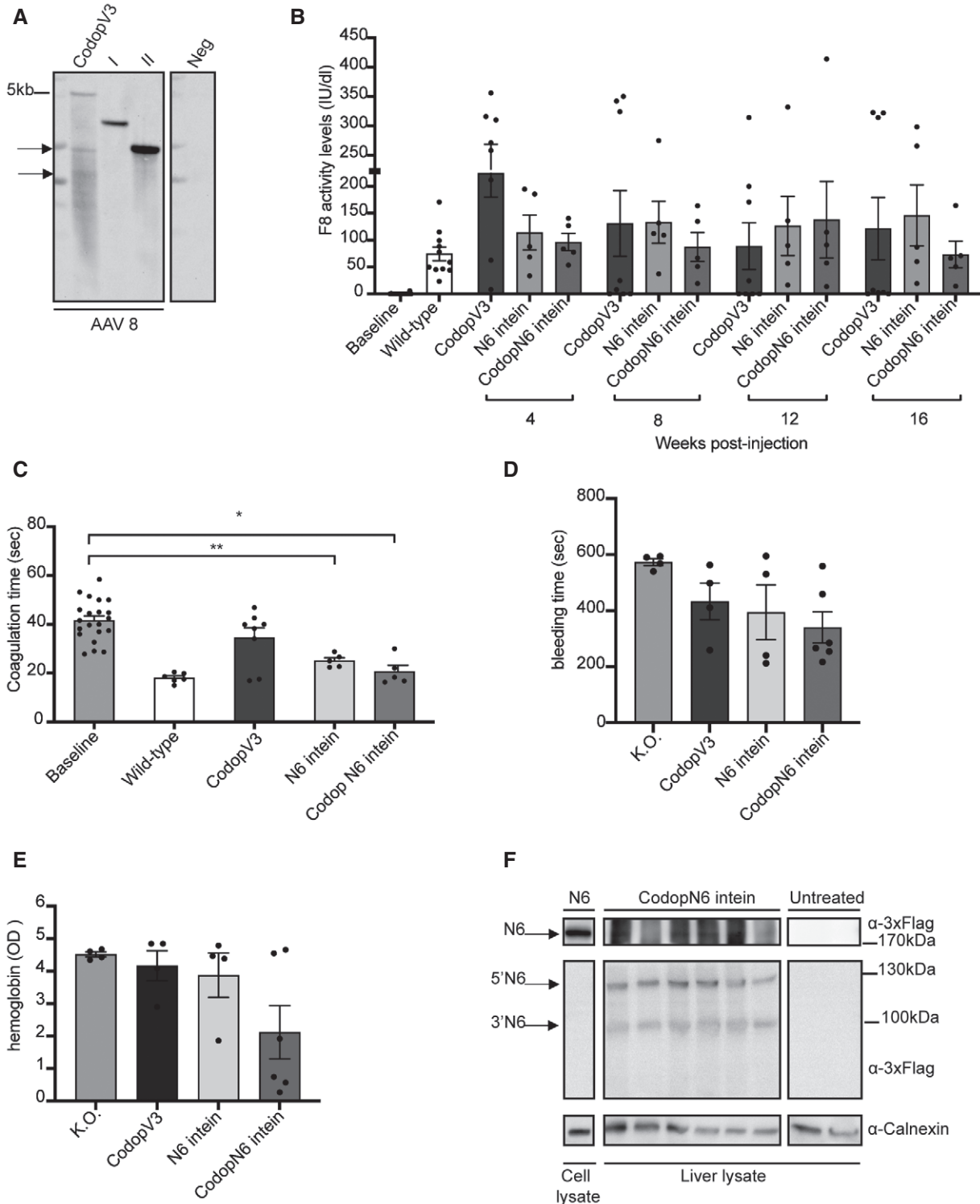


Figure 5.

Figure 5. AAV-N6 intein administration results in therapeutic F8 activity levels.

- A Alkaline gel Southern blot analysis of AAV DNA. AAV DNA was hybridised to a probe specific for the HLP promoter. Neg, AAV DNA treated with Dnase I; CodopV3, AAV-CodopV3; I, AAV-5'N6-N-intein; II, AAV-C-intein-3' N6.
- B Chromogenic assay performed on plasma samples to detect F8 activity in AAV-treated mice compared to controls groups. Data are presented as mean \pm SEM. The same animals were analysed at the various time points. Each dot within the same group and within different groups of treatment corresponds to a single animal. The baseline includes all animals ($n = 20$) before the treatment: CodopV3: $n = 8$; N6 intein: $n = 5$; CodopN6 intein: $n = 5$. The statistical difference between groups has been assessed at 4-week post-injection (wpi) with the one-way ANOVA $P = 0.056$; at 8 wpi with the Kruskal–Wallis test $P = 0.68$; at 12 wpi with the Kruskal–Wallis test $P = 0.45$; at 16 wpi with the Kruskal–Wallis test $P = 0.58$. All P -values are reported in Appendix Table S1.
- C Activated partial thromboplastin time (aPTT) assay performed on plasma samples both at the baseline and at the last time point of the analysis (16 wpi). Data are presented as mean \pm SEM. Each dot within each group of treatment corresponds to different animals: The baseline includes all animals before the treatment $n = 21$; CodopV3: $n = 8$; N6 intein: $n = 5$; CodopN6 intein: $n = 5$. Significant differences between groups were assessed using the Kruskal–Wallis test. **indicates the significant difference between the baseline and the N6 intein groups: $P \leq 0.01$. *indicates the significant difference between the baseline and the CodopN6 intein groups: $P \leq 0.05$. All P -values are reported in Appendix Table S1.
- D Tail-clip assay reported as bleeding time in seconds. Significant differences between groups were assessed using one-way ANOVA test P -value is 0.11 . Data are presented as mean \pm SEM. Each dot corresponds to a different animal. Knockout (K.O.) group: $n = 4$; CodopV3: $n = 4$; N6 intein: $n = 4$; CodopN6 intein: $n = 6$.
- E Haemoglobin content measured as optical density (OD) at 416 nm after the tail-clip assay. Significant differences between groups were assessed using one-way ANOVA test. Data are reported as mean \pm SEM. Each dot corresponds to a single animal. Knockout (K.O.) group: $n = 4$; CodopV3: $n = 4$; N6 intein: $n = 4$; CodopN6 intein: $n = 6$.
- F Western blot analysis of liver lysates (100 μ g) from either CodopN6 intein-treated mice ($n = 6$) or untreated haemophilic mice ($n = 2$). A lysate from HEK293 cells transfected with the N6 full-length plasmid was used as positive control (50 μ g). Arrows point at N6 full-length protein (N6), the 5' half of N6 (5'N6) and 3' half of N6 (3'N6).

Source data are available online for this figure.

levels of F8 expression and secretion (McIntosh *et al*, 2013), but clinical translatability is limited by the poor characterisation of over-size genomes upon truncated genome re-assembly. In this study, we overcome this limitation by effectively delivering N6 using two separate AAV vectors, each well within the AAV packaging capacity.

The therapeutic levels of F8 achieved *in vivo* by a single systemic administration of AAV-N6 intein are comparable to those obtained with the single packageable AAV-codon-optimised F8-V3 (CodopV3; Nathwani *et al*, 2018) which is in clinical development (NCT03001830) and expresses one of the most promising B-domain deleted (BDD) versions of F8 (Nathwani *et al*, 2018). Yet, the size of the AAV-F8-CodopV3 genome is over the canonical vector cargo capacity and results in truncated genomes.

Importantly, we provide evidence that our strategy does not lead neither to the development of anti-F8 antibodies or to increased levels of pro/anti-inflammatory cytokines, whereas this occurred in AAV-CodopV3 treated animals. There could be several reasons for this: while the CodopV3 coding sequence (CDS) is fully contained within the longer N6 CDS, it is possible that the difference in their B-domain structure is responsible for the higher immune-reactivity of V3 than N6; F8 antigen levels may differ between the various groups, as we engineered N6 to be expressed at similar therapeutic

levels than V3 using lower vector doses, which improves the burden of both AAV manufacturing and anti-AAV immune responses; the single oversized AAV-CodopV3 vector contains truncated genomes that may result in shorter immunogenic products.

One of the limitations of the AAV-intein platform is the production of half proteins derived from non-*trans*-spliced polypeptides (for instance, in cells infected by only one of the two AAV-intein vectors) as well as of the inteins excised from the mature protein, which is an expected by-product of PTS. Reports of intein-mediated *trans*-splicing also occurring in the cell medium of independently expressed and secreted intein halves (Zhu *et al*, 2010, 2011) suggest that this could contribute to the overall F8 levels even if not all cells are coinfecting. The excised inteins bioproduct could raise immunological concerns as it is non-mammalian; however, no apparent toxicity has been observed in previous studies (Chen *et al*, 2007; Zhu *et al*, 2010, 2011, 2013; Tornabene *et al*, 2019) nor in ours, though our study was not designed to assess potential toxicity. Independently, we have recently incorporated a degron in the AAV-intein vectors that results in selective intein degradation following PTS, therefore without significantly impacting on levels of full-length protein (Tornabene *et al*, 2021). This could be incorporated in the future in the AAV-N6 intein vectors, if necessary.

Figure 6. AAV-N6 intein administration results in therapeutic F8 levels without eliciting anti-F8 antibodies.

- A The amount of anti-F8 antibodies analysed by indirect ELISA is reported in Arbitrary Units/millilitre (AU/ml). Each numbered bar represents a single mouse. CodopV3, AAV-CodopV3 injected group $n = 8$; N6 intein, AAV-N6 intein injected group $n = 5$; CodopN6 intein, AAV-CodopN6 intein injected group $n = 5$. Significant differences were assessed as follow: Paired T -test has been used for CodopV3 $n = 5$: $P \leq 0.001$; Wilcoxon test for CodopV3 $n = 3$: $P \leq 0.05$; Paired T -test has been used for N6 intein $n = 5$: $P \leq 0.05$; Paired T -test has been used for CodopN6 intein $n = 5$: $P \leq 0.01$.
- B Bethesda assay performed on plasma samples mice injected with AAV-CodopV3; on the plasma of animals injected with AAV-N6 intein $n = 3$ and the plasma of animals injected with AAV-CodopN6 intein $n = 2$; plasma of a wild-type animal was used as a control. The dotted line indicates the threshold above which anti-F8 antibodies are considered inhibitors.
- C Pro-inflammatory cytokines levels followed over time and reported as percentage of the baseline levels (time point before the injection). Data are represented as mean \pm SEM. Five animals belonging to the CodopV3 group were analysed. Significant differences were assessed using the Kruskal–Wallis test; for IP-10: *indicates the $P \leq 0.05$ between 0 and 4 wpi; * indicates the $P \leq 0.05$ between 0 and 8 wpi; *indicates the $P \leq 0.05$ between 0 and 16 wpi. ($n = 20$); for eotaxin: *indicates the $P \leq 0.05$. All P -values are reported in Appendix Table S1.

Source data are available online for this figure.

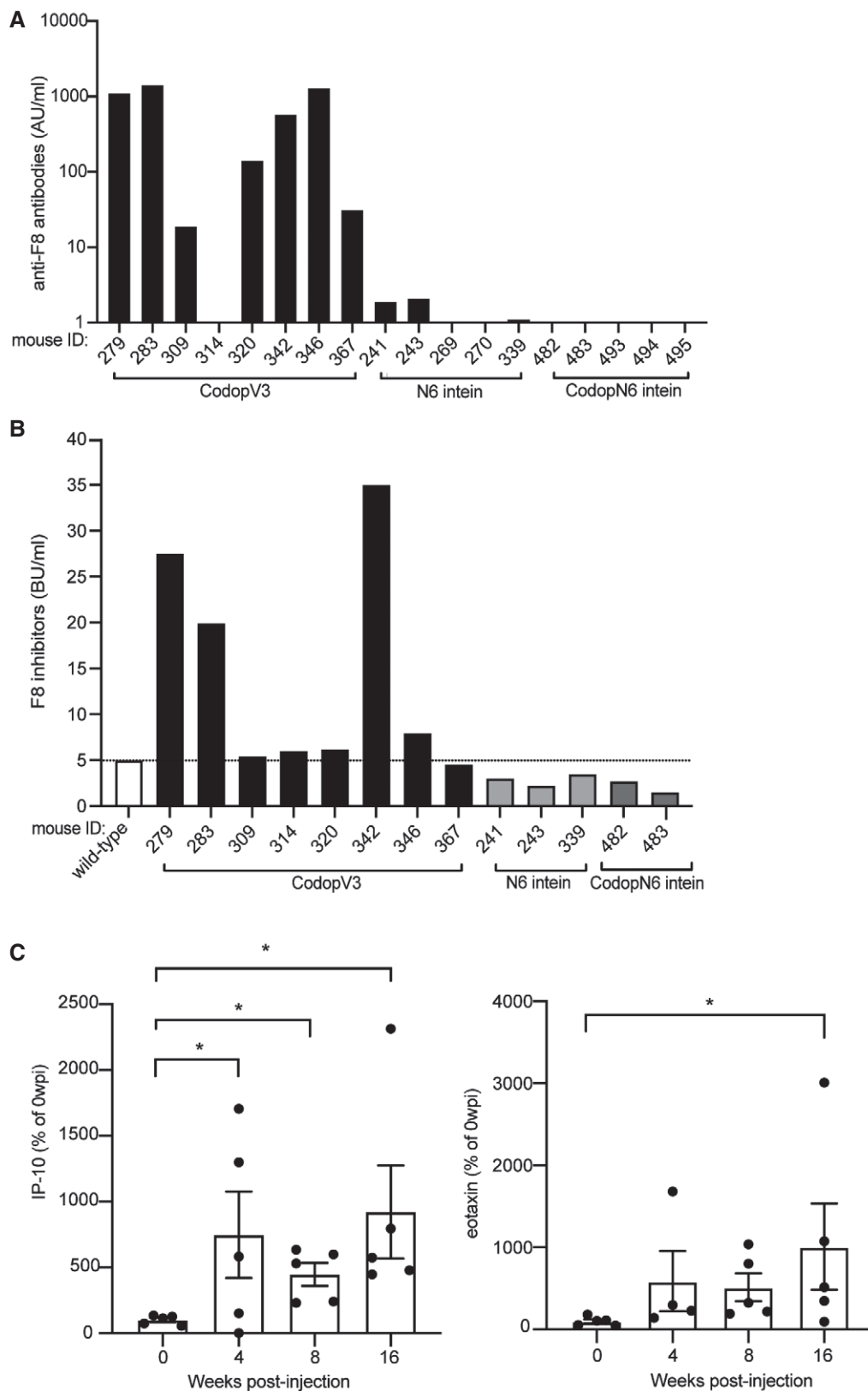


Figure 6.

In conclusion, our results support liver gene therapy with a single intravenous administration of AAV-N6 intein as a potential therapeutic strategy for HemaA.

Materials and Methods

Study design

This study was designed to define the efficiency of AAV-intein-mediated protein *trans*-splicing (PTS) in reconstituting the full-length F8-N6 protein in mouse liver. This was defined *in vitro* by assessing the expression (Western blot) and the activity (chromogenic assay) of the reconstituted protein achieved via protein *trans*-splicing and *in vivo*. To initially evaluate PTS efficiency in liver, a proof-of-concept study was performed in wild-type mice where we compared AAV-intein ($n = 5$) to single AAV vectors ($n = 5$) using the enhanced green fluorescent protein (eGFP) as reporter. The AAV-N6 intein platform was tested in an adult mouse model of haemophilia A in comparison with the single AAV-codon-optimised BDD F8-V3 used as golden standard (chromogenic assay, activated partial thromboplastin time and Western blot). In the *in vivo* studies that involved the haemophilic model, males only were used (given that haemophilia A is inherited as X-linked recessive). To evaluate the efficacy of the treatment over time, different time points were selected for the analysis as indicated in the results section.

Statistical analysis

The experimenters in the efficacy studies were blind to the treatment of the animals, and within the same litter, animals were randomly assigned to each treatment group. Sample sizes were determined on the basis of previous experience and technical feasibility; at least three biological replicates in *in vitro* studies or four animals per group were used in all the experiments, as indicated in the results section and figure legends.

Data are presented as mean \pm SEM, and statistical $P \leq 0.05$ were considered significant. The normality assumption was verified using the Shapiro–Wilk test. Levene's test was applied to check the homogeneity of variances. Data were analysed by the Student's *t*-test, ANOVA test or, when data were not normally distributed (Shapiro–Wilk test $P \leq 0.05$), either the Kruskal–Wallis rank-sum test or the Wilcoxon rank-sum test (non-parametric tests) were used. Specific statistical values are reported in Appendix Table S1.

Generation of AAV vector plasmids

The plasmids used for AAV vector production are derived from the pTigem AAV plasmid that contains the ITRs of AAV serotype 2. The enhanced green fluorescent protein (eGFP) coding sequence was split at Cysteine71, while the F8-N6 protein was split at Serin 962 (Ser962) considering the signal peptide exclusively within the N6 linker (in place of the B domain), aiming to preserve the integrity of the other more critical protein domains. Further split considerations were taken into account based on the intrinsic amino acid residue requirements for efficient protein *trans*-splicing with the *Npu*

inteins. In particular, the main prerequisite is the presence of an amino acid containing either a thiol or hydroxyl group (Cysteine, Serine or Threonine) as the first residue in the 3' half of the coding sequence (Shah *et al*, 2013; Cheriyan *et al*, 2014).

Split-inteins included in the plasmids were the split-inteins of DnaE from *Nostoc punctiforme* (*Npu*; Iwai *et al*, 2006). The plasmids used in the study were under the control of either the ubiquitous cytomegalovirus (CMV) promoter (Tornabene *et al*, 2019) or the liver-specific hybrid liver promoter (HLP) (McIntosh *et al*, 2013) or the human thyroxin binding globulin (TBG) promoter (Yan *et al*, 2012). The polyadenylation signal (polyA) used was either the short synthetic polyA (Levitt *et al*, 1989) or the bovine growth hormone (BGH) polyA signal. For the generation of the heterologous split-inteins, the same splitting point (Ser962) was used. The N-split-intein flanking the 5' half plasmid was the N-intein of DnaB from *Rhodothermus marinus* (*Rma*; Zhu *et al*, 2013; Tornabene *et al*, 2019), while the C-split-intein flanking the 3' half plasmid was the C-intein of the DnaE. Heterologous split-intein plasmids were produced under the control of the ubiquitous cytomegalovirus (CMV) promoter since they were only used for *in vitro* purposes. The codon-optimised BDD F8-V3 plasmid used as golden standard was kindly provided by Dr Amit C. Nathwani (McIntosh *et al*, 2013).

AAV vector production and characterisation

Adeno-associated viral vectors were produced by InnovaVector srl (Pozzuoli, Napoli, Italy) by triple transfection of HEK293 cells as already described (Doria *et al*, 2013). No differences in vector yields were observed between AAV vectors, which include the split-intein sequences or not.

Southern blot analyses of AAV vector DNA

DNA was extracted from 6×10^{10} viral particles measured as genome copies (GC). To digest unpackaged genomes, the vector solution was incubated with 30 μ l of DNase I (04536282001; Roche, Italy) in a total volume of 300 μ l, containing 50 mM Tris pH 7.5, and 1 mM MgCl₂ for 2 h at 37°C. The DNase was then inactivated with 50 mM EDTA, followed by incubation at 50°C for 1 h with proteinase K and 2.5% *N*-lauryl-sarcosil solution to lyse the capsids. The DNA was extracted twice with phenol-chloroform and precipitated with 2 volumes of ethanol 100% and 10% sodium acetate (3 M) and 1 μ l of Glycogen (1090139300; Roche, Italy) was performed as previously described (Sambrook & Russell, 2001). Single-stranded DNA was quantified with Qubit® ssDNA Kit (Q10212; ThermoFisher Scientific, Germany). A probe specific for the HLP promoter was used; 1.4×10^{10} GC for the single vector AAV-Codop V3 and for both the 5' and the 3' AAV-N6 intein were loaded on an alkaline agarose gel electrophoresis (Fig 5A).

Transfection of HEK293 cells

HEK293 cells were maintained and transfected using the calcium phosphate method (1 μ g of each plasmid/well in 6-well plate format) as already described (Maddalena *et al*, 2018). The total amount of DNA transfected in each well was kept equal by the addition of a

scramble plasmid when necessary. 12-hour post-transfection (hpt) medium was switched to Opti-MEM reduced serum medium (31985062; Gibco, ThermoFisher Scientific, Germany) 1 ml/well until the time point of 72 hpt when cells were harvested and medium was collected.

Western blot analysis

Samples (HEK293 cells or liver lysates) were lysed in RIPA buffer to extract F8 protein. Lysis buffer was supplemented with protease inhibitors (11697498001; Roche, Basel, Switzerland) and 1 mM phenylmethylsulfonyl. For medium samples, upon cell harvesting at 72-hour post-transfection (hpt) medium samples were centrifuged at 4°C for 15 min to remove cell debris. Purified medium was collected; 30 µl of medium mixed with 1× Laemmli sample buffer. All samples were denatured at 99°C for 5 min in 1× Laemmli sample buffer. Liver lysates (100 µg), cell lysates (50 µg) and medium samples were separated by either 12% (for excised intein detection) or 6% (for full-length F8 protein and single halves detection) SDS-polyacrylamide gel electrophoresis (SDS-PAGE). The antibodies used for immuno-blotting are as follows: anti-3xFlag (Dilution 1:2,000; A8592; Sigma-Aldrich, Saint Louis, MO, USA) to detect the full-length F8-N6 protein and both the 5' and the 3' halves; anti-β-Actin (Dilution 1:1,000; NB600-501; Novus Biological LLC, Littleton, CO, USA) to detect β-Actin proteins which were used as loading controls for the 12% SDS-PAGE; anti-Calnexin (Dilution 1:2,000; ADI-SPA-860; Enzo Life Sciences Inc, New York, NY, USA) to detect Calnexin, used as loading controls for the 6% SDS-PAGE. The quantification of the full-length F8-N6 bands detected by Western blot was performed using ImageJ software (free download is available at <http://rsbweb.nih.gov/ij/>).

Immunoprecipitation and mass spectrometry analysis

Cells were plated in 100 mm plates (5×10^5 cells/plates) and transfected with either the single CodopN6 plasmid or CodopN6 intein plasmids using the calcium phosphate method (20 µg of each plasmid/plate). Cells were harvested 72 hpt, and both the single CodopN6 and the CodopN6 intein proteins were immunoprecipitated using anti-flag M2 magnetic beads (M8823; Sigma-Aldrich), according to the manufacturer instructions. Proteins were eluted from the beads by incubation for 15 min in sample buffer supplemented with 4 M urea at 37°C and 10 min at 99°C. Samples were then loaded on a gradient 4–10% SDS-polyacrylamide gel electrophoresis. In total, 8 protein bands (from HEK293 cells transfected 5 times independently with CodopN6 intein plasmids) were cut after staining with Instant Blue (ISB1L; Sigma-Aldrich) and were used for protein sequencing. Briefly, 8 gel slides were used for digestion by the following enzymes: Lysin and Trypsin. The resulting peptides were identified using nanoscale liquid chromatography coupled to tandem mass spectrometry (nano-LC-MS/MS) analysis. Data obtained were processed using MaxQuant and the implemented Andromeda search engine.

Animal model

Animals were housed at the TIGEM animal facility (Pozzuoli, Italy). C57Bl/6 mice used in the proof-of-concept study with the

The paper explained

Medical issue

With an incidence of 1 in 5,000 males, haemophilia A (HemA) is the most common inherited bleeding disorder which is caused by the deficiency of coagulation factor VIII (F8). The size of F8 coding sequence exceeds the cargo capacity of adeno-associated viral (AAV) vectors; therefore, current HemA gene therapy clinical trials use AAV with oversize genomes.

Results

We tested if intein-mediated protein trans-splicing (PTS) allows to reconstitute F8 in mouse liver transduced by AAV, thus overcoming the limitations imposed by the vector transfer capacity. We show that AAV-intein reconstitute F8 to therapeutic levels in HemA mice and this occurs without the development of anti-F8 antibodies at the vector doses tested.

Clinical impact

Liver gene therapy with AAV-intein represents a potential therapeutic strategy for HemA using relatively low doses of vectors with defined genomes which do not elicit anti-F8 antibodies.

reporter enhanced green fluorescent protein were purchased from Envigo.

The haemophilic mouse model (B6;129S-F8tm1Kaz/J) was imported from The Jackson Laboratory (JAX stock). Mice were maintained by crossing knockout homozygous females with knockout hemizygous males.

Retro-orbital injection of AAV vectors in mice

All procedures on mice were approved from the Italian Ministry of Health; department of Public Health, Animal Health, Nutrition and Food Safety number 379/2019-PR.

Adult C57Bl/6 mice (5 weeks of age) were retro-orbitally injected with AAV8 at the dose of 5×10^{11} GC of each vector per animal.

Adult knockout males (between 7 and 11 weeks of age) were retro-orbitally injected with AAV8 with either AAV-N6 intein or the single AAV-CodopV3 as a positive control at the dose of 5×10^{11} GC of each vector per animal.

AAV-CodopN6 intein were retro-orbitally injected with the dose of 1.5×10^{11} GC of each vector per animal.

Plasma collection and F8 assays

Briefly, nine parts of blood were collected by retro-orbital withdrawal into one part of buffered trisodium citrate 0.109 M (5T31.363048; BD, Franklin Lakes, NJ, USA). Blood plasma was collected after samples centrifugation at 3,000 rpm at 4°C for 15 min.

To evaluate F8 activity, chromogenic assay was performed on plasma samples using a Coatest® SP4 FVIII-kit (K824094; Chromogenix, Werfen, Milan, Italy) according to the manufacturer's instructions. Standard curve was generated by serial dilution of commercial human F8 (Refacto, Pfizer). Results are expressed as International Units (IU) per decilitre (dl).

Activated partial thromboplastin time (aPTT) was measured on plasma samples with Coatron M4 (Teco, Bünde, Germany) using the aPTT programme following the manufacturer's manual.

To quantify F8 antigen levels, the ELISA kit (FVIII-AG; VisuLize FVIII ELISA kit, Affinity Biologicals, Arcore, Italy) was used according to the manufacturer's instructions.

Tail-clip assay

Mice were anaesthetised, and the distal part of the tails was cut at 2–3 mm of diameter and immediately put in a prewarmed 0.9% saline solution and allowed to bleed for 10 min without disturbance. Tails were then cauterised, and mice were sacrificed. The mixture of collected blood and physiological saline solution was centrifuged at 1,500 g for 5 min. The collected erythrocytes were lysed with water, and the haemoglobin content was measured at an optical density of 416 nm.

Indirect enzyme-linked immunosorbent assay (ELISA) to detect anti-F8 antibodies

To evaluate the presence of anti-F8 antibodies, an indirect enzyme-linked immunosorbent assay (ELISA) was performed using ZYMUTEST™ Anti-VIII Monostrip IgG (RK039A; HYPHEN BioMed, France) according to the manufacturer's instructions. The secondary antibody used to detect mouse IgG is the goat-anti-mouse IgG (H + L) HRP conjugate (Dilution 1:3000; AP308P; Sigma-Aldrich).

Bethesda assay to detect F8 inhibitors

Plasma samples containing high levels of F8 were heat inactivated at 58°C for 90 min. A standard curve was generated by serial dilution of the commercial human F8 (Refacto, Pfizer) in F8-deficient plasma. Serial dilutions of all samples were done in F8-deficient plasma and then mixed 1:1 with 100% Refacto (Pfizer) diluted in F8-deficient plasma. All experimental samples and controls were then incubated at 37°C for 2 h. After that, all samples and the standard curve were analysed by aPTT following the manufacturer's manual.

Cytokines and chemokines assay

Serum samples were analysed with mouse cytokine & chemokine 36-Plex ProcartaPlex 1A Panel (EPX360-26092-901; ThermoFisher) according to the manufacturer's instructions.

Data availability

All data associated with this study are present in the paper or in the Expanded View. The mass spectrometry proteomics data have been deposited to the ProteomeXchange Consortium via the PRIDE (Perez-Riverol *et al*, 2022) partner repository and are available in the following database (<http://www.ebi.ac.uk/pride/archive/projects/PXD031884>). Mass spectrometry proteomics data: identifier PXD031884.

Expanded View for this article is available online.

Acknowledgements

We acknowledge the TIGEM Proteomics core for mass spectrometry analysis and Phoebe Kim Ashley Norman (TIGEM Scientific Office) for the critical

reading of this manuscript. This work was supported by the European Research Council (ERC) (grant number 694323 "EYEGET" to AA.) and the Telethon Foundation (grant number TGM16MT1 to AA.).

Author contributions

Federica Esposito: Conceptualization; Data curation; Formal analysis; Supervision; Validation; Investigation; Visualization; Methodology; Writing—original draft; Project administration; Writing—review and editing. **Hristiana Lyubanova:** Data curation; Investigation; Visualization; Methodology; Writing—review and editing. **Patrizia Tornabene:** Investigation; Methodology; Writing—review and editing. **Stefano Auricchio:** Validation; Investigation; Writing—review and editing. **Antonella Iuliano:** Formal analysis; Writing—review and editing. **Edoardo Nusco:** Resources; Investigation; Writing—review and editing. **Simone Merlin:** Resources; Supervision; Writing—review and editing. **Cristina Olgasi:** Resources; Supervision; Writing—review and editing. **Marco Gargaro:** Resources; Supervision; Writing—review and editing. **Giorgia Manni:** Data curation; Investigation; Writing—review and editing. **Francesca Fallarino:** Resources; Supervision; Writing—review and editing. **Antonia Follenzi:** Resources; Supervision; Writing—review and editing. **Alberto Auricchio:** Conceptualization; Resources; Supervision; Funding acquisition; Methodology; Writing—original draft; Project administration; Writing—review and editing.

In addition to the CRediT author contributions listed above, the contributions in detail are:

The study was conceived, designed and written by AA and FE. All data were generated by FE and HL with the technical help of SA. HL and FE performed the *in vitro* experiments, and FE performed the *in vivo* experiments in Hema mice. HL and PT performed the *in vivo* experiments in wild-type mice with eGFP. AI performed statistical analysis. EN performed the experimental procedures in the animals; SM and CO supervised the technical set-up of the experiments. PT contributed to the editing of the manuscript. AF, PT and FF contributed to data analysis and interpretation. MG and GM performed cytokines and chemokines analysis.

Disclosure and competing interests statement

AA., F.E. and H.L. are coinventors on the patent application number EP201697125. AA. and P.T. are coinventors on the patent application WO2020079034A2. Alberto Auricchio is an editorial advisory board member. This has no bearing on the editorial consideration of this article for publication. The other authors declare that they have no conflict of interest.

References

- Antonarakis SE, Kazazian HH, Tuddenham EGD (1995) Molecular etiology of factor VIII deficiency in hemophilia A. *Hum Mutat* 5: 1–22
- Boström EA, Kindstedt E, Sulniute R, Palmqvist PY, Majster M, Holm CK, Zwicker S, Clark R, Önell S, Johansson I *et al* (2015) Increased eotaxin and MCP-1 levels in serum from individuals with periodontitis and in human gingival fibroblasts exposed to pro-inflammatory cytokines. *PLoS One* 10: 1–19
- Bowen DJ (2002) Haemophilia A and haemophilia B: molecular insights. *Mol Pathol* 55: 1–18
- Burton M, Nakai H, Colosi P, Cunningham J, Mitchell R, Couto L (1999) Coexpression of factor VIII heavy and light chain adeno-associated viral vectors produces biologically active protein. *Proc Natl Acad Sci USA* 96: 12725–12730

- Butterfield JSS, Hege KM, Herzog RW, Kaczmarek R (2019) A molecular revolution in the treatment of hemophilia. *Mol Ther* 28: 997–1015
- Cafuir LA, Kempton CL (2017) Current and emerging factor VIII replacement products for hemophilia A. *Ther Adv Hematol* 8: 303–313
- Chen L, Lu H, Wang J, Sarkar R, Yang X, Wang H, High KA, Xiao W (2009) Enhanced factor VIII heavy chain for gene therapy of Hemophilia A. *Mol Ther* 17: 417–424
- Chen L, Zhu F, Li J, Lu H, Jiang H, Sarkar R, Arruda VR, Wang J, Zhao J, Pierce GF et al (2007) The enhancing effects of the light chain on heavy chain secretion in split delivery of factor VIII gene. *Mol Ther* 15: 1856–1862
- Cheriyian M, Chan SH, Perler F (2014) Traceless splicing enabled by substrate-induced activation of the *Nostoc punctiforme* Npu DnaE intein after mutation of a catalytic cysteine to serine. *J Mol Biol* 426: 4018–4029
- Dong B, Nakai H, Xiao W (2010) Characterization of genome integrity for oversized recombinant AAV vector. *Mol Ther* 18: 87–92
- Doria M, Ferrara A, Auricchio A (2013) AAV2/8 vectors purified from culture medium with a simple and rapid protocol transduce murine liver, muscle, and retina efficiently. *Hum Gene Ther Methods* 24: 392–398
- Grieger JC, Samulski RJ (2005) Packaging capacity of adeno-associated virus serotypes: impact of larger genomes on infectivity and postentry steps. *J Virol* 79: 9933–9944
- Hirsch ML, Agbandje-Mckenna M, Samulski RJ (2010) Little vector, big gene transduction: fragmented genome reassembly of adeno-associated virus. *Mol Ther* 18: 6–8
- Iwai H, Züger S, Jin J, Tam PH (2006) Highly efficient protein trans-splicing by a naturally split DnaE intein from *Nostoc punctiforme*. *FEBS Lett* 580: 1853–1858
- Levitt N, Briggs D, Gil A, Proudfoot NJ (1989) Definition of an efficient synthetic poly(A) site. *Genes Dev* 3: 1019–1025
- Li M, Chen Y, Li H, Yang D, Zhou Y, Chen Z, Zhang Y (2021) Serum CXCL10/IP-10 may be a potential biomarker for severe Mycoplasma pneumoniae pneumonia in children. *BMC Infect Dis* 21: 1–8
- Li Y (2015) Split-inteins and their bioapplications. *Biotechnol Lett* 37: 2121–2137
- Maddalena A, Tornabene P, Tiberi P, Minopoli R, Manfredi A, Mutarelli M, Rossi S, Simonelli F, Naggert JK, Cacchiarelli D et al (2018) Triple vectors expand AAV transfer capacity in the retina. *Mol Ther* 26: 524–541
- Mahlangu J, Oldenburg J, Paz-Priel I, Negrier C, Niggli M, Mancuso ME, Schmitt C, Jiménez-Yuste V, Kempton C, Dhalluin C et al (2018) Emicizumab prophylaxis in patients who have hemophilia A without inhibitors. *N Engl J Med* 379: 811–822
- Makris M (2020) Gene therapy 1.0 in haemophilia: effective and safe, but with many uncertainties. *Lancet Haematol* 7: e186–e188
- Manco-Johnson MJ, Abshire TC, Shapiro AD, Riske B, Hacker MR, Kilcoyne R, Ingram JD, Manco-Johnson ML, Funk S, Jacobson L et al (2007) Prophylaxis versus episodic treatment to prevent joint disease in boys with severe hemophilia. *N Engl J Med* 357: 535–544
- McIntosh J, Lenting PJ, Rosales C, Lee D, Rabbanian S, Raj D, Patel N, Tuddenham EGD, Christophe OD, McVey JH et al (2013) Therapeutic levels of FVIII following a single peripheral vein administration of rAAV vector encoding a novel human factor VIII variant. *Blood* 121: 3335–3344
- Miao HZ, Sirachainan N, Palmer L, Kucab P, Cunningham MA, Kaufman RJ, Pipe SW (2004) Bioengineering of coagulation factor VIII for improved secretion. *Blood* 103: 3412–3419
- Mills KV, Johnson MA, Perler FB (2014) Protein splicing: How Inteins escape from precursor proteins. *J Biol Chem* 289: 14498–14505
- Nathwani AC, Davidoff AM, Tuddenham EGD (2004) Prospects for gene therapy of haemophilia. *Haemophilia* 10: 309–318
- Nathwani AC, Davidoff AM, Tuddenham EGD (2017) Advances in gene therapy for Hemophilia. *Hum Gene Ther* 28: 1004–1012
- Nathwani AC, Tuddenham E, Chowdhary P, McIntosh J, Lee D, Rosales C, Phillips M, Pie J, Junfang Z, Meagher MM et al (2018) GO-8: preliminary results of a phase I/II dose escalation trial of gene therapy for Haemophilia A using a novel human factor VIII variant. *Blood* 132 (Supplement 1): 489
- Oldenburg J, Mahlangu JN, Bujan W, Trask P, Callaghan MU, Young G, Asikanius E, Peyvandi F, Santagostino E, Kruse-Jarres R et al (2018) Emicizumab prophylaxis and health-related outcomes in persons with hemophilia A (PwHA) with inhibitors: HAVEN 1 study. *Haemophilia* 25: 33–44
- Pasi KJ, Rangarajan S, Mitchell N, Lester W, Symington E, Madan B, Laffan M, Russell CB, Li M, Pierce GF et al (2020) Multiyear follow-up of aav5-hfviii-sq gene therapy for hemophilia A. *N Engl J Med* 382: 29–40
- Perez-Riverol Y, Bai J, Bandla C, García-Seisdedos D, Hewapathirana S, Kamatchinathan S, Kundu D, Prakash A, Frericks-Zipper A, Eisenacher M et al (2022) The PRIDE database resources in 2022: a hub for mass spectrometry-based proteomics evidences. *Nucleic Acids Res* 50: D543–D552
- Pipe SW (2009) Functional roles of the factor VIII B domain. *Haemophilia* 15: 1187–1196
- Rosenkilde MM, Schwartz TW (2004) The chemokine system – A major regulator of angiogenesis in health and disease. *Apmis* 112: 481–495
- Sambrook J, Russell DW (2001) *Molecular cloning: a laboratory manual*, 999 pp. Cold Spring Harbor, New York: Cold Spring Harbor Laboratory Press
- Sandberg H, Almstedt A, Brandt J, Gray E, Holmquist L, Oswaldsson U, Sebring S, Mikaelsson M (2001) Structural and functional characteristics of the B-domain-deleted recombinant factor VIII protein, r-VIII SQ. *Thromb Haemost* 85: 93–100
- Scallan CD, Liu T, Parker AE, Patarroyo-White SL, Chen H, Jiang H, Vargas J, Nagy D, Powell SK, Wright JF et al (2003) Phenotypic correction of a mouse model of hemophilia A using AAV2 vectors encoding the heavy and light chains of FVIII. *Blood* 102: 3919–3926
- Shah NH, Eryilmaz E, Cowburn D, Muir TW (2013) Extein residues play an intimate role in the rate-limiting step of protein trans-splicing. *J Am Chem Soc* 135: 5839–5847
- Toole JJ, Pittman DD, Orr EC (1986) A large region (~95 kDa) of human factor VIII is dispensable for *in vitro* procoagulant activity. *Proc Natl Acad Sci USA* 83: 5939–5942
- Tornabene P, Trapani I, Minopoli R, Centrulo M, Lupo M, de Simone S, Tiberi P, Dell'Aquila F, Marrocco E, Iodice C et al (2019) Intein-mediated protein trans-splicing expands adeno-associated virus transfer capacity in the retina. *Sci Transl Med* 11: eaav4523
- Tornabene P, Trapani I, Centrulo M, Marrocco E, Minopoli R, Lupo M, Iodice C, Gesualdo C, Simonelli F, Surace EM et al (2021) Inclusion of a degenon reduces levelsof undesired inteins after AAV-mediated proteintans-splicing in the retina. *Mol Ther Methods Clin Dev* 23: 448–459
- Ward NJ, Buckley SMK, Waddington SN, VandenDriessche T, Chuah MKL, Nathwani AC, McIntosh J, Tuddenham EGD, Kinnon C, Thrasher AJ et al (2011) Codon optimization of human factor VIII cDNAs leads to high-level expression. *Blood* 117: 798–807
- White II GC, Rosendaal F, Aledort LM, Lusher JM, Rothschild C, Ingerslev J (2001) Definitions in Hemophilia. *Thromb Haemost* 85: 560
- Wu Z, Yang H, Colosi P (2010) Effect of genome size on AAV vector packaging. *Mol Ther* 18: 80–86
- Yan Z, Yan H, Ou H (2012) Human thyroxine binding globulin (TBG) promoter directs efficient and sustaining transgene expression in liver-specific pattern. *Gene* 506: 289–294

- Zhu FX, De YS, Liu ZL, Miao J, Qu HG, Chi XY (2011) The effect of a secretion-enhanced heavy chain on improving intein-based dual-vector co-delivery of a full-length factor VIII gene. *Chinese Sci Bull* 56: 158–163
- Zhu FX, Liu ZL, Chi XY, Qu HG (2010) Protein trans-splicing based dual-vector delivery of the coagulation factor VIII gene. *Sci China Life Sci* 53: 683–689
- Zhu FX, Liu ZL, Miao J, Qu HG, Chi XY (2012) Enhanced plasma factor VIII activity in mice via cysteine mutation using dual vectors. *Sci China Life Sci* 55: 521–526

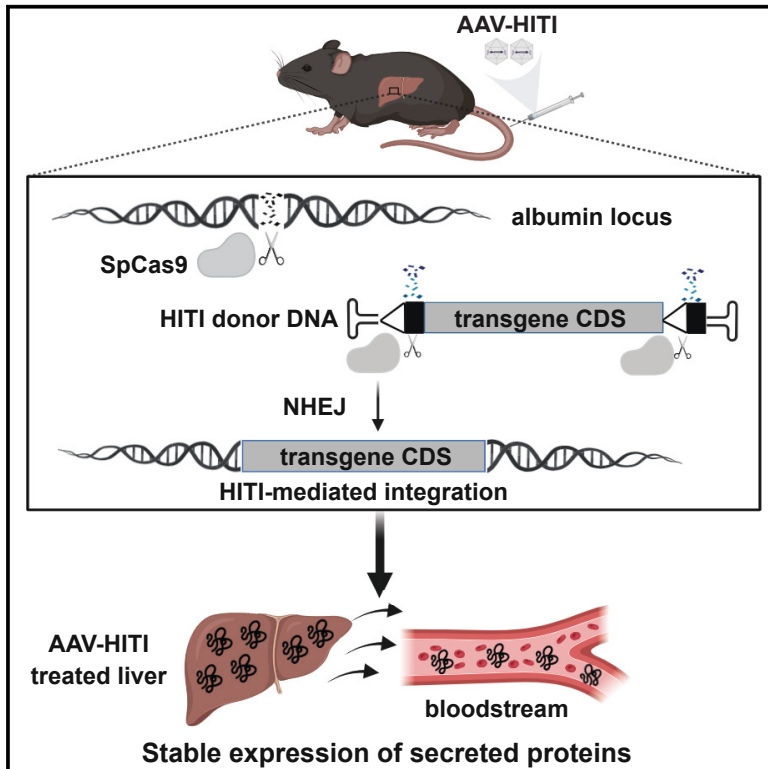
- Zhu FX, Liu ZL, Wang XL, Miao J, Qu HG, Chi XY (2013) Inter-chain disulfide bond improved protein trans-splicing increases plasma coagulation activity in C57BL/6 mice following portal vein FVIII gene delivery by dual vectors. *Sci China Life Sci* 56: 262–267



License: This is an open access article under the terms of the Creative Commons Attribution License, which permits use, distribution and reproduction in any medium, provided the original work is properly cited.

Safe and effective liver-directed AAV-mediated homology-independent targeted integration in mouse models of inherited diseases

Graphical abstract



Authors

Federica Esposito, Fabio Dell'Aquila, Manuel Rhiel, ..., Ivana Trapani, Toni Cathomen, Alberto Auricchio

Correspondence

auricchio@tigem.it

In brief

Esposito et al. explore the therapeutic potential of liver-directed adeno-associated viral vector-mediated homology-independent targeted integration (AAV-HITI) through CRISPR-Cas9 at the mouse albumin locus. Effective integration yields stable therapeutic protein levels in mouse models of inherited diseases without adverse effects, supporting AAV-HITI as a safe and efficient liver-directed knockin strategy.

Highlights

- AAV-HITI provides sustained transgene expression from newborn and adult liver
- Liver-directed AAV-HITI is effective in mouse models of inherited diseases
- AAV-HITI results in undetectable off-targets and large gene rearrangements
- AAV-HITI is safe at the doses tested up to 1 year after AAV-HITI delivery



Article

Safe and effective liver-directed AAV-mediated homology-independent targeted integration in mouse models of inherited diseases

Federica Esposito,¹ Fabio Dell'Aquila,^{1,2} Manuel Rhiel,^{3,4} Stefano Auricchio,¹ Kay Ole Chmielewski,^{3,4,5} Geoffroy Andrieux,^{6,7} Rita Ferla,¹ Paula Sureda Horrach,¹ Arjun Padmanabhan,¹ Roberto Di Cunto,¹ Simone Notaro,¹ Manel Llado Santeularia,¹ Melanie Boerries,^{6,7,8} Margherita Dell'Anno,¹ Edoardo Nusco,¹ Agnese Padula,¹ Sofia Nutarelli,⁹ Tatjana I. Cornu,^{3,4,7} Nicolina Cristina Sorrentino,^{1,10} Pasquale Piccolo,¹ Ivana Trapani,^{1,2} Toni Cathomen,^{3,4,7,8} and Alberto Auricchio^{1,11,12,*}

¹Telethon Institute of Genetics and Medicine (TIGEM), Pozzuoli, Italy

²Medical Genetics, Department of Advanced Biomedical Sciences, University of Naples Federico II, Naples, Italy

³Institute for Transfusion Medicine and Gene Therapy, Medical Center – University of Freiburg, Freiburg, Germany

⁴Center for Chronic Immunodeficiency (CCI), Medical Center – University of Freiburg, Freiburg, Germany

⁵PhD Program, Faculty of Biology, University of Freiburg, Freiburg, Germany

⁶Institute of Medical Bioinformatics and Systems Medicine, Medical Center – University of Freiburg, Freiburg, Germany

⁷Faculty of Medicine, University of Freiburg, Freiburg, Germany

⁸German Cancer Consortium (DKTK), Partner site Freiburg, a partnership between DKFZ and Medical Center - University of Freiburg, Freiburg, Germany

⁹Department of Life Science and Public Health, Catholic University of the Sacred Heart, Rome, Italy

¹⁰Department of Clinical Medicine and Surgery, University of Naples Federico II, Naples, Italy

¹¹Gene Therapy Joint lab, Dept. of Advanced Biomedical Sciences and Dept. of Translational Medicine, University of Naples “Federico II”, Naples, Italy

¹²Lead contact

*Correspondence: auricchio@tigem.it

<https://doi.org/10.1016/j.xcrm.2024.101619>

SUMMARY

Liver-directed adeno-associated viral (AAV) vector-mediated homology-independent targeted integration (AAV-HITI) by CRISPR-Cas9 at the highly transcribed albumin locus is under investigation to provide sustained transgene expression following neonatal treatment. We show that targeting the 3' end of the albumin locus results in productive integration in about 15% of mouse hepatocytes achieving therapeutic levels of systemic proteins in two mouse models of inherited diseases. We demonstrate that full-length HITI donor DNA is preferentially integrated upon nuclease cleavage and that, despite partial AAV genome integrations in the target locus, no gross chromosomal rearrangements or insertions/deletions at off-target sites are found. In line with this, no evidence of hepatocellular carcinoma is observed within the 1-year follow-up. Finally, AAV-HITI is effective at vector doses considered safe if directly translated to humans providing therapeutic efficacy in the adult liver in addition to newborn. Overall, our data support the development of this liver-directed AAV-based knockin strategy.

INTRODUCTION

Adeno-associated viral (AAV) vectors are considered the most effective tool for *in vivo* gene therapy due to their safety, efficacy, and long-term therapeutical transgene expression.^{1–3} In AAV-based liver-directed gene therapy, a single intravenous AAV administration has been demonstrated to be sufficient to convert hepatocytes into a factory for efficient and sustained transgene expression and secretion of proteins into the bloodstream, providing long-term therapeutic effects in both preclinical studies and humans.^{4–9} Despite their therapeutic potential, the non-integrative nature of AAV genomes excludes the use of AAV vectors from neonatal treatments,^{10–13} which is the

preferred stage of intervention for diseases such as early-onset inborn errors of metabolism. Liver growth in young subjects leads to AAV genome loss¹⁴ over time resulting in the decline of the therapeutic efficacy following cell division.¹ For this reason, patients under 4 years of age were excluded from our recent successfully completed phase 1/2 clinical trial of AAV-based liver gene therapy for mucopolysaccharidosis type VI (MPS VI)⁵ (Database: [ClinicalTrials.gov](https://clinicaltrials.gov), number NCT03173521). Furthermore, antibodies against the AAV vector capsid that are generated after the first administration may prevent a second round of treatment.^{1,15–19} To address these shortcomings, genome editing via CRISPR-Cas nucleases alone or in combination with knockin strategies is being explored



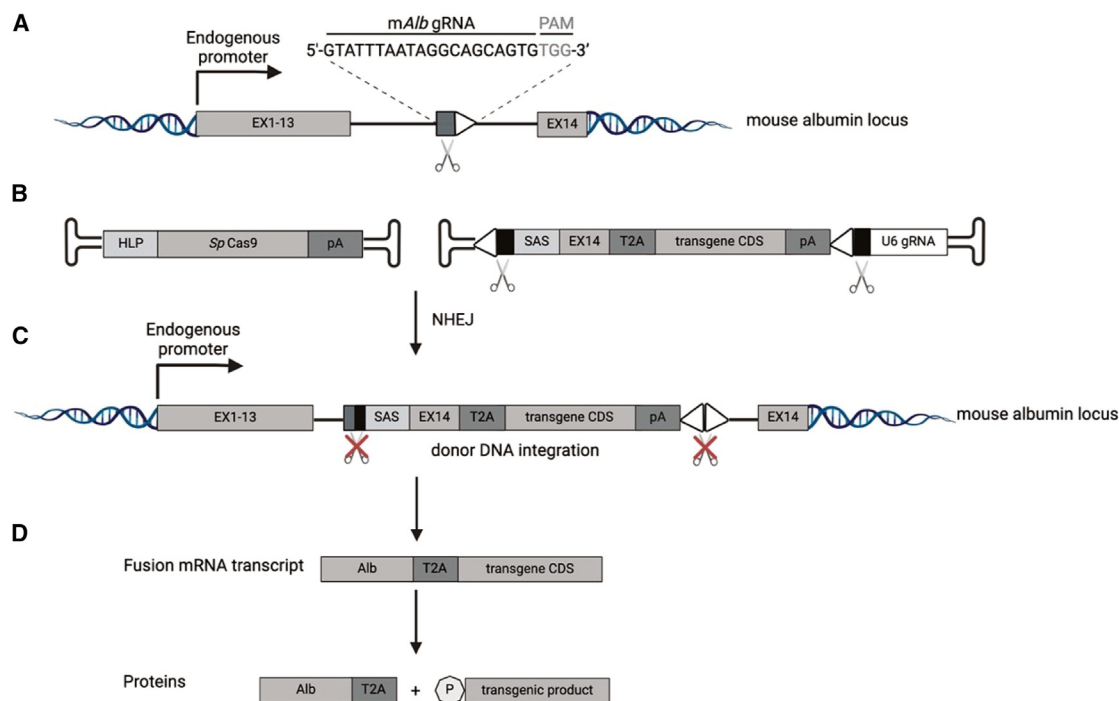


Figure 1. Schematic representation of homology-independent targeted integration (HITI)

(A) The on-target mouse albumin locus and the gRNA sequence designed within the intron 13 are depicted. EX1-13, mouse albumin exons; EX14, last mouse albumin exon; PAM, protospacer adjacent motif.

(B) Schematic representation of the two AAVs. One AAV carries the nuclease *SpCas9* under control of the small hybrid liver-specific promoter (HLP). The other AAV contains the HITI donor DNA with the desired promoter-less transgene coding sequence (CDS). SAS, splicing acceptor signal; EX14, mouse albumin exon 14; T2A, *Thosea asigna* virus 2A skipping peptide; pA, polyadenylation signal (synthetic or bovine growth hormone); U6 gRNA, expression cassette for the gRNA (depicted) or the scRNA sequence; EX1-13, mouse albumin exons 1–13; gRNA and PAM sequences are represented with black (inverted gRNA sequences at the extremities of the donor DNA) and gray (within the mouse albumin locus) boxes and white triangle, respectively.

(C) The non-homologous end-joining (NHEJ) repair pathway of the cell leads to the integration of the cleaved donor DNA at the on-target site.

(D) Upon transgene integration a single fusion transcript is produced, and this results in the expression of both a modified albumin (Alb-2A) and a therapeutic transgene product containing a proline (P) residue at its N terminus.

extensively.^{1,20–30} In particular, homology-independent targeted integration (HITI) of therapeutic transgenes^{21,25,31–34} into the mouse albumin (*mAlb*) locus, which occurs via the cell cycle-independent non-homologous end-joining (NHEJ) repair machinery, is being considered to achieve stable expression following newborn liver gene therapy.^{25,28,35–38} Here, we show that AAV-HITI directed to the 3' end of the albumin locus results in the integration of the donor DNA after its processing by CRISPR-Cas9 as expected based on HITI design. This provides significant therapeutic benefit in the absence of major off-target (OT) and toxic effects in different mouse models of inherited human diseases.

RESULTS

Liver-directed AAV-HITI results in robust transgene expression following neonatal treatment

Our AAV vector-based CRISPR-Cas9-mediated HITI (AAV-HITI) approach was designed to target intron 13 of the *mAlb* locus, similarly to previous reports³⁴ (Figure 1A). The system relies on the co-delivery of two different AAV8 vectors. AAV8 has high liver tropism^{39,40} and has been safely and effectively used in various AAV-liver-directed genome editing preclinical studies^{21,30,41} as

well as by us and others in liver-directed gene therapy clinical trials.^{5,8} One AAV delivers the large *S. pyogenes* Cas9 (*SpCas9*) nuclease together with a small hybrid liver-specific promoter (HLP),^{21,42,43} while the other carries the HITI donor DNA which is designed to contain a synthetic splicing acceptor signal (SAS) followed by the last *mAlb* exon (exon 14), the *Thosea asigna* virus 2A skipping peptide (T2A), and the promoter-less coding sequence (CDS) of a desired transgene together with a polyadenylation signal (pA) and the guide (g) RNA (or scramble RNA [scRNA]) expression cassette including the U6 promoter (Figure 1B). As previously described,^{21,32,33} the HITI donor DNA is flanked at its 5' and 3' extremities by the same gRNA sequence of the endogenous target site (*mAlb* intron 13) but in an inverted orientation. Upon CRISPR-Cas9-mediated cleavage at both the endogenous locus and the extremities of the HITI donor DNA, the NHEJ repair pathway of the cell promotes donor DNA integration at the nuclease-induced double-strand breaks (DSBs) in the endogenous locus^{21,32–34} (Figure 1C). Once proper integration has occurred, the therapeutic transgene is expressed under the control of the endogenous promoter. A single fusion mRNA transcript is generated; at the protein levels, this will result in the production of both a modified albumin (Alb-2A) and a

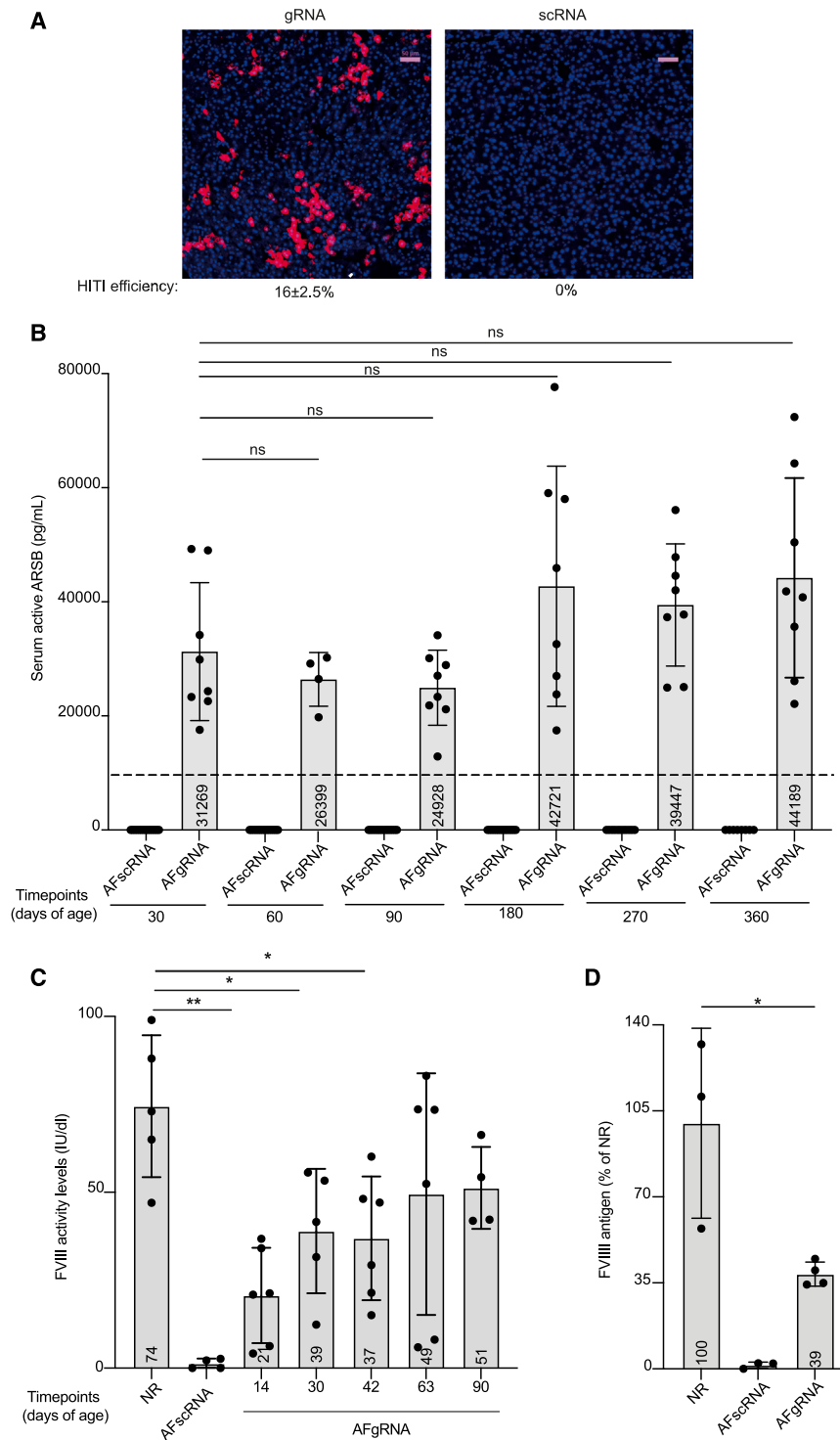


Figure 2. AAV-HITI-mediated transgene expression from newborn liver

(A) Representative fluorescence microscopy images of OCT liver cryo-sections from wild-type mice injected with AAV-HITI using the dsRed transgene (gRNA, $N = 5$ or scRNA, $N = 5$) at the total dose of 1.2×10^{14} total GCs/kg. HITI efficiency is reported below the images. Scale bar, 50 μm .

(B) Serum ARSB activity was analyzed at different time points after AAV-HITI treatment. AFgRNA, MPS VI mice treated with AAV-HITI-gRNA ($N = 8$); AFscRNA ($N = 14$ and $N = 8$ survived up to P360), MPS VI mice treated with AAV-HITI-scRNA. Dotted line corresponds to normal (NR) serum ARSB activity (NR = $11,825 \pm 334$ pg/mL; Alliegro et al., 2016⁴⁴). ARSB measurements in all AFscRNA animals are equal to zero while all treated mice show ARSB activity levels higher than zero; therefore all the comparisons between the two groups are significant. No statistically significant differences were observed in AFgRNA-treated mice among the different time points. (B–C) Each dot corresponds to a single animal within each group at different time points.

(C) FVIII activity levels evaluated in HemA mice by chromogenic assay at different time points after AAV-HITI treatment. Statistical differences were assessed by ordinary one-way ANOVA test. $**p = 0.0025$, between normal (NR, $N = 5$) and AFgRNA ($N = 6$) at 14 days; $*p = 0.0190$, between NR and AFgRNA ($N = 5$, one sample was excluded) at 30 days; $*p = 0.0389$, between NR and AFgRNA ($N = 6$) at 42 days. No statistically significant differences were observed between NR and AFgRNA at the following time points.

(D) FVIII antigen levels measured in AFgRNA ($N = 4$) HemA mice at 90 days of age. $*p = 0.0262$ between NR and AFgRNA at 90 days. All data are represented as mean \pm standard deviation. See also Figures S1, S2, and Table S1.

therapeutic transgene product containing a proline (P) residue at its N terminus (Figure 1D). To evaluate the efficiency of the system at targeting newborn hepatocytes, we used an AAV-HITI donor carrying the CDS of the *Discosoma* sp.-Red (dsRed) fluorescent protein together with the expression cassette encoding either the gRNA or an scRNA which served as a negative control

scRNA. This indicates that our AAV-HITI approach provides robust transgene expression following neonatal delivery in mice. We then investigated the persistence of the AAV-HITI donor DNA following newborn delivery and found a significant drop after a month, as expected based on hepatocyte proliferation at that age, with similar very low levels at 1 and 12 months

after vector delivery (Figure S1B). We therefore hypothesized that the majority of the HITI donor DNA at 1 month after newborn delivery is integrated and performed a customized DNA hybridization analysis with a probe specific for the HITI donor DNA vector on liver cryo-sections to assess the rate of its integration. We found about 40% more positive hepatocyte nuclei in gRNA- than scRNA-treated samples, presumably resulting from HITI donor DNA integration whether full or partial (Figure S1C).

We next investigated the therapeutic potential of our strategy in two different mouse models of human inherited diseases. Liver-directed AAV-HITI efficacy was first assessed in a mouse model of MPS VI,⁴⁵ a lysosomal storage disorder due to arylsulfatase B (ARSB) deficiency. In this setting, the AAV-HITI donor vector contained the *ARSB* CDS in place of dsRed (Table S1). AAV-HITI vectors were co-delivered systemically in newborn MPS VI mice as described earlier, and the mice were monitored over a period of 1 year. Since ARSB is secreted into the bloodstream, it can be measured non-invasively⁴⁵ as a readout for AAV-HITI treatment. Starting from 1-month post-treatment, serum ARSB activity was found to be higher in AAV-HITI-gRNA-treated MPS VI (AFgRNA) than in wild-type mice⁴⁴ (Figure 2B) while AAV-HITI-scRNA-treated littermates (AFscRNA) had undetectable levels of ARSB at all time points (Figure 2B). Interestingly, ARSB activity in AFgRNA mice showed a non-statistically significant trend toward increase over time (Figure 2B). Next, we investigated whether following AAV-HITI serum albumin includes the T2A modification (Alb-2A) as predicted based on the AAV donor DNA design (Figure 1). Western blot analysis of AAV-HITI-treated sera samples collected at different time points confirmed the presence of Alb-2A of correct size (Figure S2A). In addition to MPS VI, AAV-HITI efficacy was assessed in a mouse model of hemophilia A (HemA), the most common X-linked bleeding disorder caused by mutations in the *F8* gene.⁴⁶ Since the full-length *F8* CDS (~7 kb) exceeds the cargo capacity (~4.9 kb) of the AAV vector, we designed an HITI donor DNA carrying the promoter-less CDS of a previously described human B domain-deleted (BDD) *F8* variant⁴⁷ (CodopV3 ~4.5 kb; Table S1). Newborn HemA male mice were injected systemically at P1–2 with AAV-HITI vectors (gRNA or scRNA) at a total dose of 3.9×10^{13} GCs/kg. Plasma samples were collected from AAV-HITI-treated HemA mice (AFgRNA and AFscRNA) and unaffected controls at different time points, and FVIII activity and FVIII antigen were measured. Therapeutic levels of FVIII were observed in plasma samples of AFgRNA- but not AFscRNA-treated mice up to 90 days of age by chromogenic assay^{42,48} (Figure 2C), and FVIII protein levels were found to be around 40% of normal FVIII levels at 90 days post AAV-HITI delivery (Figure 2D). Lastly, Alb-2A expression was confirmed in AFgRNA mice at different time points by western blot analysis (Figure S2B).

Liver-directed AAV-HITI improves the phenotype of MPS VI and HemA mice

ARSB deficiency results in systemic abnormal storage and urinary excretion of glycosaminoglycans (GAGs). The measurement of urinary GAGs levels is considered a useful biomarker for MPS VI.^{5,49,50} To evaluate AAV-HITI-mediated phenotypic improvement, we collected urine samples from treated mice

and unaffected littermates at different time points. Normalized urinary GAG levels were found in urinary samples from AFgRNA-treated MPS VI mice starting from 3 months post-treatment (P90) until the last time point of the analysis (P360; Figure 3A). One-year post-treatment, MPS VI mice were sacrificed, and different organs were collected for further analysis. GAG levels in liver, kidney, and spleen lysates were normal in AFgRNA-treated MPS VI mice (Figure 3B). Accordingly, GAGs storage was significantly decreased in histological sections of these tissues (Figure S3) as well as in the heart mitral valve and myocardium of the AFgRNA-treated MPS VI mice (Figure 3C). Indeed, MPS VI patients suffer from heart failure, predominantly due to mitral valve insufficiency.⁵¹ A further feature of MPS VI patients is skeletal abnormalities,^{49,52} which have also been described in the mouse model of MPS VI.⁵³ Therefore, we assessed if AAV-HITI can improve these disease manifestations. Radiographic images from the AAV-HITI-treated MPS VI mice (AFgRNA or AFscRNA) and unaffected normal controls (NR) were used to evaluate the skull and long bones (femurs and tibias); male and female mice were considered separately given the sex-dependent growth differences. In AFgRNA-treated mice we observed an improvement in the skull width/length ratio compared to AFscRNA-treated mice of the same sex (Figure 3D). In AFgRNA-treated male mice we found a significant amelioration in the femur (Figure 3E) and tibia (Figure 3F) lengths. Altogether, our data indicate that AAV-HITI is effective following newborn delivery to MPS VI mice. Lastly, we assessed AAV-HITI efficacy in newborn AAV-HITI-treated (AFgRNA or AFscRNA) HemA mice by measuring the hemostasis activity by tail-clip and activated partial thromboplastin time (aPTT) assays.

We found that AFgRNA-treated male mice exhibited a significant reduction of bleeding time (Figure 3G) and blood loss (Figure 3H) at 63 days of age and improved coagulation compared to AFscRNA-treated mice at 90 days of age (Figure 3I). These findings support the use of AAV-HITI for therapies directed to newborn liver.

AAV-HITI at the on-target site

Having established the physiological benefits of AAV-HITI in two disease models, we thoroughly characterized AAV-HITI at the on-target site by molecular analysis and next-generation sequencing (NGS). Genomic DNA extracted from liver samples of AAV-HITI-treated MPS VI animals was used to evaluate SpCas9-gRNA efficiency 1-year post-treatment. For each treatment (gRNA or scRNA), a pool of 3 different DNA samples was analyzed by targeted amplicon NGS. Small insertions/deletions (indels) were observed in ~30% of reads from gRNA but not scRNA samples (~0.1%; Figure 4A). Interestingly, in ~1% ($n = 603$) of the total obtained reads ($n = 61,260$) from the gRNA DNA pool, we observed insertions longer than 10 nucleotides which were found to align with the AAV-HITI donor and the AAV-SpCas9 vector genomes. The vast majority of these insertions originated from the inverted-terminal repeat (ITR) regions (Figure 4B). We then investigated if the AAV donor DNA was integrated before or after being processed by CRISPR-Cas9 (therefore with or without the ITRs, respectively). To this end, we generated, as control, a donor DNA lacking the inverted gRNA sites at both its 5' and 3' extremities (donor DNA without

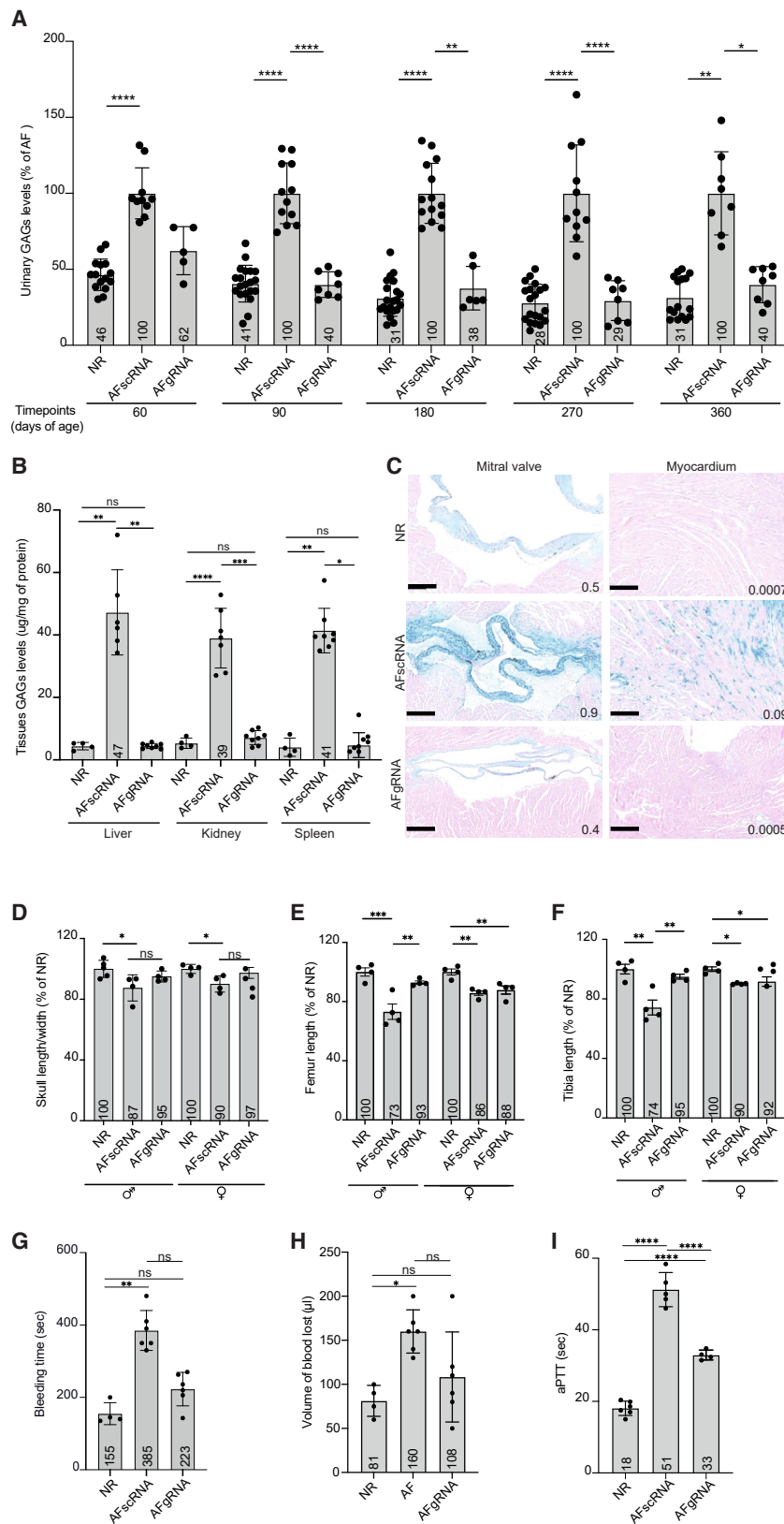


Figure 3. Liver-directed AAV-HITI therapeutic efficacy in newborn mice

(A) Urinary levels of glycosaminoglycans (GAGs) reported as a percentage of GAG levels in affected MPS VI mice (% of AF). Statistical differences were assessed by Kruskal-Wallis test and Dunn's multiple comparisons test. p values: * $p = 0.0379$, ** $p = 0.0022$, and **** $p < 0.0001$. AFgRNA ($N = 8$), MPS VI mice treated with AAV-HITI-gRNA; AFscRNA ($N = 14$ and only $N = 8$ survived up to P360), MPS VI mice treated with AAV-HITI-scRNA. Each dot corresponds to a single animal within each group at different time points.

(B) Quantification of GAGs in the liver, kidney, and spleen. Statistical differences were assessed by Brown-Forsythe and Welch ANOVA tests. For the liver: ** $p = 0.0016$ between NR ($N = 4$) and AFscRNA ($N = 6$); ** $p = 0.0016$ between AFscRNA and AFgRNA ($N = 8$); $p = 0.9996$ between NR and AFgRNA. For the kidney: **** $p = 0.0001$ between NR ($N = 4$) and AFscRNA ($N = 7$); *** $p = 0.0002$ between AFscRNA and AFgRNA ($N = 8$); $p = 0.3784$ between NR and AFgRNA. For the spleen the Kruskal-Wallis test was used: ** $p = 0.0029$ between NR ($N = 4$) and AFscRNA ($N = 8$); * $p = 0.0113$ between AFscRNA and AFgRNA ($N = 8$); $p > 0.9999$ between NR and AFgRNA. (A and B) Each dot corresponds to a single animal within each group at different time points. The differences in the number of analyzed samples within the same group of treatment at different time points were due to sample availability.

(C) Representative histological images of GAG storage in mitral heart valve and myocardium. Scale bar, 100 μ m. Alcian blue quantification is reported inside the images as Alcian blue-positive area/total area. NR, $N = 4$; AFscRNA, $N = 8$; AFgRNA, $N = 8$.

(D–F) Measurement of skull length/width ratio, femur, and tibia lengths; data are reported as the percentage of normal length (% of NR). Males and females were kept separate in the analysis. AFgRNA, $N = 8$; AFscRNA, $N = 8$. Statistical differences were assessed by ordinary one-way ANOVA and Tukey's multiple comparisons test. (D) p value * $= 0.0336$ between NR and AFscRNA males; $p = 0.4847$ between NR and AFgRNA males; * $p = 0.0191$ between NR and AFscRNA females; $p = 0.6887$ between NR and AFgRNA females. (E) *** $p = 0.0011$ between NR and AFscRNA males; $p = 0.4491$ between NR and AFgRNA males; ** $p = 0.0099$ between AFscRNA and AFgRNA males; ** $p = 0.0122$ between NR and AFscRNA females; ** $p = 0.0055$ between NR and AFgRNA females. (F) ** $p = 0.0019$ between NR and AFscRNA males; ** $p = 0.0089$ between NR and AFgRNA males. * $p = 0.0238$ between NR and AFscRNA females; * $p = 0.0398$ between NR and AFgRNA females.

(G and H) Tail-clip assay performed at 63 days of age in Hema AAV-HITI-treated male mice (AFgRNA, $N = 6$; AFscRNA, $N = 6$) and unaffected (NR; $N = 4$) controls. (G) ** $p = 0.0019$; (H) * $p = 0.0129$.

(I) Activated partial thromboplastin time (aPTT) measured at 90 days of age in Hema AAV-HITI (AFgRNA, $N = 4$ and AFscRNA, $N = 5$) mice and unaffected (NR, $N = 6$) controls. p values: **** $p < 0.0001$ between NR and AFscRNA; **** $p < 0.0001$ between NR and AFgRNA. All data are represented as mean \pm standard deviation. See also Figure S3.

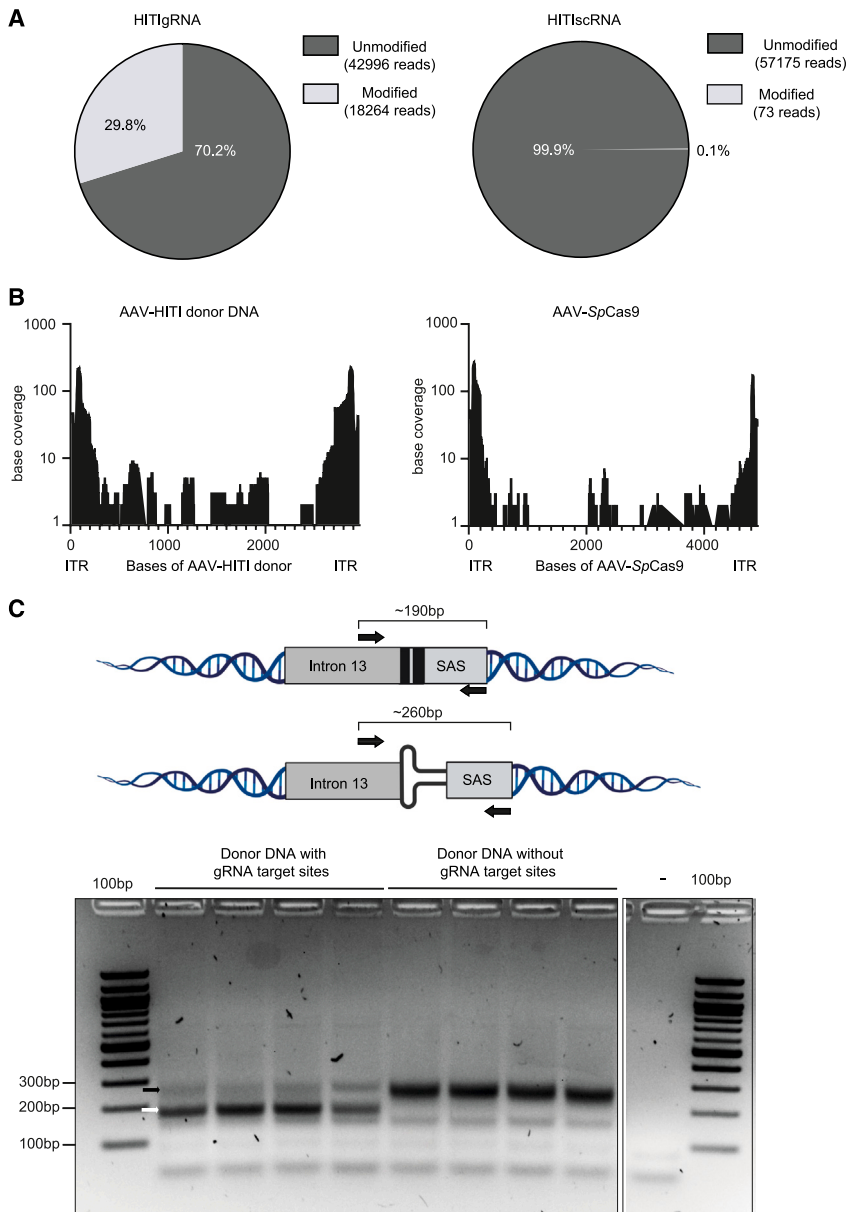


Figure 4. AAV-HITI molecular characterization at the on-target site

(A) Pie chart showing the modified reads observed in AAV-HITI (HITIgRNA or HITiscRNA)-treated mice analyzed by next-generation sequencing (NGS). The expected amplicon size is 285 bp, which was covered by 2x250 bp reads in NGS. The percentage of the modified reads is used as an indication of the gRNA efficiency at the on-target site (HITIgRNA ~30% of indel).

(B) Sequences from different portions of both AAV vectors (AAV-HITI donor DNA and AAV-SpCas9) are captured at the induced double-strand breaks, mostly ITR sequences (ITR).

(C) Schematic representation of the strategy with the expected PCR amplicons and the position of the primers (up) and representative images of the 5' junction PCR run on a 2% agarose gel (down). Four different biological samples for each group are shown in the gel. The white arrow indicates proper HITI-mediated donor DNA integration band (~190 bp); the black arrow indicates the ITR-mediated donor DNA integration band (~260 bp). See also [Table S1](#).

observed in samples treated with the donor DNA without gRNA target sites and the presence of ITRs confirmed by Sanger sequencing. Two junction PCR products of different sizes (~260 and ~190 bp; [Figure 4C](#)) were found in the samples from the AAV-HITI group. Sanger sequencing analysis showed that the smaller and more abundant PCR product (~190 bp) corresponded to the expected HITI-mediated integration while the higher (~260 bp) and less represented PCR product to the result of ITR-mediated integration.

To further evaluate the role of AAV ITRs in mediating full-length HITI donor DNA integration, we analyzed DNA samples from AFGRNA-treated MPS VI mice (previously injected to assess AAV-HITI efficacy) by long-read (LR) sequencing. We initially tried to amplify the target site upon HITI integration, hoping to detect the full-length integrated donor DNA.

However, we obtained only small PCR products resembling the target site without HITI donor integration. This is very likely due to the strong bias toward amplification of smaller fragments during PCR. Here, the fragment derived from wild-type alleles is ~10-fold smaller than the expected fragment after HITI. In order to circumvent this PCR bias yet visualize the target site after successful HITI, we PCR-amplified in separate reactions two different long PCR products (5' and 3' junctions; [Figure 5A](#)) whose size corresponded to the full-length donor DNA integrated at the on-target (~2 kb; [Figure 5B](#)). These long PCR fragments were analyzed by LR sequencing using Nanopore technology with specific primers ([Table S3](#)). We found that the majority of the obtained reads corresponded to the expected HITI-mediated integration; however, a small

gRNA target sites; [Table S1](#)). This donor should be integrated exclusively with its ITRs. Next, wild-type newborn C57BL/6 mice were randomly assigned to two different treatment groups and injected systemically by temporal vein at P1–2 at a total dose of 3.9×10^{13} GCs/kg. The same AAV vector encoding for the nuclease (AAV-SpCas9) was used in both groups and co-delivered with a second AAV carrying either the previously described ([Figure 1B](#)) dsRed HITI donor DNA (HITI donor) or the newly generated donor DNA without gRNA target sites. One-month post-treatment, genomic DNA was extracted from liver samples for molecular analysis. The 5' junction was PCR amplified with specific primers ([Figure 4C](#); [Table S2](#)) on DNA samples obtained from all the treated mice. A PCR product corresponding to the expected size (~260 bp) of the ITR-mediated integration was

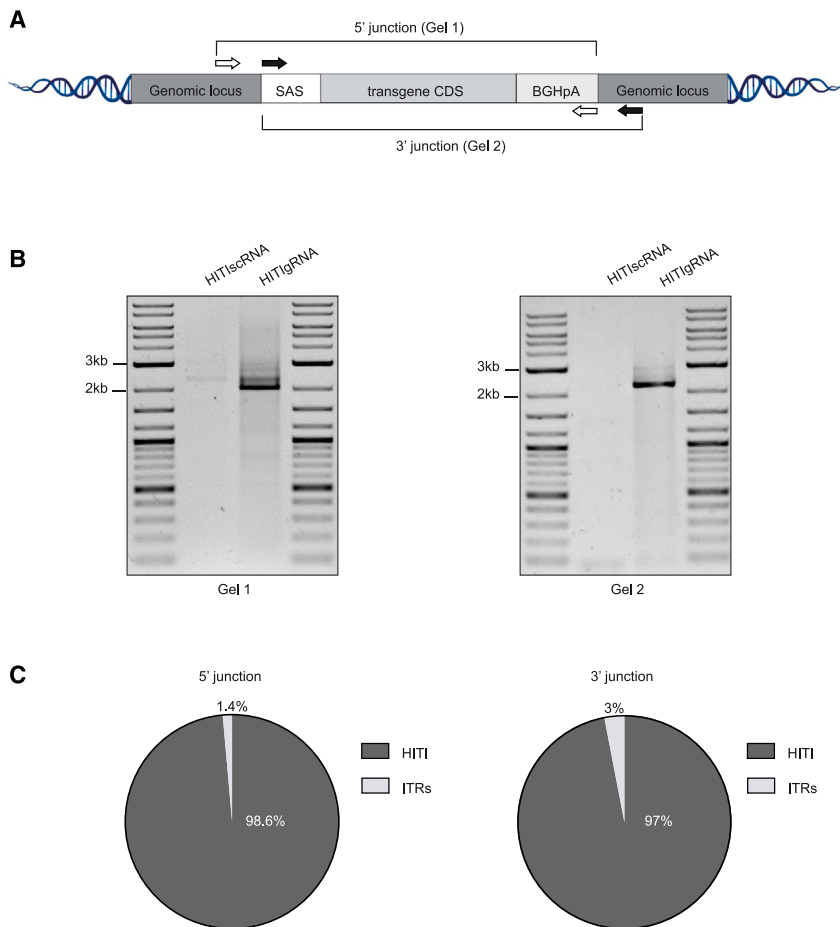


Figure 5. Long-reads analysis shows that full-length HITI donor DNA is integrated predominantly after ITR cleavage

(A) Schematic of the different long PCR junction products. White arrows indicate the primers designed to amplify the 5' junction: the forward primer (white left) was designed in the endogenous locus right before the cleavage site; the reverse primer (white right) was designed at the end of the donor DNA on the polyadenylation signal (BGHpA). Black arrows indicate the primers designed to amplify the 3' junction: the forward primer (black left) was designed at the beginning of the donor DNA on the splicing acceptor signal (SAS); the reverse primer (black right) was designed in the endogenous locus right after the cleavage site.

(B) Representative images of the 5' and 3' junction PCR products run on an agarose gel for the detection of the full-length HITI donor DNA (~2 kb). The 5' junction is shown in Gel 1 and the 3' junction in Gel 2.

(C) Pie chart showing the percentage (%) of long reads in which donor DNA integration was HITI mediated or ITRs mediated (ITRs) at the junction sites. See also Figures S4, S6, and Tables S2 and S3.

fraction of reads presented with remnants of ITRs. We then tailored a bioinformatics pipeline to count the reads that contained ITR sequences, and we found that 1.4% of the 5' junction reads and 3% of the 3' junction reads contained substantial (>9 bp) parts of the ITR sequences (Figure 5C). To assess the frequency of the ITR-mediated donor DNA integration by a method complementary to LR sequencing, we performed Illumina-based short-read sequencing on samples treated with AAV-HITI. Short fragments (~200 bp) covering the 5' junction were produced, and the number of reads containing (partial) ITRs was counted. Across three samples, we found that on average 9.8% (range 8.3%–11.3%) of the reads contained substantial (>9 bp) parts of an ITR. In line with the LR sequencing data, the vast majority of integrated fragments seem to have been released from the viral sequences prior to integration via HITI (Figure S4). To assess the various HITI donor DNA integration outcomes, we performed chromosomal aberrations analysis by single targeted linker-mediated PCR sequencing (CAST-Seq)⁵⁴ analysis (Figure S5) of liver DNA samples. CAST-Seq revealed six predominant integration events (Figure S6A): (1) the correct HITI event in the desired orientation (peak 1), (2) a fusion of intron 13 with the pA-encoding region of the AAV vector (peak 2), and (3) ITR-containing AAV fragments in both forward and reverse orientations (peaks 3–6; Figure S6A). Based on read coverage, we es-

estimate that the intended HITI fusion product accounts for about 20% of integration events which is slightly higher than the integration in the reverse orientation (14.5%). The most frequent integration event is capturing of ITR-containing AAV fragments, maybe because they are shorter than the transgene-containing DNA sections (Figures S6A and S6B). In Figure S6C, only a sub-fraction of CAST-Seq reads was analyzed, i.e., only reads representing integration of cleaved (ITR-free) HITI donor template. This analysis includes peak 1 (19.7% of all integration events) and peak 2 (14.5% of all integration events) of Figures S6A and S6B but none of the other peaks (peaks 3–6). Of the total 34.2% (i.e., 19.7% + 14.5%) ITR-free HITI donor integration events, 48% are productive (Figure S6C). These 16.4% (48% of 34.2%) align very well with the 16% dsRed-positive hepatocytes observed by fluorescence microscopy (Figure 2A). Furthermore, the 34.2% of HITI integration events converge with the 49% HITI-positive nuclei observed in Figure S1C.

Safety of AAV-HITI following neonatal delivery

To assess the safety of AAV-HITI following neonatal treatment, we evaluated over time the amount of AAV-SpCas9 genomes following delivery in newborn mice and found a significant drop of about 30-fold after a month (Figure S7A), which is in line with data in Figure S1B.

To further investigate AAV-SpCas9 genome integration at the target site, we used CAST-Seq. We observed predominantly ITR-mediated capture of the AAV-SpCas9 genome without preference for either ITR (Figure S7B); however, Cas9 integration events were found to be less abundant (peak at 60,000 reads

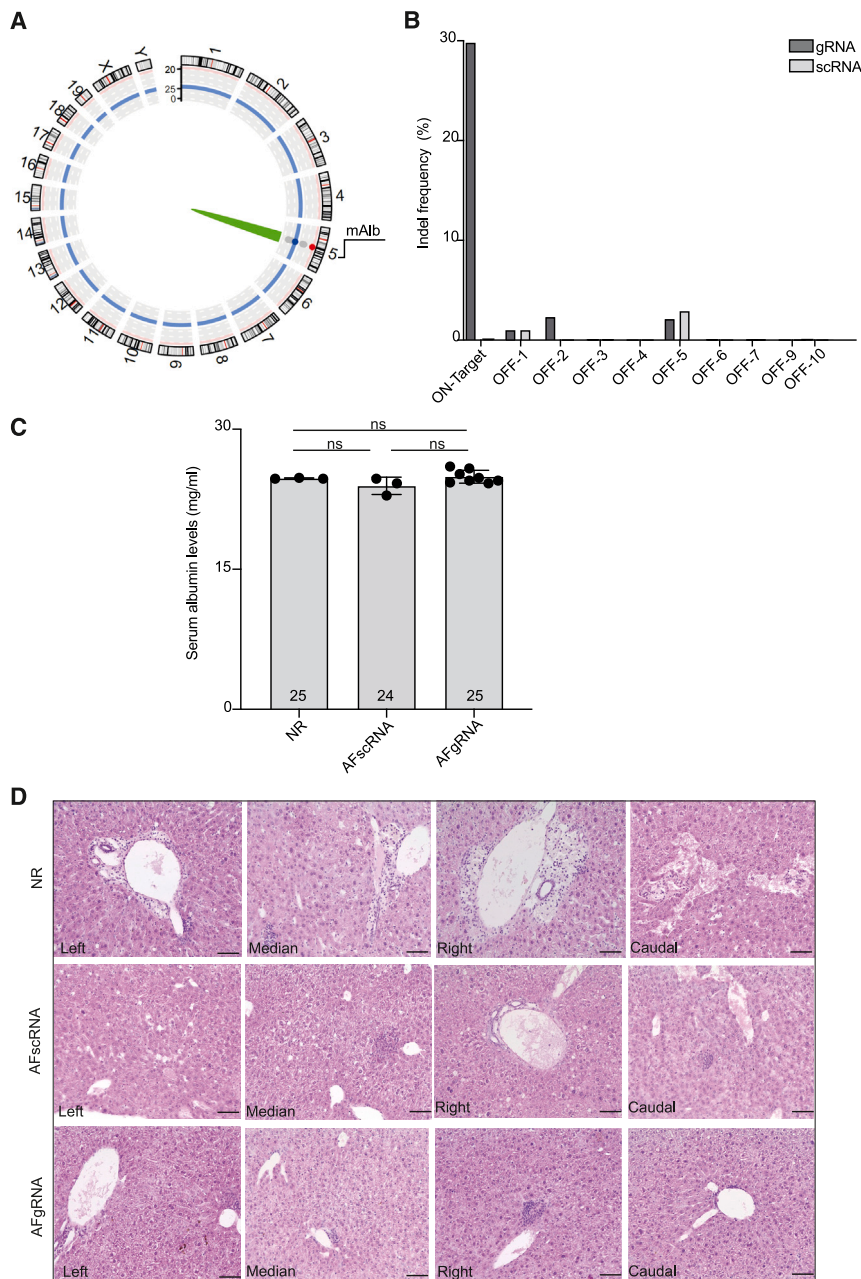


Figure 6. Safety following neonatal delivery of high doses of AAV-HITI

(A) The circos plot summarizes the CAST-Seq analysis performed on genomic DNA extracted from liver samples of AAV-HITI-treated MPS VI mice. The on-target is reported in green. No chromosomal aberrations were found.

(B) Off-target activity (indel frequency) measured at the top predicted off-target loci by next-generation sequencing (NGS) analysis on genomic DNA extracted from liver samples of AAV-HITI-treated MPS VI. The off-target 8 (OFF-8) was excluded due to technical issues.

(C) Serum albumin levels measured 1-year post-treatment in sera samples from normal controls (NR, $N = 3$) or AAV-HITI-treated MPS VI mice (AFgRNA, $N = 8$; AFscRNA, $N = 3$); data are represented as mean \pm standard deviation. Statistical differences were assessed by ordinary one-way ANOVA test.

(D) Representative images from histopathological analysis performed on paraffin sections from different liver lobes from AAV-HITI-treated MPS VI mice (AFgRNA, $N = 8$; AFscRNA, $N = 8$) and untreated normal controls (NR, $N = 4$) 1-year post-treatment. Scale bar, 50 μ m. See also Figures S7, S8 and Tables S5–S7.

liver lysates 1 year after vector delivery, and no Cas9 expression was detected (Figure S7D) suggesting that the risk of unwanted genetic editing due to long-term SpCas9 expression appears low under these conditions.

To evaluate potential CRISPR-Cas9-induced chromosomal rearrangement in an unbiased fashion, we performed CAST-Seq designed to this aim. We have shown before that CAST-Seq allows for the nomination of off-target (OT) sites through detection of OT-cleavage-induced translocations.⁵⁴ It furthermore enables assessment of DNA aberrations at the target site post nuclease treatment, including large deletions and inversions. CAST-Seq performed on genomic DNA extracted from liver samples of 3 different MPS VI mice treated

with AAV-HITI (gRNA or scRNA; Table S5) revealed an exquisite safety profile of our nuclease. We did not detect any OT-mediated translocations (OMTs; Figure 6A) but only large deletions/inversions surrounding the on-target site (Figure S8A), in extreme cases reaching up to 35 kb. CAST-Seq also allowed us to assess the relative frequencies of gross chromosomal aberrations at the target site. We found that 2.4% of CAST-Seq reads indicate deletions and inversions larger than 200 bp, whereas only 0.6% of reads were detected in AAV-HITI scRNA-treated mice (Figure S8B).

Moreover, we used *in silico* prediction to identify putative OTs and selected the top 10 candidates for downstream analysis (Table S6). We PCR-amplified the region surrounding the

in Figure S7B) than HITI donor DNA integration events (peak at 200,000 reads in Figure S6A). Detection of internal AAV regions, in addition to the ITRs, suggests that internal regions were likely captured upon end resection of the vector genome (Figure S7B). To qualitatively assess potential full-length AAV-SpCas9 integration at the on-target site, we used specific primers as depicted in Figure S7C (Table S4). A faint PCR fragment corresponding to the expected size (~4.5 kb) was amplified in the AFgRNA- but not in the AFscRNA-treated sample (Figure S7C). Full-length SpCas9 integration was confirmed by Sanger sequencing analysis. To understand whether this could result in SpCas9 expression, we performed western blot analysis on AAV-HITI-treated

expected OT cleavage site with primers specific for each locus (Table S7). PCR products were analyzed by NGS for the presence of indel mutations. Indels were found to be almost undetectable or present at similar frequency in AFgRNA- and AFscRNA-treated samples (Figure 6B), underlining that the employed CRISPR-Cas9 nuclease is highly specific. Furthermore, we measured serum albumin levels in AAV-HITI-treated (gRNA or scRNA) MPS VI mice and unaffected littermates at P360 and confirmed that our AAV-HITI approach does not alter endogenous albumin expression (Figure 6C). Histopathological analysis performed on liver sections from all AAV-HITI-treated (AFgRNA or AFscRNA) mice and unaffected controls showed no evidence of hepatocellular carcinoma (HCC) at this stage (P360; Figure 6D).

Dose response of liver-directed AAV-HITI in newborn mice

We next performed a dose-response study with two additional doses of AAV-HITI: a medium dose (MD) of 3.9×10^{13} total GCs/kg and a low dose (LD) of 1.2×10^{13} total GCs/kg. AAV-HITI efficiency at these new doses was assessed in newborn C57BL/6 mice using the dsRed HITI donor DNA. Animals were randomly assigned to the MD or LD group and injected systemically at P1–2, as described earlier. The percentage of hepatocytes expressing dsRed as a result of the integration (used to evaluate AAV-HITI efficiency) was quantified on liver cryo-sections 1-month post-treatment and found to be AAV dose dependent (Figure S9A). Next, the efficacy of AAV-HITI at these same doses (MD and LD) was evaluated in newborn MPS VI mice. A similar dose-dependent effect on serum ARSB activity was observed. Mice administered with AAV-HITI at MD exhibited sustained and stable serum ARSB activity levels starting from 1-month post-treatment, while mice treated with AAV-HITI at LD stably achieved ~50% of the normal ARSB levels (Figure S9B). Urinary (Figure S9C) and tissue GAG levels were normalized in AFgRNA-treated MPS VI mice (Figures S10A–S10D). GAGs storage was significantly decreased also in histological sections from the heart mitral valve and myocardium (Figure S10E) regardless of the dose used. In MD AFgRNA-treated mice, we also observed a significant amelioration in the skull width/length ratio and in the femur length compared to AF controls (Figures S10F–S10H).

Liver-directed AAV-HITI is effective in adult mice

To understand the applicability and efficiency of AAV-HITI in the adult liver, MPS VI and HemA mice were randomly administered systemically at 6 weeks of age an LD of 1.2×10^{13} GCs/kg of AAV-HITI vectors. For MPS VI mice detectable serum ARSB activity was measured in the AFgRNA-treated animals at 90 days of age, and this activity became supraphysiological at the subsequent time points (Figure 7A). Moreover, AFgRNA-treated mice showed decreased levels of urinary (Figure 7B) and tissue GAGs compared to the AF control mice (Figures S11A–S11D). GAGs storage was also reduced in histological sections from the heart mitral valve and myocardium (Figure S11E) while no significant improvement was observed in the analyzed bones (Figures S11F–S11H). In HemA mice at 30 days post AAV-HITI delivery, we observed FVIII protein levels around 36% of normal (Figure 7C), therapeutic levels of FVIII activity (Figure 7D), and reduced

clotting time (Figure 7E). These data indicate that AAV-HITI is effective in the adult liver at moderate AAV doses in addition to newborn.

DISCUSSION

In this study, we have demonstrated the therapeutic efficacy of liver-directed AAV-HITI at the highly transcribed *mAlb* locus both in the newborn and in the adult liver. Several previous studies have reported targeting of the albumin locus^{30,37,55} with overall similar levels of transgene integration to those we obtained here. HITI, however, hijacks NHEJ able to target both newborn and adult tissues^{21,22,25,34} without the need for long homology arms in the donor template. This allows to accommodate larger therapeutic sequences. Importantly, here we show that the majority of the full-length donor DNA integration happened after CRISPR-Cas9 cleavage of the ITRs, as intended by its design, which is in line with the lower integration rate of the AAV-*SpCas9* vector which lacks the inverted gRNA sites. This, combined with the slightly favored desired integration of the donor DNA that we observed using CAST-Seq, highlights the importance of the inverted gRNA sites at both extremities of the donor DNA. In addition, we found that integration of internal AAV-HITI donor DNA sequences was rare, suggesting that excessive end resection upon CRISPR-Cas-mediated cleavage of the HITI donor DNA does not occur.

Furthermore, we demonstrated the safety of AAV-HITI following neonatal delivery at high doses. AAV-HITI combines two different technologies whose safety is under evaluation: AAV vectors and CRISPR-Cas9 nuclease. AAV vectors are predominantly non-integrative; however, it has been shown that portions of their genome can integrate into pre-existing DSBs at a low frequency.⁵⁶ Despite this low level of integrations, a number of studies have been conducted in mice to investigate potential genotoxicity associated with these events particularly after neonatal treatment.^{57,58} Data collected in animal studies suggest that several factors such as age of treatments, vector doses, and vector design may influence genotoxic events related to AAV vectors.⁵⁷ However, no confirmed genotoxicity associated with AAV therapies has been described in humans to date.⁵⁷ In our recent publication,²¹ we performed genome-wide analysis of liver genomic DNA following AAV neonatal delivery and found partial AAV integrations at spontaneous DSBs. Here, we showed that portions of the AAV vector genomes can be found at the CRISPR-Cas9-induced DSBs with most of these integrations falling within the AAV ITR sequences, in line with previously reported data.^{59–61} To further investigate the safety of our approach, we thoroughly assessed AAV-*SpCas9* integration and long-term expression and found that, albeit detectable, full-length integration occurs at low levels and does not result in long-term detectable protein expression in the transduced liver.

Moreover, when nuclease-based strategies are proposed for therapeutic applications, the need to assess nuclease specificity and genome integrity is crucial to reduce the risk of genotoxicity.⁵⁴ Indeed, poor nuclease specificity may result in indel mutations at OT sites and large chromosomal aberrations.⁵⁴ Notably, the CAST-Seq data combined with the assessment of *in silico*-predicted OT sites showed that, despite low rates of partial

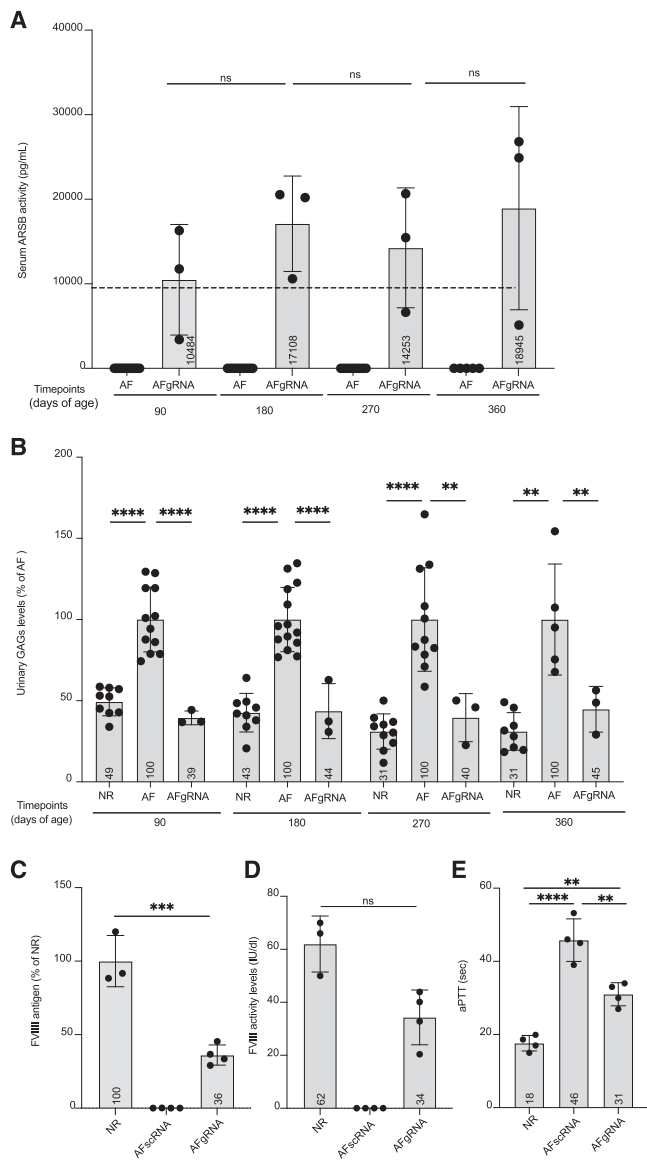


Figure 7. Liver-directed AAV-HITI in adult mice

(A) Serum ARSB activity analyzed at different time points in MPS VI mice left untreated (AF, $N = 14$) or treated with AAV-HITI-gRNA (AFgRNA, $N = 3$) at the total dose of 1.2×10^{13} total GCs/kg.

(B) Urinary GAG levels at different time points in MPS VI mice left untreated (AF, $N = 14$) or treated with AAV-HITI-gRNA (AFgRNA, $N = 3$) reported as a percentage of GAG levels in untreated MPS VI mice. NR, sera samples from normal animals. Statistical differences were assessed at P90 by Brown-Forsythe and Welch ANOVA tests: **** $p < 0.0001$ between NR and AF; **** $p < 0.0001$ between AF and AFgRNA; by Kruskal-Wallis test at P180: **** $p < 0.0001$ between NR and AF; **** $p < 0.0001$ between AF and AFgRNA; by ordinary one-way ANOVA test at P270: **** $p < 0.0001$ between NR and AF; ** $p < 0.0007$ between AF and AFgRNA; at P360: ** $p = 0.0012$ between NR and AF; $p = 0.9999$ between NR and AFgRNA; ** $p = 0.0078$ between AF and AFgRNA. The differences in the number of analyzed samples within the same group of treatment were due to sample availability. Each dot corresponds to a single animal within each group at different time points. (A and B) The differences in the number of analyzed samples within the same group of treatment at different time points were due to sample availability.

AAV integrations at the on-target site, neither intra-chromosomal rearrangements nor OT indels could be detected. CAST-Seq further revealed that a minor portion of reads (2.4%) from the target locus pointed at large chromosomal aberrations. Despite their low frequency, these events warrant consideration for potential safety implications. Of note, these data are in stark contrast to the high frequency (often exceeding 50%) at which such reads are found in cells that were exposed to a CRISPR-Cas9 nuclease in the absence of a donor DNA template (Kiermund et al., in revision; Rhie et al., in preparation), suggesting that the presence of an AAV donor DNA template could mitigate these chromosomal aberrations. However, more experiments, and in particular proper side-by-side comparisons, are needed to confirm this hypothesis.

Additionally, the absence of HCC up to 1 year after neonatal treatment supports the safety of the AAV-HITI platform. Of note, our AAV-HITI approach is based on the use of a weak HLP to drive SpCas9 expression and no promoter in the donor DNA. This design should limit the risk of genotoxicity, as also demonstrated by Chandler et al.⁶² Nonetheless, to exclude potential AAV-HITI-induced genotoxicity associated with HCC development in mice, longer follow-up up to 18–24 months of age will be necessary.⁶³

The unaltered secreted albumin levels support the safe design of HITI in albumin intron 13, as correct HITI insertions are not predicted to affect albumin gene expression. However, we should not underestimate the risk that undesired integration events may introduce potential cryptic acceptor splice sites that could alter expression from the endogenous locus. While this does not affect albumin levels in our case, it should not be overlooked, especially if HITI is performed in other genes.

Since high doses of AAVs may lead to adverse events,^{64,65} we performed a dose-response study in which we found that AAV-HITI administered in neonatal mice at 1.2×10^{13} total GCs/kg resulted in $\sim 50\%$ of the normal levels of serum ARSB activity, which significantly improved several features of the mouse disease phenotype. If directly translatable to humans, this dose is well tolerated. We also tested this same AAV-HITI dose in adult MPS VI and HemA mice and found it to be highly effective thus expanding the potential applications of AAV-HITI to conditions that require intervention in the adult liver.

Overall, our data support the use of the liver-directed AAV-HITI for sustained and stable expression of therapeutic transgenes to treat inborn genetic disorders. However, additional studies are required to further assess its translational potential. For instance,

(C) FVIII antigen levels detected in AAV-HITI (AFscRNA, $N = 4$; AFgRNA, $N = 4$)-treated adult HemA mice and normal controls (NR, $N = 3$) 1-month post AAV-HITI treatment. *** $p = 0.0001$ between NR and AFgRNA.

(D) FVIII activity levels evaluated in HemA mice (AFgRNA, $N = 4$; AFscRNA, $N = 4$) and normal controls (NR, $N = 3$) 1-month post AAV-HITI treatment. Statistical differences were assessed by ordinary one-way ANOVA test. p value between NR and AFgRNA = 0.0783.

(E) Activated partial thromboplastin time (aPTT) measured 1 month post AAV-HITI treatment in HemA AAV-HITI (AFgRNA, $N = 4$ and AFscRNA, $N = 4$) mice and normal controls (NR, $N = 4$). **** $p < 0.0001$ between NR and AFscRNA; ** $p = 0.0028$ between NR and AFgRNA; ** $p = 0.0014$ between AFscRNA and AFgRNA. All data are represented as mean \pm standard deviation. See also Figure S11.

unwanted AAV genome integration at the on-target site could be mitigated using low doses of AAV-HITI,²⁵ or by using non-viral systems such as lipid nanoparticles (LNPs) for nuclease delivery which provide transient expression.⁶⁶

Finally, validating gRNA sequences tailored for the human albumin locus and assessing the effectiveness and safety of AAV-HITI in mice with humanized liver could represent a significant step toward advancing this approach for clinical application.

Limitations of the study

Future implementations of this study could include longer animal follow-up and formal Investigational New Drug (IND)-enabling studies to further support the safety of the AAV-HITI platform and unbiased LR whole-genome sequencing to further strengthen the characterization of HITI-mediated editing events.

STAR★METHODS

Detailed methods are provided in the online version of this paper and include the following:

- [KEY RESOURCES TABLE](#)
- [RESOURCE AVAILABILITY](#)
 - Lead contact
 - Materials availability
 - Data and code availability
- [EXPERIMENTAL MODEL AND SUBJECT DETAILS](#)
 - Animal models
- [METHODS DETAILS](#)
 - Study design
 - Systemic vector administration
 - Generation of the AAV vector plasmids
 - AAV vector production and characterization
 - Liver fluorescence imaging
 - *In situ* hybridization
 - Serum ARSB enzymatic activity
 - Chromogenic assay
 - FVIII antigen detection
 - GAG level analysis in urine and tissues
 - Alcian blue staining in histological sections
 - Bone analysis
 - Tail-clip assay
 - Activated partial thromboplastin time (aPTT) assay
 - Western blot analysis
 - Serum albumin measurement
 - Histopathological analysis
 - DNA extraction
 - Quantitative PCR (qPCR)
 - CAST-Seq
 - Nanopore long-read sequencing
 - Short-read sequencing
 - Off-target site analysis
- [QUANTIFICATION AND STATISTICAL ANALYSIS](#)

SUPPLEMENTAL INFORMATION

Supplemental information can be found online at <https://doi.org/10.1016/j.xcrm.2024.101619>.

ACKNOWLEDGMENTS

We thank TIGEM Advanced Histopathology Facility for tissue processing and embedding of liver, spleen, kidney, and heart tissues; imaging; quantification of Alcian blue staining in heart tissue; and for DNAscope experiments. We

thank Cogentech s.r.l. for the liver histopathology analysis; NEGEDIA s.r.l. for the off-target analysis; InnovaVector s.r.l. for AAV vectors preparation; TIGEM Bioinformatics Core, particularly Eugenio Del Prete, for the statistical analysis; and [Biorender.com](https://www.biorender.com) for the cartoons used. We gratefully acknowledge Dr. Cathal Wilson (TIGEM) for editing of the text. This work was supported by the European Union Horizon 2020 grant “UPGRADE” (grant 825825), the Italian UniNA and “Compagnia di San Paolo” Star Plus 2020 Established Principal Investigator (grant 21-UNINA-EPIG-007), the European Union’s EIC Pathfinder program AAVolution (grant 101071041), and the ERC EXPEDITE grant (grant 101097155). We also acknowledge funding from the European Union, project geneTIGA grant-101057438 to T.C., and the German Federal Ministry of Education and Research (BMBF) within the Medical Informatics Funding Scheme: MIRACUM-FKZ 01ZZ1801B and PM⁴Onco-FKZ 01ZZ2322A (M.B.), and EkoEstMed-FKZ 01ZZ2015 (G.A.).

AUTHOR CONTRIBUTIONS

F.E. and A.A. conceived the study and wrote the manuscript. F.E., P.S.H., S.A., and M.L.S. generated plasmids for AAV production. F.E., F.D.A., R.F., and M.D.A. performed the experiments in MPS VI mice. F.E., P.S.H., and S.A. performed the experiments in C57BL/6 mice. F.E. and S.A. performed the experiments in HemA mice. F.E., F.D.A., E.N., S.A., R.D.C., and M.D.A. performed *in vivo* procedures. A. Padmanabhan and S. Notaro processed the different MPS VI tissues. A. Padula and F.E. designed and performed the western blot analysis on sera samples. F.E. and S.A. performed the western blot analysis on liver samples. P.P. and I.T. contributed to the interpretation of the results. F.E. performed the off-target NGS experiments and analyzed the data. M.R., K.O.C., G.A., M.B., T.I.C., and T.C. designed, performed, and analyzed CAST-Seq, on-target NGS, and long-read sequencing experiments. F.E. designed and performed the short-read experiments. M.R. and K.O.C. analyzed the short-read sequencing data. N.C.S. and S. Nutarelli developed customized ISH protocols and performed and analyzed the ISH experiments.

DECLARATION OF INTERESTS

F.E., F.D.A., R.F., M.L.S., and A.A. are listed as inventors on the patent WO2023213831 “Homology independent targeted integration for gene editing” related to this work. A.A. is founder, shareholder, and consultant of InnovaVector s.r.l. and of AAVantgarde Bio s.r.l. R.F. is currently an employee of AAVantgarde Bio s.r.l. T.C., M.B., and G.A. are listed as inventors of CAST-Seq (EP3856928B1).

Received: October 4, 2023

Revised: February 13, 2024

Accepted: May 27, 2024

Published: June 18, 2024

REFERENCES

1. Zabaleta, N., Unzu, C., Weber, N.D., and Gonzalez-Aseguinolaza, G. (2023). Gene therapy for liver diseases — progress and challenges. *Nat. Rev. Gastroenterol. Hepatol.* *20*, 288–305. <https://doi.org/10.1038/s41575-022-00729-0>.
2. Mendell, J.R., Al-Zaidy, S.A., Rodino-Klapac, L.R., Goodspeed, K., Gray, S.J., Kay, C.N., Boye, S.L., Boye, S.E., George, L.A., Salazar, S., et al. (2021). Current Clinical Applications of In Vivo Gene Therapy with AAVs. *Mol. Ther.* *29*, 464–488. <https://doi.org/10.1016/j.ymthe.2020.12.007>.
3. Au, H.K.E., Isalan, M., and Mielcarek, M. (2021). Gene Therapy Advances: A Meta-Analysis of AAV Usage in Clinical Settings. *Front. Med.* *8*, 809118–809214. <https://doi.org/10.3389/fmed.2021.809118>.
4. Jeyakumar, J.M., Kia, A., Tam, L.C.S., McIntosh, J., Spiewak, J., Mills, K., Heywood, W., Chisari, E., Castaldo, N., Verhoef, D., et al. (2023). Preclinical evaluation of FLT190, a liver-directed AAV gene therapy for Fabry disease. *Gene Ther.* *30*, 487–502. <https://doi.org/10.1038/s41434-022-00381-y>.

5. Brunetti-Pierri, N., Ferla, R., Ginocchio, V.M., Rossi, A., Fecarotta, S., Romano, R., Parenti, G., Yildiz, Y., Zancan, S., Pecorella, V., et al. (2022). Liver-Directed Adeno-Associated Virus-Mediated Gene Therapy for Mucopolysaccharidosis Type VI. *NEJM Evid. 1*, EVIDo2200052-12. <https://doi.org/10.1056/evidoa2200052>.
6. Ginocchio, V.M., Ferla, R., Auricchio, A., and Brunetti-Pierri, N. (2019). Current Status on Clinical Development of Adeno-Associated Virus-Mediated Liver-Directed Gene Therapy for Inborn Errors of Metabolism. *Hum. Gene Ther. 30*, 1204–1210. <https://doi.org/10.1089/hum.2019.151>.
7. Miesbach, W., Meijer, K., Coppens, M., Kampmann, P., Klamroth, R., Schutgens, R., Tangelder, M., Castaman, G., Schwäble, J., Bonig, H., et al. (2018). Gene therapy with adeno-associated virus vector 5–human factor IX in adults with hemophilia B. *Blood 131*, 1022–1031. <https://doi.org/10.1182/blood-2017-09-804419>.
8. Nathwani, A.C., Tuddenham, E.G.D., Rangarajan, S., Rosales, C., McIntosh, J., Linch, D.C., Chowdhary, P., Riddell, A., Pie, A.J., Harrington, C., et al. (2011). Adenovirus-Associated Virus Vector-Mediated Gene Transfer in Hemophilia B. *N. Engl. J. Med. 365*, 2357–2365. <https://doi.org/10.1056/nejmoa1108046>.
9. Nathwani, A.C., Reiss, U.M., Tuddenham, E.G.D., Rosales, C., Chowdhary, P., McIntosh, J., Peruta, M.D., Lheriteau, E., Patel, N., Raj, D., et al. (2015). Long term gene therapy for Fx. *N. Engl. J. Med. 371*, 1994–2004. <https://doi.org/10.1056/NEJMoa1407309>. Long-Term.
10. Ehrhardt, A., Xu, H., and Kay, M.A. (2003). Episomal Persistence of Recombinant Adenoviral Vector Genomes during the Cell Cycle In Vivo. *J. Virol. 77*, 7689–7695. <https://doi.org/10.1128/jvi.77.13.7689-7695.2003>.
11. Cotugno, G., Annunziata, P., Barone, M.V., Karali, M., Banfi, S., and Auricchio, A. (2012). Impact of age at administration, lysosomal storage, and transgene regulatory elements on AAV2/8-mediated rat liver transduction. *PLoS One 7*, e33286. <https://doi.org/10.1371/journal.pone.0033286>.
12. Wang, L., Wang, H., Bell, P., McMenamin, D., and Wilson, J.M. (2012). Hepatic gene transfer in Neonatal mice by Adeno-associated virus serotype 8 vector. *Hum. Gene Ther. 23*, 533–539. <https://doi.org/10.1089/hum.2011.183>.
13. Cunningham, S.C., Spinoulas, A., Carpenter, K.H., Wilcken, B., Kuchel, P.W., and Alexander, I.E. (2009). AAV2/8-mediated correction of OTC deficiency is robust in adult but not neonatal Spfash mice. *Mol. Ther. 17*, 1340–1346. <https://doi.org/10.1038/mt.2009.88>.
14. Cunningham, S.C., Dane, A.P., Spinoulas, A., and Alexander, I.E. (2008). Gene delivery to the juvenile mouse liver using AAV2/8 vectors. *Mol. Ther. 16*, 1081–1088. <https://doi.org/10.1038/mt.2008.72>.
15. Earley, J., Piletska, E., Ronzitti, G., and Piletsky, S. (2023). Evading and overcoming AAV neutralization in gene therapy. *Trends Biotechnol. 41*, 836–845. <https://doi.org/10.1016/j.tibtech.2022.11.006>.
16. Hamilton, B.A., and Wright, J.F. (2021). Challenges Posed by Immune Responses to AAV Vectors: Addressing Root Causes. *Front. Immunol. 12*, 675897–675898. <https://doi.org/10.3389/fimmu.2021.675897>.
17. Mingozzi, F., Maus, M.V., Hui, D.J., Sabatino, D.E., Murphy, S.L., Rasko, J.E.J., Ragni, M.V., Manno, C.S., Sommer, J., Jiang, H., et al. (2007). CD8(+) T-cell responses to adeno-associated virus capsid in humans. *Nat. Med. 13*, 419–422. <https://doi.org/10.1038/nm1549>.
18. Manno, C.S., Pierce, G.F., Arruda, V.R., Glader, B., Ragni, M., Rasko, J.J., Ozelo, M.C., Hoots, K., Blatt, P., Konkle, B., et al. (2006). Successful transduction of liver in hemophilia by AAV-Factor IX and limitations imposed by the host immune response. *Nat. Med. 12*, 342–347. <https://doi.org/10.1038/nm1358>.
19. Ertl, H.C.J. (2022). Immunogenicity and toxicity of AAV gene therapy. *Front. Immunol. 13*, 975803–975809. <https://doi.org/10.3389/fimmu.2022.975803>.
20. Chavez, M., Chen, X., Finn, P.B., and Qi, L.S. (2023). Advances in CRISPR therapeutics. *Nat. Rev. Nephrol. 19*, 9–22. <https://doi.org/10.1038/s41581-022-00636-2>.
21. Tornabene, P., Ferla, R., Llado-Santaeularia, M., Centruolo, M., Dell’Anno, M., Esposito, F., Marrocco, E., Pone, E., Minopoli, R., Iodice, C., et al. (2022). Therapeutic homology-independent targeted integration in retina and liver. *Nat. Commun. 13*, 1963–2014. <https://doi.org/10.1038/s41467-022-29550-8>.
22. Wang, Q., Zhong, X., Li, Q., Su, J., Liu, Y., Mo, L., Deng, H., and Yang, Y. (2020). CRISPR-Cas9-Mediated In Vivo Gene Integration at the Albumin Locus Recovers Hemostasis in Neonatal and Adult Hemophilia B Mice. *Mol. Ther. Methods Clin. Dev. 18*, 520–531. <https://doi.org/10.1016/j.omtm.2020.06.025>.
23. Li, T., Yang, Y., Qi, H., Cui, W., Zhang, L., Fu, X., He, X., Liu, M., Li, P.F., and Yu, T. (2023). CRISPR/Cas9 therapeutics: progress and prospects. *Signal Transduct. Target. Ther. 8*, 36. <https://doi.org/10.1038/s41392-023-01309-7>.
24. Frangoul, H., Altshuler, D., Cappellini, M.D., Chen, Y.-S., Domm, J., Eustace, B.K., Foell, J., de la Fuente, J., Grupp, S., Handgretinger, R., et al. (2021). CRISPR-Cas9 Gene Editing for Sickle Cell Disease and β -Thalassemia. *N. Engl. J. Med. 384*, 252–260. <https://doi.org/10.1056/nejmoa2031054>.
25. He, X., Zhang, Z., Xue, J., Wang, Y., Zhang, S., Wei, J., Zhang, C., Wang, J., Urip, B.A., Ngan, C.C., et al. (2022). Low-dose AAV-CRISPR-mediated liver-specific knock-in restored hemostasis in neonatal hemophilia B mice with subtle antibody response. *Nat. Commun. 13*, 7275. <https://doi.org/10.1038/s41467-022-34898-y>.
26. Gillmore, J.D., Gane, E., Taubel, J., Kao, J., Fontana, M., Maitland, M.L., Seitzer, J., O’Connell, D., Walsh, K.R., Wood, K., et al. (2021). CRISPR-Cas9 In Vivo Gene Editing for Transthyretin Amyloidosis. *N. Engl. J. Med. 385*, 493–502. <https://doi.org/10.1056/nejmoa2107454>.
27. Bart P. L., Koenekoop, R.K., Porto, F.B.O., Russell, S.R., and Girach, A. (2011). Leber Congenital Amaurosis Due to Cep290 Mutations — Severe Vision Impairment with a High Unmet Medical. 898–907.
28. Ou, L., Przybilla, M.J., Ahlat, O., Kim, S., Overn, P., Jarnes, J., O’Sullivan, M.G., and Whitley, C.B. (2020). A Highly Efficacious PS Gene Editing System Corrects Metabolic and Neurological Complications of Mucopolysaccharidosis Type I. *Mol. Ther. 28*, 1442–1454. <https://doi.org/10.1016/j.ymthe.2020.03.018>.
29. Tao, J., Bauer, D.E., and Chiarle, R. (2023). Assessing and advancing the safety of CRISPR-Cas tools: from DNA to RNA editing. *Nat. Commun. 14*, 212. <https://doi.org/10.1038/s41467-023-35886-6>.
30. De Caneva, A., Porro, F., Bortolussi, G., Sola, R., Lisjak, M., Barzel, A., Giacca, M., Kay, M.A., Vlahoviček, K., Zentilin, L., and Muro, A.F. (2019). Coupling AAV-mediated promoterless gene targeting to SaCas9 nuclease to efficiently correct liver metabolic diseases. *JCI Insight 5*, e128863. <https://doi.org/10.1172/jci.insight.128863>.
31. Hong, S.A., Seo, J.H., Wi, S., Jung, E.S., Yu, J., Hwang, G.H., Yu, J.H., Baek, A., Park, S., Bae, S., and Cho, S.R. (2022). In vivo gene editing via homology-independent targeted integration for adrenoleukodystrophy treatment. *Mol. Ther. 30*, 119–129. <https://doi.org/10.1016/j.ymthe.2021.05.022>.
32. Suzuki, K., and Izpisia Belmonte, J.C. (2018). In vivo genome editing via the HITI method as a tool for gene therapy. *J. Hum. Genet. 63*, 157–164. <https://doi.org/10.1038/s10038-017-0352-4>.
33. Suzuki, K., Tsunekawa, Y., Hernandez-Benitez, R., Wu, J., Zhu, J., Kim, E.J., Hatanaka, F., Yamamoto, M., Araoka, T., Li, Z., et al. (2016). In vivo genome editing via CRISPR/Cas9 mediated homology-independent targeted integration. *Nature 540*, 144–149. <https://doi.org/10.1038/nature20565>.
34. Chen, X., Niu, X., Liu, Y., Zheng, R., Yang, L., Lu, J., Yin, S., Wei, Y., Pan, J., Sayed, A., et al. (2022). Long-term correction of hemophilia B through CRISPR/Cas9 induced homology-independent targeted integration. *J. Genet. Genomics 49*, 1114–1126. <https://doi.org/10.1016/j.jgg.2022.06.001>.
35. Chen, H., Shi, M., Gilam, A., Zheng, Q., Zhang, Y., Afrikanova, I., Li, J., Gluzman, Z., Jiang, R., Kong, L.J., and Chen-Tsai, R.Y. (2019). Hemophilia

- A ameliorated in mice by CRISPR-based in vivo genome editing of human Factor VIII. *Sci. Rep.* 9, 16838–16915. <https://doi.org/10.1038/s41598-019-53198-y>.
36. Porro, F., Bortolussi, G., Barzel, A., De Caneva, A., Iaconcig, A., Vodret, S., Zentilin, L., Kay, M.A., and Muro, A.F. (2017). Promoterless gene targeting without nucleases rescues lethality of a Crigler-Najjar syndrome mouse model. *EMBO Mol. Med.* 9, 1346–1355. <https://doi.org/10.15252/emmm.201707601>.
 37. Barzel, A., Paulk, N.K., Shi, Y., Huang, Y., Chu, K., Zhang, F., Valdmans, P.N., Spector, L.P., Porteus, M.H., Gaensler, K.M., and Kay, M.A. (2015). Promoterless gene targeting without nucleases ameliorates haemophilia B in mice. *Nature* 517, 360–364. <https://doi.org/10.1038/nature13864>.
 38. Sharma, R., Anguela, X.M., Doyon, Y., Wechsler, T., DeKolver, R.C., Sproul, S., Paschon, D.E., Miller, J.C., Davidson, R.J., Shivak, D., et al. (2015). In vivo genome editing of the albumin locus as a platform for protein replacement therapy. *Blood* 126, 1777–1784. <https://doi.org/10.1182/blood-2014-12-615492>.
 39. Zhao, L., Yang, Z., Zheng, M., Shi, L., Gu, M., Liu, G., Miao, F., Chang, Y., Huang, F., and Tang, N. (2024). Recombinant adeno-associated virus 8 vector in gene therapy: Opportunities and challenges. *Genes Dis.* 11, 283–293. <https://doi.org/10.1016/j.gendis.2023.02.010>.
 40. Gao, G.-P., Alvira, M.R., Wang, L., Calcedo, R., Johnston, J., and Wilson, J.M. (2002). Novel adeno-associated viruses from rhesus monkeys as vectors for human gene therapy. *Proc. Natl. Acad. Sci. USA* 99, 11854–11859.
 41. Martinez-Turrillas, R., Martin-Mallo, A., Rodriguez-Diaz, S., Zapata-Linares, N., Rodriguez-Marquez, P., San Martin-Uriz, P., Vilas-Zornoza, A., Calleja-Cervantes, M.E., Salido, E., Prosper, F., and Rodriguez-Madoz, J.R. (2022). In vivo CRISPR-Cas9 inhibition of hepatic LDH as treatment of primary hyperoxaluria. *Mol. Ther. Methods Clin. Dev.* 25, 137–146. <https://doi.org/10.1016/j.omtm.2022.03.006>.
 42. Esposito, F., Lyubenova, H., Tornabene, P., Auricchio, S., Iuliano, A., Nusco, E., Merlin, S., Olgasi, C., Manni, G., Gargaro, M., et al. (2022). Liver gene therapy with intein-mediated F8 trans-splicing corrects mouse haemophilia A. *EMBO Mol. Med.* 14, 151999–e15215. <https://doi.org/10.15252/emmm.202115199>.
 43. McIntosh, J., Lenting, P.J., Rosales, C., Lee, D., Rabbanian, S., Raj, D., Patel, N., Tuddenham, E.G.D., Christophe, O.D., McVey, J.H., et al. (2013). Therapeutic levels of FVIII following a single peripheral vein administration of rAAV vector encoding a novel human factor VIII variant. *Blood* 121, 3335–3344. <https://doi.org/10.1182/blood-2012-10-462200>.
 44. Alliegro, M., Ferla, R., Nusco, E., De Leonibus, C., Settembre, C., and Auricchio, A. (2016). Low-dose gene therapy reduces the frequency of enzyme replacement therapy in a mouse model of lysosomal storage disease. *Mol. Ther.* 24, 2054–2063. <https://doi.org/10.1038/mt.2016.181>.
 45. Ferla, R., Claudiani, P., Cotugno, G., Saccone, P., De Leonibus, E., and Auricchio, A. (2014). Similar therapeutic efficacy between a single administration of gene therapy and multiple administrations of recombinant enzyme in a mouse model of lysosomal storage disease. *Hum. Gene Ther.* 25, 609–618. <https://doi.org/10.1089/hum.2013.213>.
 46. Bowen, D.J. (2002). Haemophilia A and haemophilia B: molecular insights [erratum appears in *Mol Pathol* 2002 Jun;55(3):208]. *Mol Pathol.* 55, 127–144.
 47. Nathwani, A.C., Tuddenham, E., Chowdhury, P., McIntosh, J., Lee, D., Rosales, C., Phillips, M., Pie, J., Junfang, Z., Meagher, M.M., et al. (2018). GO-8: Preliminary Results of a Phase I/II Dose Escalation Trial of Gene Therapy for Haemophilia a Using a Novel Human Factor VIII Variant. *Blood* 132, 489. <https://doi.org/10.1182/blood-2018-99-118256>.
 48. Peyvandi, F., Mannucci, P.M., Garagiola, I., El-Beshlawy, A., Elalfy, M., Ramanan, V., Eshghi, P., Hanagavadi, S., Varadarajan, R., Karimi, M., et al. (2016). A Randomized Trial of Factor VIII and Neutralizing Antibodies in Hemophilia A. *N. Engl. J. Med.* 374, 2054–2064. <https://doi.org/10.1056/nejmoa1516437>.
 49. D'Avanzo, F., Zanetti, A., De Filippis, C., and Tomanin, R. (2021). Mucopolysaccharidosis type vi, an updated overview of the disease. *Int. J. Mol. Sci.* 22, 13456. <https://doi.org/10.3390/ijms222413456>.
 50. Harmatz, P., and Shediac, R. (2017). Mucopolysaccharidosis VI: Pathophysiology, diagnosis and treatment. *Front. Biosci.* 22, 385–406. <https://doi.org/10.2741/4490>.
 51. Sestito, S., Rinninella, G., Rampazzo, A., D'Avanzo, F., Zampini, L., Santoro, L., Gabrielli, O., Fiumara, A., Barone, R., Volpi, N., et al. (2022). Cardiac involvement in MPS patients: incidence and response to therapy in an Italian multicentre study. *Orphanet J. Rare Dis.* 17, 251–312. <https://doi.org/10.1186/s13023-022-02396-5>.
 52. Muenzer, J. (2011). Overview of the mucopolysaccharidoses. *Rheumatology* 50, 4–12. <https://doi.org/10.1093/rheumatology/ker394>.
 53. Evers, M., Saftig, P., Schmidt, P., Hafner, A., McLoughlin, D.B., Schmahl, W., Hess, B., Von Figura, K., and Peters, C. (1996). Targeted disruption of the arylsulfatase B gene results in mice resembling the phenotype of mucopolysaccharidosis VI. *Proc. Natl. Acad. Sci. USA* 93, 8214–8219. <https://doi.org/10.1073/pnas.93.16.8214>.
 54. Turchiano, G., Andrieux, G., Klermund, J., Blattner, G., Pennucci, V., el Gaz, M., Monaco, G., Poddar, S., Mussolino, C., Cornu, T.I., et al. (2021). Quantitative evaluation of chromosomal rearrangements in gene-edited human stem cells by CAST-Seq. *Cell Stem Cell* 28, 1136–1147.e5. <https://doi.org/10.1016/j.stem.2021.02.002>.
 55. Wang, L., Yang, Y., Breton, C.A., White, J., Zhang, J., Che, Y., Saveliev, A., McMenamin, D., He, Z., Latshaw, C., et al. (2019). CRISPR/Cas9-mediated in vivo gene targeting corrects hemostasis in newborn and adult factor IX-knockout mice. *Blood* 133, 2745–2752. <https://doi.org/10.1182/blood.2019000790>.
 56. Deyle, D.R., and Russell, D.W. (2009). Adeno-associated virus vector integration. *Curr. Opin. Mol. Ther.* 11, 442–447.
 57. Sabatino, D.E., Bushman, F.D., Chandler, R.J., Crystal, R.G., Davidson, B.L., Dolmetsch, R., Eggan, K.C., Gao, G., Gil-Farina, I., Kay, M.A., et al. (2022). Evaluating the state of the science for adeno-associated virus integration: An integrated perspective. *Mol. Ther.* 30, 2646–2663. <https://doi.org/10.1016/j.ymthe.2022.06.004>.
 58. Chandler, R.J., LaFave, M.C., Varshney, G.K., Burgess, S.M., and Venditti, C.P. (2016). Genotoxicity in mice following AAV gene delivery: A safety concern for human gene therapy? *Mol. Ther.* 24, 198–201. <https://doi.org/10.1038/mt.2016.17>.
 59. Hanlon, K.S., Kleinstiver, B.P., Garcia, S.P., Zaborowski, M.P., Volak, A., Spirig, S.E., Muller, A., Sousa, A.A., Tsai, S.Q., Bengtsson, N.E., et al. (2019). High levels of AAV vector integration into CRISPR-induced DNA breaks. *Nat. Commun.* 10, 4439–4511. <https://doi.org/10.1038/s41467-019-12449-2>.
 60. Nelson, C.E., Wu, Y., Gemberling, M.P., Oliver, M.L., Waller, M.A., Bohning, J.D., Robinson-Hamm, J.N., Bulaklak, K., Castellanos Rivera, R.M., Collier, J.H., et al. (2019). Long-term evaluation of AAV-CRISPR genome editing for Duchenne muscular dystrophy. *Nat. Med.* 25, 427–432. <https://doi.org/10.1038/s41591-019-0344-3>.
 61. Simpson, B.P., Yrigollen, C.M., Izda, A., and Davidson, B.L. (2023). Targeted long-read sequencing captures CRISPR editing and AAV integration outcomes in brain. *Mol. Ther.* 31, 760–773. <https://doi.org/10.1016/j.ymthe.2023.01.004>.
 62. Chandler, R.J., La Fave, M.C., Varshney, G.K., Trivedi, N.S., Carrillo-Carrasco, N., Senac, J.S., Wu, W., Hoffmann, V., Elkahloun, A.G., Burgess, S.M., and Venditti, C.P. (2015). Vector design influences hepatic genotoxicity after adeno-associated virus gene therapy. *J. Clin. Invest.* 125, 870–880. <https://doi.org/10.1172/JCI79213>.
 63. Ferla, R., Alliegro, M., Dell'Anno, M., Nusco, E., Cullen, J.M., Smith, S.N., Wolfsberg, T.G., O'Donnell, P., Wang, P., Nguyen, A.D., et al. (2021). Low incidence of hepatocellular carcinoma in mice and cats treated with systemic adeno-associated viral vectors. *Mol. Ther. Methods Clin. Dev.* 20, 247–257. <https://doi.org/10.1016/j.omtm.2020.11.015>.

64. Hinderer, C., Katz, N., Buza, E.L., Dyer, C., Goode, T., Bell, P., Richman, L.K., and Wilson, J.M. (2018). Severe Toxicity in Nonhuman Primates and Piglets Following High-Dose Intravenous Administration of an Adeno-Associated Virus Vector Expressing Human SMN. *Hum. Gene Ther.* 29, 285–298. <https://doi.org/10.1089/hum.2018.015>.
65. (2020). High-dose AAV gene therapy deaths. *Nat. Biotechnol.* 38, 910. <https://doi.org/10.1038/s41587-020-0642-9>.
66. Han, J.P., Kim, M., Choi, B.S., Lee, J.H., Lee, G.S., Jeong, M., Lee, Y., Kim, E.A., Oh, H.K., Go, N., et al. (2022). In vivo delivery of CRISPR-Cas9 using lipid nanoparticles enables antithrombin gene editing for sustainable hemophilia A and B therapy. *Sci. Adv.* 8, eabj6901-10. <https://doi.org/10.1126/sciadv.abj6901>.
67. Lampe, S.E.G., Kaspar, B.K., and Foust, K.D. (2014). Intravenous injections in neonatal mice. *J. Vis. Exp.* 11, 2–7. <https://doi.org/10.3791/52037>.
68. Nakai, H., Fuess, S., Storm, T.A., Muramatsu, S.i., Nara, Y., and Kay, M.A. (2005). Unrestricted Hepatocyte Transduction with Adeno-Associated Virus Serotype 8 Vectors in Mice. *J. Virol.* 79, 214–224. <https://doi.org/10.1128/jvi.79.1.214-224.2005>.
69. Tornabene, P., Trapani, I., Centrulo, M., Marrocco, E., Minopoli, R., Lupo, M., Iodice, C., Gesualdo, C., Simonelli, F., Surace, E.M., and Auricchio, A. (2021). Inclusion of a degron reduces level of undesired inteins after AAV-mediated protein trans-splicing in the retina. *Mol. Ther. Methods Clin. Dev.* 23, 448–459. <https://doi.org/10.1016/j.omtm.2021.10.004>.
70. Auricchio, A., Hildinger, M., O'Connor, E., Gao, G.P., and Wilson, J.M. (2001). Isolation of highly infectious and pure adeno-associated virus type 2 vectors with a single-step gravity-flow column. *Hum. Gene Ther.* 12, 71–76. <https://doi.org/10.1089/104303401450988>.
71. Doria, M., Ferrara, A., and Auricchio, A. (2013). AAV2/8 vectors purified from culture medium with a simple and rapid protocol transduce murine liver, muscle, and retina efficiently. *Hum. Gene Ther. Methods* 24, 392–398. <https://doi.org/10.1089/hgtb.2013.155>.
72. Wang, F., Flanagan, J., Su, N., Wang, L.C., Bui, S., Nielson, A., Wu, X., Vo, H.T., Ma, X.J., and Luo, Y. (2012). RNAscope: A novel in situ RNA analysis platform for formalin-fixed, paraffin-embedded tissues. *J. Mol. Diagn.* 14, 22–29. <https://doi.org/10.1016/j.jmoldx.2011.08.002>.
73. Rhiel, M., Geiger, K., Andrieux, G., Rositzka, J., Boerries, M., Cathomen, T., and Cornu, T.I. (2023). T-CAST: An optimized CAST-Seq pipeline for TALEN confirms superior safety and efficacy of obligate-heterodimeric scaffolds. *Front. Genome Ed.* 5, 1130736–1130814. <https://doi.org/10.3389/fged.2023.1130736>.
74. Currin, A., Swainston, N., Dunstan, M.S., Jervis, A.J., Mulherin, P., Robinson, C.J., Taylor, S., Carbonell, P., Hollywood, K.A., Yan, C., et al. (2019). Highly multiplexed, fast and accurate nanopore sequencing for verification of synthetic DNA constructs and sequence libraries. *Synth. Biol.* 4, ysz025-8. <https://doi.org/10.1093/synbio/ysz025>.
75. Tange, O. (2018). GNU Parallel 2018 (Ole Tange).
76. Srivathsan, A., Lee, L., Katoh, K., Hartop, E., Narayanan Kutty, S., Wong, J., Yeo, D., and Meier, R. (2021). MinION barcodes: biodiversity discovery and identification by everyone, for everyone. Preprint at bioRxiv. <https://doi.org/10.1186/s12915-021-01141-x>.
77. Li, H. (2018). Minimap2: Pairwise alignment for nucleotide sequences. *Bioinformatics* 34, 3094–3100. <https://doi.org/10.1093/bioinformatics/bty191>.
78. Danecek, P., Bonfield, J.K., Liddle, J., Marshall, J., Ohan, V., Pollard, M.O., Whitwham, A., Keane, T., McCarthy, S.A., Davies, R.M., and Li, H. (2021). Twelve years of SAMtools and BCFtools. *GigaScience* 10, giab008-4. <https://doi.org/10.1093/gigascience/giab008>.
79. Clement, K., Rees, H., Canver, M.C., Gehrke, J.M., Farouni, R., Hsu, J.Y., Cole, M.A., Liu, D.R., Joung, J.K., Bauer, D.E., and Pinello, L. (2019). CRISPResso2 provides accurate and rapid genome editing sequence analysis. *Nat. Biotechnol.* 37, 224–226. <https://doi.org/10.1038/s41587-019-0032-3>.
80. Li, H. (2013). Aligning Sequence Reads, Clone Sequences and Assembly Contigs with BWA-MEM. Preprint at arXiv. <https://doi.org/10.48550/arXiv.1303.3997>.
81. Concordet, J.P., and Haeussler, M. (2018). CRISPOR: Intuitive guide selection for CRISPR/Cas9 genome editing experiments and screens. *Nucleic Acids Res.* 46, W242–W245. <https://doi.org/10.1093/nar/gky354>.

STAR★METHODS

KEY RESOURCES TABLE

REAGENT or RESOURCE	SOURCE	IDENTIFIER
Antibodies		
2A	Novus Biologicals	Cat#NBP259627H, RRID:AB_3101802
Cas9	Thermo Fisher Scientific	Cat# MA1-201, RRID:AB_2610640
Calnexin	Enzo Life Sciences	Cat#ADI-SPA-860F, RRID:AB_11178981
hARSB polyclonal antibody	Covalab	Custom
Chemicals, peptides and recombinant proteins		
SubX	Leica Biosystems	Cat# 3803670E
Alcian blue	Merck	Cat#A5268-25G
Nuclear Fast Red	Merck	Cat#N8002-5G
Aluminum sulfate hydrate 98%	Merck	Cat# 36,845-8
Critical commercial assays		
Coatest® SP4 FVIII-kit	Chromogenix, Werfen, Milan	Cat#K824094
Activated partial thromboplastin time (aPTT)	Teco, Bunde, Germany	Coatron M4
Mouse albumin ELISA kit	Abcam	Cat# 108791
VisuLizeFVIII ELISA kit	Affinity Biologicals	Cat# FVIII-AG
Deposited data		
BSgenome.Mmusculus.UCSC.mm10 1.4.3	Bioconductor	https://bioconductor.org/packages/release/data/annotation/html/BSgenome.Mmusculus.UCSC.mm10.html
TxDb.Mmusculus.UCSC.mm10.knownGene 3.10.0	Bioconductor	https://bioconductor.org/packages/release/data/annotation/html/TxDb.Mmusculus.UCSC.mm10.knownGene.html
org.Mm.e.g.,.db 3.16.0	Bioconductor	https://bioconductor.org/packages/release/data/annotation/html/org.Mm.e.g.,.db.html
Experimental models: Organisms/strains		
C57BL/6 mice	Envigo	Cat#057
B6; 129S F8tm1Kaz/J	Jackson Laboratory	Cat#004424
MPS VI mice	Institute of Molecular Medicine and Cell Research, University of Freiburg, Germany	N/A
Software and algorithms		
Fiji	ImageJ	http://rsbweb.nih.gov/ij/
GraphPad	Prism GraphPad	https://www.graphpad.com/features
Benchling	Benchling	www.benchling.com
Zen Blue	ZEISS ZEN	https://www.zeiss.com/microscopy/en/products/software/zeiss-zen-lite.html
Qpath	Qpath	https://qupath.github.io/
Biorender	Biorender	https://www.biorender.com/
CRISPResso2	CRISPResso2	http://crispresso2.pinellolab.org/submission
CRISPOR web tool	CRISPOR web tool	CRISPOR.org
MinKNOW version 23.04.6	Oxford Nanopore Technologies	https://nanoporetech.com
Minimap2 v. 2.24-r1122	minimap2	https://github.com/lh3/minimap2/releases
BBmap	SOURCEFORGE	https://sourceforge.net/projects/bbmap/
BWA MEM v0.7.17	SOURCEFORGE	https://bio-bwa.sourceforge.net/bwa.shtml
GNU parallel 20220922	GNU Operating System	https://www.gnu.org/software/parallel/
Samtools 1.16.1	Samtools	http://www.htslib.org/

(Continued on next page)

Continued

REAGENT or RESOURCE	SOURCE	IDENTIFIER
Pcregrep 8.45 2021-06-15		https://man7.org/linux/man-pages/man1/pcregrep.1.html
BBduk	BBTools	https://jgi.doe.gov/data-and-tools/software-tools/bbtools/bb-tools-user-guide/bbduk-guide/
bedtools v2.27.1	Bedtools website	https://bedtools.readthedocs.io
Biostrings 2.46.0	Bioconductor	https://bioconductor.org/packages/release/bioc/html/Biostrings.html
ChIPseeker 1.14.2	Bioconductor	https://bioconductor.org/packages/release/bioc/html/ChIPseeker.html
CAST-Seq	CAST-Seq github	https://github.com/AG-Boerries/CAST-Seq
R 4.2.2	CRAN	https://www.r-project.org

Other

TaqMan-PCR	Applied Biosystems	Cat# 4304437
O.C.T. matrix	Kaltek	Cat# 0782
Vectashield with DAPI	Vector Laboratories	Cat# H-1200-10
Trisodium citrate 0.109 M	BD	Cat# 5T31.363048
Bradford Reagent	Bio-Rad	Cat#5000006
Protease inhibitor cocktail	Merck	Cat#78430
Ponceau	Merck	Cat#P7170-1L
KAPA HiFi Hotstart Polymerase	Roche	Cat#07958927001
Ampure XP beads	Beckman Coulter	Cat# A63881
DNasey Blood & Tissue kit	Qiagen	Cat# 69504
QIAquick® Gel Extraction Kit	Qiagen	Cat# 28706
Ligation Sequencing Kit V14	Oxford Nanopore Technologies	Cat# SQK-LSK114
LightCycler 480 SYBR Green I Master	Roche	Cat#04707516001

RESOURCE AVAILABILITY

Lead contact

Further information and requests for resources and reagents as well as datasets and protocols should be directed to and will be fulfilled by the lead contact, Alberto Auricchio (auricchio@tigem.it).

Materials availability

This study did not generate new unique reagents.

Data and code availability

- All data reported in this paper will be shared by the [lead contact](#) upon request.
- This study does not report original code.
- Any additional information required to reanalyze the data reported in this work paper is available from the [lead contact](#) upon request.

EXPERIMENTAL MODEL AND SUBJECT DETAILS

Animal models

Mice were housed at the TIGEM animal house (Pozzuoli, Italy) and maintained under a 12 h light/dark cycle at $23 \pm 1^\circ\text{C}$ and humidity of $50\% \pm 5\%$ with food and water available *ad libitum*. Animals were raised in accordance with the Institutional Animal Care and Use Committee guidelines for the care and use of animals in research. C57BL/6J mice were purchased from Envigo Italy SRL (Udine, Italy). The hemophilic A (HemA) mouse model (Cat# B6; 129S-F8tm1Kaz/J) was imported from the Jackson Laboratory (JAX stock). The MPS VI mice were kindly provided by Prof. C. Peters (Institute of Molecular Medicine and Cell Research, University of Freiburg, Germany). HemA mice were maintained by crossing knockout homozygous females with knockout hemizygous males to produce knockout experimental mice. MPS VI mice were maintained as heterozygotes and crossed to produce homozygous knockout experimental mice.

METHODS DETAILS

Study design

This study was designed to evaluate the efficacy and safety of the AAV vector mediated HITI approach in the liver. Editing efficiency in the liver was defined in cryo-section fluorescent images by using the ImageJ software to count and calculate the percentage of hepatocyte positive for the *Discosoma* sp.-Red (dsRed) fluorescent protein. In all *in vivo* studies, mice were randomly assigned to each treatment group. Therapeutic efficacy in the liver was assessed by evaluating the impact of neonatal systemic delivery of AAV-HITI on the phenotype of two different animal models of Mucopolysaccharidosis type VI (MPS VI) and Hemophilia A (HemA) while for safety studies only MPS VI mice were used. In addition, in the studies involving the MPS VI disease model, female and male mice were considered equivalent and randomly assigned to treatment groups whereas in the study involving hemophilic animals only males were used. Littermate controls were used when available. In both cases, observers were blind to both genotype and treatment of the animals. Sample sizes were determined based on previous experience and technical feasibility. Any difference in the numbers of analyzed samples within the same group of treatment at different timepoints was due to sample availability.

Systemic vector administration

Studies in animals were carried out in accordance with the Italian Ministry of Health regulation for animal procedures (Ministry of Health authorization number: 352/2020-PR and 626/2022-PR). The injections were performed under general anesthesia, as previously described.²¹ Temporal vein injections in neonatal mice (C57BL/6J or MPS VI, or HemA) were performed at post-natal p1-2 following the protocol published by Gombash Lampe et al.⁶⁷ For adult treatments, (C57BL/6J, MPS VI or HemA) retro-orbital injections were performed. The following doses were used in the experiments aimed at evaluating HITI efficiency in C57BL/6J and MPSVI newborn mice: high doses 1.2×10^{14} total genome copies (GC/Kg; 6×10^{13} GC/kg for each vector); medium doses 3.9×10^{13} total GC/Kg (1.95×10^{13} GC/kg for each vector); low doses 1.2×10^{13} total GC/Kg (6×10^{12} GC/kg for each vector). For rescue experiments in neonatal HemA mice, we used 3.9×10^{13} total GC/Kg (1.95×10^{13} GC/kg for each vector). For rescue experiments in MPS VI and Hema adult mice, we used 1.2×10^{13} total GC/Kg (6×10^{12} GC/kg for each vector). AAV8 vectors were used for all *in vivo* studies because of their high liver transduction efficiency.⁶⁸

Generation of the AAV vector plasmids

The plasmids used for AAV vector production were derived from either the pAAV2.1²¹ or the pTIGEM⁶⁹ plasmids both containing the inverted terminal repeats of AAV serotype 2.⁷⁰ The mouse albumin (mAlb) gRNA (5'-GTATTTAATAGGCAGCAGTG-3') was selected using the benchling gRNA design tool (www.benchling.com), targeting the intron 13 of the albumin locus considering the best predicted on-target and off-target scores. The scramble RNA was designed so as not to align with any sequences in the mouse genome.

AAV vector production and characterization

AAV serotype 8 vectors (AAV8) were produced by InnovaVector s.r.l by triple transfection of HEK293 cells followed by two rounds of CsCl₂ purification.⁷¹ For each viral preparation, vector titers (genome copies/ml) were determined by averaging the titer achieved by dot-blot and by TaqMan-PCR (Cat#4304437, Applied Biosystems, Carlsbad, California, USA) quantification analysis.⁷¹

Liver fluorescence imaging

To evaluate dsRed expression in liver, C57BL/6J mice were injected at post-natal day (P) 1–2. Livers were harvested at p30 under anesthesia as previously described.²¹ A small piece of each lobe was dissected, fixed in 4% PFA overnight, infiltrated with 15% sucrose over the course of a day and 30% sucrose overnight before being included in O.C.T. matrix (Cat# 0782, Kaltek) for cryo-sectioning. Five- μ m-thick liver cryo-sections were cut, distributed on slides, and mounted with Vectashield with DAPI (Cat#H-1200-10, Vector Lab). Cryo-sections were analyzed under a confocal LSM-700 microscope (Carl Zeiss), using appropriate excitation and detection settings for dsRed and DAPI. For assessment of HITI efficiency in mouse liver cryo-sections, three to four images of each liver were acquired at 20 \times magnification and then analyzed using ImageJ (Fiji) software (<http://rsbweb.nih.gov/ij/>) as previously described.²¹ We counted a minimum of 900 hepatocytes, identified by DAPI staining of the nucleus, for each image. The hepatocytes expressing the dsRed as result of the integration were unequivocally identified and counted based on their shape. The final value (~15%) was then obtained by dividing the number of dsRed positive hepatocytes over the total number of DAPI cells and multiplied by 100 to obtain the percentage (%).

In situ hybridization

Liver cryo-sections were used for the *in situ* hybridization (ISH) with the technology of Basescope (Advanced Cell Diagnostic, USA) in accordance with the manufacturer's protocol.⁷² ISH labeling of HITI donor DNA was performed using a 3-ZZ paired probe (sense) (Cat# 1134401, ACD). ISH was performed using the BaseScope Duplex Reagent Kit (Cat# 323871, ACD). Custom pre-treatment conditions included target retrieval of 30 min at 95 C–100 C, RNAscope Protease III (Cat # 322380, ACD) for 30 min at room temperature (RT). Custom counterstaining with Mayer haematoxylin for 1 min at RT was performed after probe, amplification, and chromogen steps in the kit assay. Sections were analyzed with scanned with ZEISS Axio Scan.Z1. The whole digital slides were viewed by zen blue software. Red positive spots of HITI DNA were quantified with QuPath software. For the quantitative analysis of positive

signals, we selected 4–6 liver regions at 20× magnification from mice belonging to AAV-HITlgRNA, -scRNA and PBS experimental groups, and the results were expressed as a percentage of positive nuclei over the total nuclei analyzed.

Serum ARSB enzymatic activity

Blood samples were collected at different timepoints from AAV-HITl-treated and control MPS VI mice as previously reported.²¹ Serum ARSB activity was measured by an immune capture assay based on the use of a specific custom-made anti-hARSB polyclonal antibody (Covalab, Villeurbanne, France) following a previously described protocol.²¹

Chromogenic assay

Blood sampling was performed by retro-orbital withdrawal and nine parts of blood were collected into one part of buffered trisodium citrate 0.109 M (Cat#5T31.363048; BD, Franklin Lakes, NJ, USA). Plasma was collected after centrifugation at 3,000 rpm at 4°C for 15 min. Chromogenic assay was performed on plasma samples using the Coatest SP4 FVIII-kit (Cat# K824094; Chromogenix, Werfen, Milan, Italy) according to the manufacturer's instructions. Results are expressed as International Units (IU) per decilitre (dL).

FVIII antigen detection

To quantify the levels of FVIII antigen, an ELISA kit (Cat#FVIII-AG; VisuLize FVIII ELISA kit, Affinity Biologicals, Arcore, Italy) was used according to the manufacturer's instructions.

GAG level analysis in urine and tissues

Urine samples were collected over 24 h using metabolic cages at p60, p90, p180, p270 and p360 from MPS VI-treated and control mice. Samples were centrifuged briefly to remove debris and diluted 1:50 in water to measure GAGs content. Fifty μ L of diluted urine or 250 μ g of protein lysate were then used for GAGs evaluation as previously reported.²¹

Alcian blue staining in histological sections

After methacarn fixation, livers, kidneys, spleens, and hearts were dehydrated by immersion in increasing concentrations of alcohol (70%, 80%, 90%, 100%) and then in Sub-X. All tissues were embedded in paraffin and sectioned transversally into 7- μ m-thick serial sections on a microtome. Tissue sections were de-paraffinized, rehydrated, then washed in water and stained with 1% Alcian blue (Cat#A5268-25G, Merck) in hydrochloric acid (5 min for hearts, 60 min all remaining tissues). Counter-staining was performed with 0.1% Fast-Red (Cat#N8002-5G, Merck) in water for 1 min. Liver, kidney, and spleen sections stained with Alcian blue were imaged with Leica Microscope DM5500. Heart sections stained with Alcian blue were scanned with ZEISS Axio Scan.Z1. The whole digital slides were viewed by Zen Blue software (<https://www.zeiss.com/microscopy/en/products/software/zeiss-zen-lite.html>). Quantitative analyses of Alcian blue staining in myocardial tissue and in mitral valves were performed by Qpath software (<https://qpath.github.io/>). Alcian blue quantification in myocardium was measured in two fields of identical area. Alcian blue quantification in the mitral valve was performed on the entirety of the valve. Results are expressed as Alcian blue positive area/total area.

Bone analysis

Radiography images were performed on AAV-HITl-treated MPS VI mice and unaffected controls were anesthetized with an intraperitoneal injection of ketamine (10 mg/Kg) combined with medetomidine (1 mg/Kg). Skull weight and length, and tibia and femur length, were measured using ImageJ (Fiji) software (<http://rsbweb.nih.gov/ij/>).

Tail-clip assay

Mice were anesthetized and the distal part of the tail was cut at 2–3 mm of diameter and immediately put in a prewarmed 0.9% saline solution and allowed to bleed for 10 min without disturbance and the tails were then cauterized. The mixture of collected blood and physiological saline solution was centrifuged at 1500 g for 5 min and the total volume of blood lost was measured.

Activated partial thromboplastin time (aPTT) assay

Activated partial thromboplastin time (aPTT) was measured on plasma samples with Coatron M4 (Teco, Bünde, Germany) using the aPTT program following the manufacturer's manual.

Western blot analysis

Protein concentration in AAV-HITl-treated sera samples collected from MPS VI and HemA mice was determined by Bradford Reagent (Cat#5000006, Bio-Rad). Ten microgram of sera were denatured at 100°C for 5 min in 1× Laemmli sample buffer supplemented with 1 M dithiothreitol (DTT). Next, protein samples were resolved on a 4–15% SDS-PAGE and transferred onto polyvinylidene difluoride (PVDF) membrane. After transfer to PVDF membrane, blot was blocked with TBS-Tween-20 containing 5% non-fat milk for 1 h at room temperature followed by incubation with primary antibody (Cat#NBP259627H, Novus Biologicals; dilution: 1/2,000) 1h at 4°C. Ponceau (Cat#P7170-1L, Merck) was used as normalizer in sera blot. Liver specimens were mechanically homogenized using metal beads and lysed in RIPA buffer, supplemented with protease inhibitor cocktail (Cat#78430, Merck). Samples were incubated for 30 min on ice, vortexed every 10 min, and centrifuged at 16,200 g for 20 min. Pellets were discarded and lysates were used

for Western blot analyses. After lysis, protein samples were treated as mentioned above. Hundred micrograms of liver proteins were loaded for each specimen into a 6% SDS-PAGE; after transfer to PVDF membrane, blot was blocked with TBS-Tween-20 containing 5% non-fat milk for 1 h at room temperature followed by incubation with primary antibody overnight at 4°C. The primary antibodies used for immuno-blotting were: rabbit anti-*SpCas9* (Cat# MA1-201, Thermo Fisher Scientific; dilution: 1/1,000) mouse anti-Calnexin (Cat#ADI-SPA-860F, Enzo Life Sciences; dilution: 1/2,000).

Serum albumin measurement

Blood was collected at p360 from AAV-HITI-treated and control mice via eye bleeding and centrifuged as previously described.²¹ Serum samples were diluted 1:30,000 and analyzed with a mouse albumin ELISA kit (Cat#108791, Abcam, Cambridge, UK) following the manufacturer's instructions.

Histopathological analysis

Right, left, median, and caudal liver lobes were embedded in paraffin and sectioned at a thickness of 5 μ m. To assess histological features, Haematoxylin/Eosin (Diapath) staining was performed according to standard protocols and samples were analyzed by an expert histopathologist from Histopathology Unit (Cogentech Ltd. Benefit Corporation, Milan) in blind.

DNA extraction

DNA extraction was performed using the DNeasy Blood & Tissue kit (Cat# 69504, QIAGEN) following the manufacturer's instructions.

Quantitative PCR (qPCR)

Viral genome copies (GC) were measured by qPCR analysis in 100ng of genomic DNA extracted from AAV-HITI-treated liver samples at 1-week, -month and 1-year upon AAV-HITI administration, using the LightCycler 480 SYBR Green I Master mix (Cat#04707516001, Roche). The following primers: forward HLP: 5'-CTCCTCCGATAACTGGGGTGAC-3' and reverse HLP: 5'-GCCCTGTCTC GTCCGTATTTA-3', were used to detect AAV8 -*SpCas9* vector; forward BGH 5'-TCTAGTTGCCAGCCATCTGTTGT-3'; reverse BGH 5'-TGGGAGTGGCACCTTCCA-3' were used to detect the AAV-HITI donor DNA following the qPCR protocol from Roche. Briefly, enzyme activation was set at 95°C during 20 s –3 min (1 cycle), followed by the denaturation step at 95°C during 3 s and annealing extension and acquisition at 60°C at 20 s with the last two points set at 40 cycles.

CAST-Seq

To identify chromosomal aberrations, nominate off-target sites and analyze integration events at the on-target site, we performed CAST-Seq.⁵⁴ High-throughput sequencing libraries were essentially prepared according to Turchiano et al., 2021.⁵⁴ In search for off-targets, a third decoy primer was included to prevent predominant amplification of the target locus after successful HITI. In total, three CAST-Seq libraries from liver genomic DNA samples extracted from three different 1 year-old MPS VI mice treated as newborn with high doses of AAV-HITI were prepared and compared to a single library generated from control mice samples (scrRNA). In order to analyze in depth the integration of AAVs and parts thereof, two CAST-Seq libraries of HITI-treated and a single library of a control mouse were sequenced. For these samples, the HITI-specific decoy primer was not used during library preparation. Sequencing of the samples was outsourced to GeneWiz (division of Azenta Life Sciences) who collected 2x150bp paired-end reads using an Illumina NovaSeq 6000 instrument. The bioinformatics analysis was performed using the previously published pipelines.^{54,73}

Nanopore long-read sequencing

Fragments for long-read sequencing were amplified from DNA extracted from 1 year-old MPS VI mice treated as newborn with high doses of AAV-HITI using KAPA HiFi Hotstart Polymerase (Cat#07958927001, Roche). The cycling conditions were: 3 min at 98°C followed by 35 cycles of 98°C for 20 s, 61°C (5' junction) or 63°C (3' junction) for 30 s, and 4 min at 72°C. A final elongation of 10 min at 72°C was programmed after the last cycle. Multiple PCR reactions were pooled and the pool subjected to bead purification using 0.9X Ampure XP beads (Cat# A63881, Beckman Coulter) and fragments eluted in a small volume of water (30 μ L). The thus concentrated PCR pool was subjected to agarose gel electrophoresis and the prominent PCR product was gel-extracted using the QIAquick Gel Extraction Kit (Cat# 28706, Qiagen). With the PCR step, 24-nt long barcodes were introduced, in accordance with previously published data.⁷⁴ The 5' and 3' junction PCR products were in a next step prepared for sequencing using the Ligation Sequencing Kit V14 (Cat# SQK-LSK114, Oxford Nanopore Technologies) following the manufacturer's instructions. Samples were immediately sequenced on an R10.4.1 MinION Flow Cell (Cat#FLO-MIN114, Oxford Nanopore Technologies) using a MinION sequencing device (Cat#MIN-101B, Oxford Nanopore Technologies) operated with MinKNOW software version 23.04.6. Reads were demultiplexed by employing a custom pipeline that allows for up to 4 mismatches in the barcode sequence using pcregrep and GNU Parallel.⁷⁵ We decided to allow up to 4 mismatches based on previously published data⁷⁶ as a compromise between a low false annotation rate versus loss of valuable information. Of note, the two samples described here were analyzed together during one sequencing run in the absence of other samples thus reducing the chance of wrongful read assignment. Obtained reads were aligned using Minimap2 v. 2.24-r1122,⁷⁷ and further processed with Samtools.⁷⁸ ITR sequence insertions were counted from the CIGAR string in a window of 200 bp around the integration site junctions using a custom script.

Short-read sequencing

Assessment of Indels in short sequencing reads was performed using CRISPResso2.⁷⁹ For the quantification of ITR sequence integration, raw FASTQ files were processed using BBduk (<https://sourceforge.net/projects/bbmap/>) and aligned to the reference amplicon using BWA MEM v0.7.17.⁸⁰ Correctly mapped reads were extracted from the FASTQ file and aligned to the ITR sequence. The total number of all alignments and the number of all alignments to the ITR sequence were quantified and the relative frequency was calculated.

Off-target site analysis

The top 10 predicted off-target sites were identified using the CRISPOR web tool (CRISPOR.org)⁸¹ based on GRCm39/mm39 mouse genome reference, and sorted by CFD off-target scores. Equal amounts of genomic DNA extracted from 3 AAV-HITI-gRNA-treated livers and 3-scRNA-treated livers were used to amplify between 150 and 300 bp genomic regions flanking the off-targets. PCR products were amplified with specific primers (Table S7) and quantified using Qubit 4.0 fluorometric Assay (Thermo Fisher Scientific). An equal amount of each PCR product from each liver sample was pooled together. Next-generation sequencing (NGS) amplicon library were prepared from 10 ng of pooled PCR products using the NEGEDIA DNAseq Low Input sequencing service (NEGEDIA s.r.l.) which included library preparation, quality assessment and sequencing on a NovaSeq 6000 sequencing system using a paired-end, 2x150 cycle strategy (Illumina Inc.). The resulting FASTQ files were then analyzed using CRISPRessoV2,⁷⁹ using the off-targets sequences as reference for analysis. A 17-nucleotide window (upstream and downstream of the cleavage site) was considered for evaluation. NGS analysis was performed by NEGEDIA s.r.l.

QUANTIFICATION AND STATISTICAL ANALYSIS

For all the statistical analysis, we performed the Shapiro-Wilk test to check that each condition had followed the normal distribution (null hypothesis). To assess significant differences between two conditions the non-parametric Mann-Whitney test was used in the case of rejection of the null hypothesis (p -value <0.05). If the null hypothesis was not rejected (p -value ≥ 0.05) the parametric unpaired T-test was applied and the F-test was used to check the homoscedasticity between the two compared conditions. In case of rejection of the null hypothesis (p -value <0.05) the parametric Welch's t-test was applied. For multiple comparisons and post hoc tests, non-parametric Kruskal-Wallis test was used in the case of rejection of the null hypothesis (p -value <0.05). The parametric one-way ANOVA test was applied in case of not rejection of the null hypothesis (p -value ≥ 0.05). In this case, we also performed the Brown-Forsythe test to check the homoscedasticity between the compared conditions (null hypothesis): we used the parametric Welch's one-way ANOVA in case of rejection of the null hypothesis (p -value <0.05). For completeness, we computed the p -values with post hoc tests for the pairwise multiple comparisons: Tukey's test for one-way ANOVA, Dunnett's test for Welch's one-way ANOVA, and Dunn's test for Kruskal-Wallis test. p -values are represented as follows: * p -value <0.05 ; ** p -value <0.01 ; *** p -value <0.001 ; **** p -value <0.0001 .